Astron Astrophys Rev (2009) 17:309–408
DOI 10.1007/s00159-009-0022-4

REVIEW ARTICLE

X-ray spectroscopy of stars

Manuel Güdel · Yaël Nazé

Received: 19 February 2009 / Published online: 12 May 2009

Abstract Non-degenerate stars of essentially all spectral classes are soft X-ray sources. Their X-ray spectra have been important in constraining physical processes that heat plasma in stellar environments to temperatures exceeding one million degrees. Low-mass stars on the cooler part of the main sequence and their pre-main sequence predecessors define the dominant stellar population in the galaxy by number. Their X-ray spectra are reminiscent, in the broadest sense, of X-ray spectra from the solar corona. The Sun itself as a typical example of a main-sequence cool star has been a pivotal testbed for physical models to be applied to cool stars. X-ray emission from cool stars is indeed ascribed to magnetically trapped hot gas analogous to the solar coronal plasma, although plasma parameters such as temperature, density, and element abundances vary widely. Coronal structure, its thermal stratification and geometric extent can also be interpreted based on various spectral diagnostics. New features have been identified in pre-main sequence stars; some of these may be related to accretion shocks on the stellar surface, fluorescence on circumstellar disks due to X-ray irradiation, or shock heating in stellar outflows. Massive, hot stars clearly dominate the interaction with the galactic interstellar medium: they are the main sources of ionizing radiation, mechanical energy and chemical enrichment in galaxies. High-energy emission permits to probe some of the most important processes at work in these stars, and

M. Güdel (✉)
Institute of Astronomy, ETH Zurich, 8093 Zurich, Switzerland
e-mail: guedel@astro.phys.ethz.ch

Y. Nazé
FNRS/Institut d'Astrophysique et de Géophysique, Université de Liège,
Allée du 6 Août 17, Bat B5C, 4000 Liège, Belgium
e-mail: naze@astro.ulg.ac.be

put constraints on their most peculiar feature: the stellar wind. Medium and high-resolution spectroscopy have shed new light on these objects as well. Here, we review recent advances in our understanding of cool and hot stars through the study of X-ray spectra, in particular high-resolution spectra now available from XMM-*Newton* and CHANDRA. We address issues related to coronal structure, flares, the composition of coronal plasma, X-ray production in accretion streams and outflows, X-rays from single OB-type stars, massive binaries, magnetic hot objects and evolved WR stars.

Keywords X-rays: stars · Stars: early-type · Stars: late-type

Contents

1 Introduction

Stars are among the most prominent sources accessible to modern X-ray telescopes. In fact, stars located across almost all regions of a Hertzsprung–Russell diagram have been identified as X-ray sources, with only a few exceptions, most notably A-type stars and the coolest giants of spectral type M. But even for those two classes, important exceptions exist. X-rays have been identified from the most massive and hottest stars, i.e., O-type and Wolf-Rayet stars, for which shocks forming in unstable winds are held responsible for the production of million-degree plasma and the ensuing X-rays. X-rays are therefore tracers of stellar mass loss and sensitive diagnostics of stellar-wind physics. In hot star binaries, winds may collide, thus forming very hot plasma in the wind collision region. The X-ray emission and its modulation with orbital phase then provide precise constraints on the colliding wind region, and hence the wind properties of each star.

In cooler stars of spectral classes F to M, magnetic coronae, overall analogous to the solar corona, are at the origin of X-rays, enriched by flares in which unstable magnetic fields reconnect and release enormous amounts of energy in a matter of minutes to hours. The presence of coronae in these stars testifies to the operation of an internal dynamo that generates the magnetic fields. Although X-rays provide easy diagnostics for such fields in the corona, the coronal phenomenon is by no means restricted to X-ray sources but should rather be understood as the ensemble of closed *magnetic field structures* anchored in the stellar photosphere. Some of these magnetic loops may be in the process of being heated, thus filling up with hot plasma, while others are not.

X-rays have also been detected from brown dwarfs; again, the emission mechanism is supposedly coronal. Similarly, in low-mass pre-main sequence stars, i.e., T Tauri stars (TTS) or (low-mass) protostars, intense steady and flaring X-ray radiation is also thought to originate predominantly in hot coronal plasma although the complex environment of such stars allows, in principle, additional X-ray sources to be present. Shocks forming at the photospheric footpoints of disk-to-star accretion flows have been proposed to generate detectable X-ray emission, and high-resolution X-ray spectra indeed seem to provide the corresponding diagnostics. Further, outflows and jets form X-rays in internal shocks and shocks with the interstellar medium (Herbig-Haro objects).

X-rays not only provide invaluable diagnostics for winds, magnetic fields, accretion and outflow physics. They can also become key players in their own right. In young stellar environments, for example, they act as ionizing and heating agents in circumstellar disks which then grow unstable to accretion instabilities in the presence of magnetic fields. Also, X-rays are well known to drive a complex chemistry in molecular environments such as circumstellar disks and envelopes. Once planets have formed, X-rays and the lower-energy extreme ultraviolet (EUV) radiation may

heat and evaporate significant fractions of their outer atmospheres, contributing to the loss of water and therefore playing a key role in determining the "habitability" of a planet.

Many of these topics have been addressed during the past three to four decades of stellar X-ray astronomy. A decisive boost came, however, with the introduction of high-resolution X-ray spectroscopy. While familiar to solar coronal physics for many years, high-resolution X-ray spectroscopy was the poor cousin of X-ray photometry (possibly with some low energy resolution) until recently, even though a few notable experiments like crystal spectrometers or gratings were carried on early satellites (e.g., Einstein, EXOSAT). These, however, required exceptionally bright X-ray sources. The Extreme-Ultraviolet Explorer (EUVE) gave a first taste of routine high-resolution spectroscopy in the high-energy domain, concentrating mostly on the 90–300 Å spectral region that contains many spectral lines of highly ionized species formed in million-degree plasmas. Given the large attenuation of EUV photons by the interstellar medium, only EUV bright, mostly nearby sources (predominantly cool stars) were the subject of spectroscopic observations. A summary is given by Bowyer et al. (2000).

High-resolution X-ray spectroscopy has been provided by grating instruments on the XMM-*Newton* and CHANDRA X-ray observatories which both were launched in 1999. Their broad wavelength coverage (0.07–15 keV), effective areas (up to $\approx$200 cm^2) and their impressive spectral resolving power (up to $\approx$1,000) have for the first time allowed many spectral lines to be separated, line multiplets to be resolved, and in some cases line profiles and line shifts to be measured. Such *spectroscopic* measurements have opened the window to stellar coronal and stellar wind physics, including pinpointing the location of X-ray emitting sources, determining densities of hot plasmas, measuring their composition or assessing X-ray ionization physics in stellar environments.

These topics define the main focus of the present review. We aim at summarizing our understanding of cool and hot star physics contributed by X-ray spectroscopy. Naturally, therefore, we will focus on observations and interpretations that the XMM-*Newton* and CHANDRA high-resolution spectrometers have made possible for now almost a decade. Older, complementary results from EUVE will occasionally be mentioned. However, understanding cosmic sources cannot and should not be restricted to the use of spectroscopic data alone. Although spectroscopy provides unprecedented richness of physical information, complementary results from, e.g., X-ray photometric variability studies or thermal source characterization based on low-resolution spectroscopy are invaluable in many cases. We highlight, in particular, the much higher effective areas of present-day CCD detectors that permit a rough characterization of large samples of stars inaccessible to current grating spectroscopy. A particularly important example is the study of the 6.4–7 keV line complex due to highly ionized iron in extremely hot gas on the one hand and to fluorescent emission from "cold" iron at low ionization stages on the other hand. This feature is presently best studied using CCD spectra with resolving powers of $\approx$50, in full analogy to line features at lower energies preferentially investigated with gratings.

We will, however, not concentrate on issues predominantly derived from light curve monitoring, potentially important for the localization of X-ray sources in the stellar

environments or the study of flares; we will also not focus on the thermal characterization of X-ray sources based on low-resolution spectroscopy available before the advent of XMM-*Newton* and CHANDRA; further, the many specific subclasses forming a zoo of variations of our themes, such as rapidly rotating giants, giants beyond the corona-wind dividing line, Ap stars, "Luminous Blue Variables" and others will not be treated individually as we wish to emphasize common physics related to coronae, winds, and accretion/outflow systems. Finally, this review is not concerned with evolutionary and population studies, for example in star-forming regions, in stellar clusters, or in stellar associations. These topics, equally important for a comprehensive picture of stellar physics and stellar evolution, have been reviewed elsewhere (e.g., Favata and Micela 2003; Güdel 2004).

We have structured our article as follows. The first chapter (Sect. 2) addresses X-ray spectroscopy of cool stars, focusing on the thermal and geometric coronal structure, coronal composition, and flare physics. We then turn to new features (Sect. 3) found in pre-main sequence stars with accretion and outflows. Finally, Sect. 4 reviews results from X-ray spectroscopy of massive, hot stars.

2 X-rays from cool stars

2.1 Coronal X-ray luminosities and temperatures

The Hertzsprung–Russell diagram rightward of spectral class A is dominated by stars with outer convection zones, and many of these also have inner radiative zones. In these stars, an interaction of convection with rotation produces a magnetic dynamo at the base of the convection zone, responsible for a plethora of magnetic phenomena in or above the stellar photosphere (e.g., magnetic spots, a thin chromosphere, magnetically confined coronal plasma occasionally undergoing flares, etc.).

The study of our nearby example of a cool star, the Sun, has provided a solid framework within which to interpret X-ray emission from cool stars. Indeed, essentially every type of cool star except late-type giants has meanwhile been identified in X-rays with characteristics grossly similar to what we know from the Sun. This includes objects as diverse as G- and K-type "solar-like" main-sequence stars, late-M dwarf "flare stars" and brown dwarfs (which are, however, fully convective and for which different dynamos may operate), protostars and accreting or non-accreting TTS (many of which are again fully convective), intermediate-mass A-type and pre-main-sequence Herbig Ae/Be stars, post-main sequence active binaries, and F–K-type giants. Most of these stars show variable X-ray emission at temperatures of at least 1–2 MK and occasional flaring.

As we expect from a rotation-induced internal dynamo, the luminosity level is fundamentally correlated with rotation, as was shown in the early seminal studies based on the *Einstein* stellar survey (Pallavicini et al. 1981; Walter 1981); the X-ray luminosity (L_X), the projected rotation period ($v \sin i$; in a statistical sense), the rotation period (P), the rotation rate (Ω), and the Rossby number ($Ro = P/\tau_c$, τ_c being the convective turnover time) are related by the following equations:

$$L_{\rm X} \approx 10^{27} (v \sin i)^2 \quad [\rm erg\ s^{-1}], \tag{1}$$

$$L_{\rm X} \propto \Omega^2 \propto P^{-2}, \tag{2}$$

$$F_{\rm X}, \frac{L_{\rm X}}{L_{\rm bol}} \propto Ro^{-2} \tag{3}$$

(see Pizzolato et al. 2003 for further details). These trends, however, saturate at levels of $L_{\rm X}/L_{\rm bol} \approx 10^{-3}$. At this point, a further increase of the rotation rate does not change $L_{\rm X}$ anymore. This break occurs at somewhat different rotation periods depending on spectral type but is typically located at $P \approx 1.5$–4 days, increasing toward later main-sequence spectral types (Pizzolato et al. 2003; a description in terms of Rossby number provides a more unified picture). The Sun with $L_{\rm X} \approx 10^{27}$ erg s^{-1} is located at the lower end of the activity distribution, with $L_{\rm X}/L_{\rm bol} \approx 10^{-7\ldots-6}$ and therefore far from any saturation effects. It is presently unclear why X-ray emission saturates. Possibilities include a physical saturation of the dynamo, or a complete filling of the surface with X-ray strong active regions. For the fastest rotators (v greater than about 100 km s^{-1}), $L_{\rm X}$ tends to slightly decrease again, a regime known as "supersaturation" (Randich et al. 1996).

There are some variations of the theme also for pre-main-sequence stars. Given their much deeper convective zones and ensuing longer convective turnover times, the saturation regime for typical TTS reaches up to about 30 days; almost all pre-main sequence stars may therefore be X-ray saturated (Flaccomio et al. 2003; Preibisch et al. 2005). For T Tauri samples, $L_{\rm X}/L_{\rm bol} \approx 10^{-3.5}$, although there is a large scatter around this saturation value, and the subsample of accreting TTS ("classical T Tauri" stars or CTTS) reveals ratios on average about a factor of two lower than non-accreting TTS ("weak-lined T Tauri" stars or WTTS; Preibisch et al. 2005; Telleschi et al. 2007a).

The second fundamental parameter of cool-star X-ray sources is the characteristic or "average" coronal temperature. Again, the Sun is located at the lower end of the range of coronal temperatures, showing $T_{\rm av} \approx 1.5$–3 MK, somewhat depending on the activity level (of course, individual features will reveal considerable variation around such averages at any instance). An important although unexpected finding from early surveys was a correlation between $T_{\rm av}$ and $L_{\rm X}$ (e.g., Schrijver et al. 1984; Schmitt et al. 1990; see Telleschi et al. 2005 for a recent investigation of solar analogs with similar spectral types and masses). Roughly, one finds

$$L_X \propto T^{4.5\pm0.3} \tag{4}$$

although the origin of this relation is unclear. It may involve more frequent magnetic interactions between the more numerous and more densely packed active regions on more active stars, leading to higher rates of magnetic energy release (flares) that heat the corona to higher temperatures (we will return to this point in Sects. 2.2, 2.4).

2.2 The thermal structure of coronae, and the coronal heating problem

Understanding the thermal coronal structure requires spectroscopic data of a number of lines forming at different temperatures. The advent of high-resolution X-ray

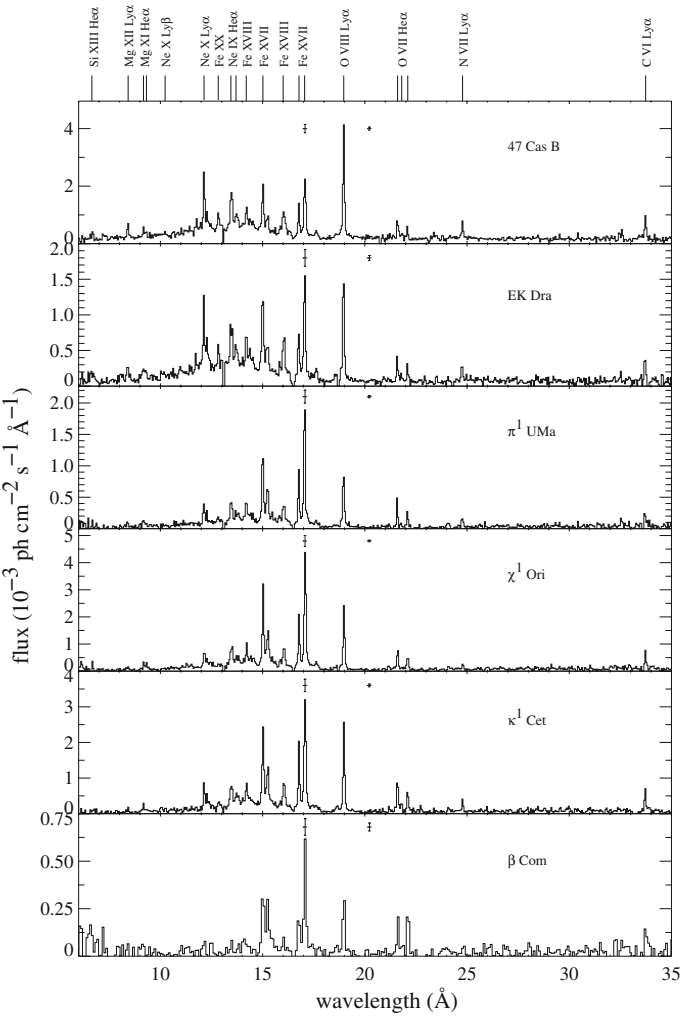

Fig. 1 XMM-*Newton* X-ray grating spectra of solar analogs at different activity levels. From *top* to *bottom*, age increases, while the overall activity level and the characteristic coronal temperatures decrease (from Telleschi et al. 2005, reproduced by permission of the AAS)

spectroscopy provided by XMM-*Newton* and CHANDRA has opened a new window to coronal structure, as summarized below. Examples of solar analog stars with different ages and therefore activity levels are shown in Fig. 1 (see also Fig. 14 for further examples of very active and inactive stars). As judged from the pattern of emission lines and the strength of the continuum, the spectra show that the dominant temperatures in the coronal plasma decrease with increasing age (from top to bottom).

Observed X-ray line fluxes as well as the continuum scale with the emission measure, $\mathrm{EM} = n_\mathrm{e} n_\mathrm{H} V$ at a given temperature, where n_e and n_H ($\approx 0.85 n_\mathrm{e}$ for a fully ionized plasma) are the number densities of electrons and hydrogen ions (protons),

respectively, and V is the emitting volume. For a distribution of emission measure in temperature, the relevant quantity is the differential emission measure (DEM), $Q(T) = n_e n_H dV(T)/d\ln T$ that gives the emission measure per unit interval in $\ln T$. Clearly, the DEM provides only a degenerate description of a complex corona, but it nevertheless contains statistical information on the average distribution of volumes in temperature and therefore—indirectly through modeling—also on the operation of heating and cooling mechanisms.

Deriving the thermal structure of an optically thin stellar corona is a problem of *spectral inversion*, using temperature-sensitive information available in spectral lines and the continuum. Many inversion methods have been designed, but regardless of the methodology, spectral inversion is an ill-conditioned problem and allows for a large number of significantly different but nevertheless "numerically correct" solutions (in the sense of reproducing a specified portion of the spectrum sufficiently well). The non-uniqueness of the inversion problem is rooted in the broad temperature range over which a given line forms, combined with the discretization of the problem (e.g., on a temperature grid) and uncertainties in the calibration, the tabulated atomic physics parameters, and even counting statistics (Craig and Brown 1976). This limitation of spectral inversion is fundamentally mathematical and cannot be removed even if data with perfect spectral resolution and perfect precision are at hand. In this sense, any inversion of a spectrum—*regardless of the inversion methodology*—is as good as any other if it reproduces the observed spectrum similarly well.[1] The discrimination between "physically acceptable" and "physically unacceptable" solutions requires that *additional conditions* be imposed on the emission measure distribution, which are in fact constraining the "physics" of the problem (e.g., smoothness of the emission measure distribution as required by thermal conduction for typical coronal features). These physical constraints obviously *cannot* be identified by any mathematical inversion technique. For further comments on this problem, see Güdel (2004).

Understanding emission measure distributions, but also reasonably constraining the spectral inversion process, requires theoretical models that link the *coronal thermal structure* with the DEM. We first summarize model predictions for non-flaring magnetic loops, and then address flaring sources.

Under the conditions of negligible gravity, i.e., constant pressure, and negligible thermal conduction at the footpoints, a hydrostatic loop (Rosner et al. 1978; Vesecky et al. 1979; Antiochos and Noci 1986) reveals a DEM given by

$$Q(T) \propto pT^{3/4-\gamma/2+\delta} \frac{1}{\left(1-[T/T_a]^{2-\gamma+\beta}\right)^{1/2}} \tag{5}$$

[1] Coronal research has developed several classes of inversion techniques, best separated into *discrete inversion techniques* that reconstruct the emission measure distribution from measured and extracted flux values of selected emission lines, and *continuous inversion techniques* that treat the spectrum as a function to be fitted with a superposition of synthetic template spectra. The often used expressions "line-based analysis" and "global fit", respectively, miss the essence of these techniques, as all methods ideally use a large fraction or the entirety of the available spectrum in which the relevant information is provided mostly by line flux ratios. Basically, equivalent solutions can be found from both classes of inversion techniques (Telleschi et al. 2005).

(Bray et al. 1991). Here, T_a is the loop apex temperature, and δ and β are power-law indices of, respectively, the loop cross section area S and the heating power q as a function of T: $S(T) = S_0 T^{\delta}$, $q(T) = q_0 T^{\beta}$, and γ is the exponent in the cooling function over the relevant temperature range: $\Lambda(T) \propto T^{\gamma}$. If T is not close to T_a, then constant cross-section loops ($\delta = 0$) have $Q(T) \propto T^{3/4-\gamma/2}$, i.e., under typical coronal conditions for non-flaring loops ($T < 10$ MK, $\gamma \approx -0.5$), the DEM slope is near unity (Antiochos and Noci 1986). If strong thermal conduction is included at the footpoints, then the slope changes to +3/2 if not too close to T_a (van den Oord et al. 1997). For a distribution of loops with different temperatures, the descending, high-T slope of the DEM is obviously related to the statistical distribution of the loops in T_a; a sharp decrease of the DEM then indicates that only few loops are present with a temperature exceeding the temperature of the DEM peak (Peres et al. 2001).

Antiochos (1980) (see also references therein) discussed DEMs of flaring loops that cool by (i) static conduction (without flows), or (ii) evaporative conduction (including flows), or (iii) radiation. The DEMs for these three cases scale like (in the above order)

$$Q_{\rm cond} \propto T^{1.5}, \quad Q_{\rm evap} \propto T^{0.5}, \quad Q_{\rm rad} \propto T^{-\gamma+1}. \tag{6}$$

Note that $\gamma \approx 0 \pm 0.5$ in the range typically of interest for stellar flares (5–50 MK). All above DEMs are therefore relatively flat (slope 1 ± 0.5).

For stellar flares that are too faint for time-resolved spectroscopy, the time-integrated DEM for a "quasi-statically" decaying flare is

$$Q \propto T^{19/8} \tag{7}$$

up to a maximum T that is equal to the temperature at the start of the decay phase (Mewe et al. 1997).

In the case of episodic flare heating (i.e., a corona that is heated by a large number of stochastically occurring flares), the average, time-integrated DEM of coronal X-ray emission is determined not by the internal thermal structure of magnetic loops but by the time evolution of the emission measure and the dominant temperature of the flaring region. In the case of dominant radiative cooling, the DEM at a given temperature is roughly inversely proportional to the radiative decay time, which implies

$$Q(T) \propto T^{-\gamma+1} \tag{8}$$

up to a maximum T_m, and a factor of $T^{1/2}$ less if subsonic draining of the cooling loop is allowed (Cargill 1994). Because the cooling function drops rapidly between 1 MK and $\lesssim 10$ MK, the DEM in this region should be steep, $Q(T) \propto T^4$.

An analytic model of a stochastically flaring corona powered by simple flares rising instantly to a peak and then cooling exponentially was presented by Güdel et al. (2003). Assuming a flare distribution in energy that follows a power law ($\mathrm{d}N/\mathrm{d}E \propto E^{-\alpha}$, see Sect. 2.4.2), and making use of a relation between flare peak temperature, T_p, and peak emission measure EM_p (Sect. 2.4.2), the DEM is

$$Q(T) \propto \begin{cases} T^{2/\zeta}, & af T^{b+\gamma} \leq L_{\min}, \\ T^{-(b+\gamma)(\alpha-2\beta)/(1-\beta)+2b+\gamma}, & af T^{b+\gamma} > L_{\min}, \end{cases} \quad (9)$$

where ζ relates temperature and density during the flare decay, $T \propto n^{\zeta}$; from the run of flare temperature and emission measure in stellar flares, one usually finds $0.5 \lesssim \zeta \lesssim 1$. The parameter b follows from the relation between flare peak temperature and emission measure, $\mathrm{EM_p} = aT_p^b$, where $b \approx 4.3$ (see Sect. 2.4.2; Güdel 2004); γ determines the plasma cooling function Λ as above, $\Lambda(T) = fT^{\gamma}$ (for typical stellar coronal abundances, $\gamma \approx -0.3$ below 10 MK, $\gamma \approx 0$ in the vicinity of 10 MK, and $\gamma \approx 0.25$ above 20 MK). Further, β describes a possible relation between flare decay time τ and the integrated radiative energy of the flare, E, $\tau \propto E^{\beta}$, with $0 \leq \beta \lesssim 0.25$ (see Güdel 2004 for further details); $L_{\min}$ is the peak luminosity of the smallest flares contributing to the DEM. For a flare-heated corona, this DEM model can, in principle, be used to assess the cooling behavior of flares (i.e., through ζ from the low-temperature DEM slope) and to derive the stochastic occurrence rate of flares (i.e., through α from the high-temperature DEM slope).

The above relations can easily be applied to DEMs reconstructed from observed spectra provided that DEM slopes have not been imposed as constraints for the inversion process. In fact, DEMs derived from stellar coronal spectra almost invariably show a relatively simple shape, namely an increasing power-law on the low-temperature side up to a peak, followed by a decreasing power-law up to a maximum temperature (Fig. 2). The DEM peak may itself be a function of activity in the sense that it shifts to higher temperatures in more active stars, often leaving very little EM at modest temperatures and correspondingly weak spectral lines of C, N, and O (see, e.g., Drake et al. 2000; Telleschi et al. 2005; Scelsi et al. 2005; Fig. 2). This behavior of course reflects the by now classic result that "stars at higher activity levels show higher average coronal temperatures" (e.g., Schmitt et al. 1990). Given the ill-conditioned inversion problem, many additional features turn up in reconstructed DEMs, such as local maxima or minima, but their reality is often difficult to assess.

Despite the models now available for a description of DEMs, we do not clearly understand which stellar parameters shape an emission measure distribution. The trend mentioned above, a correlation between average coronal temperature and "activity level", is reminiscent of a similar relation for individual stellar flares ("more-energetic flares are hotter"; Sect. 2.4.2), perhaps suggesting a connection between continuous flaring and overall coronal heating. Other parameters are less relevant. For example, active G stars at very different evolutionary stages (e.g., giants, main-sequence stars, pre-main sequence stars), with different coronal abundances and surface gravities may reveal very similar DEMs (Scelsi et al. 2005).

A principal finding of major interest are the unusually steep low-T sides of DEMs of active stars, with slopes in the range of 2–5 (Drake et al. 2000; Behar et al. 2001; Mewe et al. 2001; Argiroffi et al. 2003; Güdel et al. 2003; Telleschi et al. 2005; Scelsi et al. 2005). There is evidence that the slopes increase with increasing activity, as again illustrated in Fig. 2. Such slopes clearly exceed values expected from hydrostatic loops (1–1.5). Numerical simulations of loops undergoing repeated pulse heating at their footpoints do produce DEMs much steeper than the canonical values (Testa et al. 2005). An alternative solution may be loops with an expanding cross section from

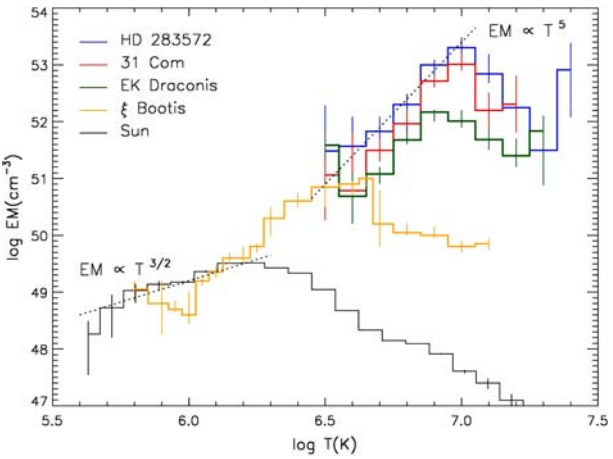

Fig. 2 DEMs derived from spectra of stars at different activity levels. The *black histogram* refers to the solar corona. Note the steeply increasing distributions for stars at higher activity levels (adapted from Scelsi et al. 2005)

the base to the apex. In that case, there is comparatively more hot plasma, namely the plasma located around the loop apex, than cooler plasma. The DEM would consequently steepen.

Steep DEMs have also been interpreted in terms of continual flaring using Eq. 9 (Güdel et al. 2003; Audard et al. 2004; Maggio et al. 2004; Telleschi et al. 2005). For solar analog stars at different activity levels, Telleschi et al. (2005) used the high-T slope of the DEMs to infer $\alpha = 2.1$–2.8 for the flare energy distribution (Sect. 2.4.2), suggesting that the ensemble of "weak", unresolved flares may generate the observed X-ray emission. Radiative flare energies in the range of 10^{25}–10^{30} erg s^{-1} would be required. From the DEM of the rapidly rotating giant FK Com, Audard et al. (2004) inferred a steep flare energy distribution with $\alpha = 2.6$–2.7; such distributions produce relatively flat light curves in which individual, strong flares are rare, compatible with the observations.

2.3 Coronal structure from X-ray spectroscopy

Understanding stellar coronal structure goes a long way in understanding stellar magnetism and dynamos. The distribution of magnetic fields near the stellar surface diagnoses type and operation of the internal magnetic dynamo; the structure of coronal magnetic fields is relevant for the energy release mechanism and determines the thermal structure of trapped hot plasma. Further, extended magnetic fields may connect to the companion star in close binaries, or the inner border of circumstellar disks in TTS or protostars; additional physical processes, such as angular momentum transfer or mass flows are important consequences.

Despite a suite of methods to infer *some* properties of coronal structure, all available methods are strongly affected by observational bias. This is principally due to the fact that the defining constituent of a corona, the *magnetic field* itself, is extremely difficult to measure; coronal structure is mostly inferred from observable signatures of magnet-

ically confined, hot plasma (as seen in the EUV or X-ray range) or trapped energetic particles (as seen in the radio range). Considering the complexity of the solar magnetic corona, its large range of size scales, and the important role that coronal *fine-structure* plays, we should not be surprised that presently available methods provide some limited qualitative sketches of what is a much more complex, highly dynamic system driven by continuous release and transformation of energy, coupled with mass motions and cooling processes. Before concentrating on high-resolution spectroscopic techniques, we briefly summarize alternative methods and results derived from them (see Güdel 2004 for more details).

2.3.1 Summary of low-resolution spectroscopic and non-spectroscopic X-ray studies

Hydrostatic loop models (Rosner et al. 1978; Vesecky et al. 1979; Serio et al. 1981) have been extensively used in solar and stellar X-ray astronomy to relate pressure, apex (peak) temperature, heating rate, and length of simple, static coronal magnetic loops anchored in the photosphere. In its simplest form, a half-circular loop of semi-length L (footpoint to apex), pressure p, apex temperature T_a, and heating rate ϵ follows the two relations (Rosner et al. 1978).

$$T_\mathrm{a} = 1{,}400(pL)^{1/3}, \quad \epsilon = 9.8 \times 10^4 p^{7/6} L^{-5/6}. \tag{10}$$

Measuring, e.g., T_a and relating the observed L_X to ϵ, the loop length can be inferred, depending on a surface-filling factor f for the loops filled with the observed plasma. Judged from such assessments, magnetically active stars require very large, moderate-pressure loops with a large surface-filling factor, or alternatively more solar-sized high-pressure compact loops with very small filling factors (<1%, e.g., Schrijver et al. 1989; Giampapa et al. 1996).

Synthetic emission spectra from *loop-structure models* of this kind have been applied to observed spectra of active stars. One typically finds mixtures of magnetic loops ranging from cool (1.5–5 MK), moderate-pressure (2–100 dyn cm^{-2}) loops to hot (10–30 MK) extreme-pressure (10^2–10^4 dyn cm^{-2}) loops reminiscent of flaring loops (Ventura et al. 1998). We need to keep in mind, however, that model solutions are degenerate in the product pL (see Eq. 10), potentially resulting in multiple solutions. Caution should therefore be applied when interpreting "best-fit" results based on the assumption of one family of identical magnetic loops.

Coronal imaging by *light-curve inversion* makes use of the fortuitous arrangement of components in binary stars producing *coronal eclipses*, or a large inclination of the rotation axis of a single star resulting in *self-eclipses* ("rotational modulation"). Image reconstruction from light curves is generally non-unique but can, in many cases, be constrained to reasonable and representative solutions. In the simplest case, *active region modeling*, similar to surface spot modeling, provides information on the location and size of the dominant coronal features (e.g., White et al. 1990). More advanced image reconstruction methods (maximum-entropy-based methods, backprojection/clean methods, etc.) provide entire maps of coronal emission (e.g., Siarkowski et al. 1996). Again, a mixture of compact, high-pressure active regions and much more extended ($\approx R_*$), lower-pressure magnetic features have been suggested for RS

CVn-type binaries (Walter et al. 1983; White et al. 1990). Light curves also provide important information on inhomogeneities and the global distribution of emitting material; X-ray bright features have been located on the leading hemispheres in binaries (Walter et al. 1983; Ottmann et al. 1993), or on hemispheres that face the companion (e.g., White et al. 1990; Siarkowski et al. 1996), perhaps suggesting some role for *intrabinary magnetic fields*. Such results indicate that even the most active stars are not entirely filled by X-ray or radio-emitting active regions, as surface-filling factors reach values of sometimes no more than 5–25% (e.g., White et al. 1990; Ottmann et al. 1993). In a few special cases, flares have been mapped using the fortuitous eclipsing by a close companion star. Such observations have located the flaring structure either at the pole or near the equator and have constrained the size of the flaring magnetic fields to typically a few tenths of R_* (for examples, see Choi and Dotani 1998; Schmitt and Favata 1999; Schmitt et al. 2003; Sanz-Forcada et al. 2007). As a by-product, characteristic electron densities of the flaring plasma can be inferred to be of order 10^{11} cm^{-3}, exceeding, as expected, typical non-flaring coronal densities (Sect. 2.3.3).

Magnetic field extrapolation using surface Doppler (or Zeeman Doppler) imaging of magnetic spots has been used in conjunction with X-ray rotational modulation observations to study distribution and radial extent of coronal magnetic fields (e.g., Jardine et al. 2002a,b; Hussain et al. 2002, 2007). Although permitting a 3-D view of a stellar corona, the method has its limitations as part of the surface is usually not accessible to Doppler imaging, and small-scale magnetic structure on the surface is not resolved. The type of field extrapolation (potential, force-free, etc.) must be assumed, but on the other hand, the 3-D coronal model can be verified if suitable rotational modulation data are available (Gregory et al. 2006).

2.3.2 Coronal structure from spectroscopic line shifts and broadening

Doppler information in X-ray spectral lines may open up new ways of imaging coronae of stars as they rotate, or as they orbit around the center of gravity in binaries. In principle, this method can be used to pinpoint the surface locations, heights, and sizes of coronal features. Applications are very limited at the present time given the available X-ray spectral resolving power of $\lesssim$ 1,000. Shifts corresponding to 100 km s^{-1} correspond to less than the instrumental resolution, but such surface (or orbital) velocities are attained only in exceptional cases of young, very rapidly rotating stars or rotationally locked, very close binaries. We summarize a few exemplary studies.

Amplitudes of $\approx$50 km s^{-1} and phases of Doppler shifts measured in the RS CVn binary HR 1099 agree well with the line-of-sight orbital velocity of the subgiant K star, thus locating the bulk of the X-ray emitting plasma on this star, rather than in the intrabinary region (Ayres et al. 2001a). In contrast, periodic line *broadening* in the dMe binary YY Gem, consisting of two nearly identical M dwarfs, indicates, as expected, that both components are similarly X-ray luminous (Güdel et al. 2001). Doppler shifts in the RS CVn binary AR Lac (Huenemoerder et al. 2003) are compatible with coronae on both companions if the plasma is close to the photospheric level. For the contact binary 44i Boo, Brickhouse et al. (2001) reported periodic line shifts corresponding to a total net velocity change over the full orbit of 180 km s^{-1}. From the amplitudes and the phase of the rotational modulation, the authors concluded that two dominant

X-ray sources were present, one being very compact and the other being extended, but both being located close to the stellar pole of the larger companion. Similar results have been obtained for another contact binary, VW Cep (Huenemoerder et al. 2006), revealing that almost all X-rays are emitted by a relatively compact corona (height 0.06–0.2R_*) almost entirely located on the primary star.

Applications are more challenging for rapidly rotating single stars. Hussain et al. (2005) did find periodic line shifts in the spectrum of the young AB Dor which, together with light curve modulation, suggested a coronal model consisting of a relatively low-lying distributed corona (height $\lesssim 0.5\ R_*$) and several more compact (height <0.3 R_*) active regions. This result, when combined with coronal extrapolations from surface Doppler imaging and spectroscopic coronal density measurements, further constrains the corona to heights of 0.3–0.4 R_*, and reasonable 3-D models of the coronal structure can be recovered (Hussain et al. 2007).

A comprehensive study of line shifts and line broadening has been presented for the Algol binary (Chung et al. 2004). Periodic line shifts corresponding to a quadrature radical velocity of 150 km s^{-1} clearly prove that the X-rays are related to the K subgiant. However, the amplitude of the shifts indicates that the source is slightly displaced toward the B star, which may be the result of tidal distortions by the latter. Excess line broadening (above thermal and rotational broadening) can be ascribed to a radially extended corona, with a coronal scale height of order one stellar radius, consistent with expected scale heights of hot coronal plasma on this star.

A rather predestined group of stars for this type of study are the rapidly rotating single giants of the FK Com class, thought to have resulted from a binary merger (Bopp and Stencel 1981). With surface velocities of order 100 km s^{-1}, shifts or broadening of bright lines can be measured. Audard et al. (2004) found significant line broadening corresponding to velocities of about 100–200 km s^{-1} in the K1 III giant YY Men; the broadening could in principle be attributed to rotational broadening of a coronal source above the equator, confined to a height of about a pressure scale height ($\approx 3R_*$). YY Men's extremely hot corona ($T \approx 40$ MK), however, makes Doppler thermal broadening of the lines a more plausible alternative (Audard et al. 2004). The prototype of the class, FK Com, also shows indications of line shifts (of order 50–150 km s^{-1}) and marginal suggestions for line broadening. The X-ray evidence combined with contemporaneous surface Doppler imaging suggests the presence of near-polar active regions with a height of $\approx 1R_*$ (Drake et al. 2008a). Taken together with other observations, there is now tentative evidence for X-ray coronae around active giants being more extended (relative to the stellar radius) than main-sequence coronae, which are predominantly compact (height $\lesssim 0.4R_*$, Drake et al. 2008a).

2.3.3 Inferences from coronal densities

High-resolution X-ray spectroscopy has opened a window to coronal densities because the X-ray range contains a series of density-sensitive lines; they happen to be sensitive to expected coronal and flare plasma densities. Electron densities have mostly been inferred from line triplets of He-like ions on the one hand and lines of Fe on the other

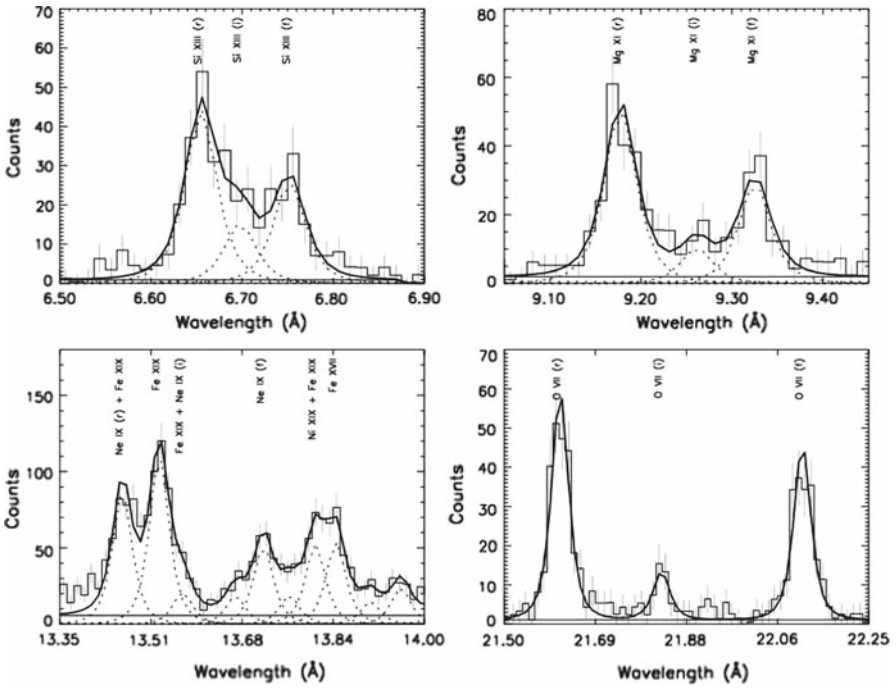

Fig. 3 He-like triplets of Si XIII (*upper left*), Mg XI (*upper right*), Ne IX (*lower left*), and O VII (*lower right*) extracted from the CHANDRA LETGS spectrum of Capella. Multi-line fits are also shown. The *horizontal lines* indicate the continuum level (from Argiroffi et al. 2003)

hand. We briefly review results from these in turn, and then summarize implications for coronal structure.

Coronal densities from He-like triplets He-like triplets of C V, N VI, O VII, Ne IX, Mg XI, and Si XIII show, in order of increasing wavelength, a resonance (r, $1s^2\ ^1S_0 - 1s2p\ ^1P_1$), an intercombination ($i$, $1s^2\ ^1S_0 - 1s2p\ ^3P_{1,2}$), and a forbidden ($f$, $1s^2\ ^1S_0 - 1s2s\ ^3S_1$) line (Fig. 3). The ratio between the f and i fluxes is sensitive to density (Gabriel and Jordan 1969) for the following reason: if the electron collision rate is sufficiently high, ions in the upper level of the forbidden transition, $1s2s\ ^3S_1$, do not return to the ground level, $1s^2\ ^1S_0$, instead the ions are collisionally excited to the upper level of the intercombination transitions, $1s2p\ ^3P_{1,2}$, from where they decay radiatively to the ground state (for a graphical presentation, see Fig. 4).

The measured ratio $\mathscr{R} = f/i$ of the forbidden to the intercombination line fluxes can be approximated by

$$\mathscr{R} = \frac{\mathscr{R}_0}{1 + n_\mathrm{e}/N_c} = \frac{f}{i}, \tag{11}$$

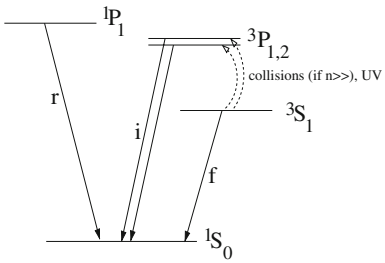

Fig. 4 Schematic diagram showing the origin of the *fir* lines in a He-like ion

Table 1 Density-sensitive He-like triplets

Ion	$\lambda(r, i, f)$ (Å)	$\mathscr{R}_0$	N_c	$\log n_e$ range[a]	T range[b] (MK)
C V	40.28/40.71/41.46	11.4	6×10^8	7.7–10	0.5–2
N VI	28.79/29.07/29.53	5.3	5.3×10^9	8.7–10.7	0.7–3
O VII	21.60/21.80/22.10	3.74	3.5×10^{10}	9.5–11.5	1.0–4.0
Ne IX	13.45/13.55/13.70	3.08	8.3×10^{11}	11.0–13.0	2.0–8.0
Mg XI	9.17/9.23/9.31	2.66[c]	1.0×10^{13}	12.0–14.0	3.3–13
Si XIII	6.65/6.68/6.74	2.33[c]	8.6×10^{13}	13.0–15.0	5.0–20

Data derived from Porquet et al. (2001) at maximum formation temperature of ion
[a] Range where $\mathscr{R}$ is within approximately [0.1, 0.9] times $\mathscr{R}_0$
[b] Range of 0.5–2 times maximum formation temperature of ion
[c] For measurement with CHANDRA HETGS-MEG spectral resolution

where $\mathscr{R}_0$ is the limiting flux ratio at low densities and N_c is the critical density at which $\mathscr{R}$ drops to $\mathscr{R}_0/2$ (we ignore the influence of the photospheric ultraviolet radiation field for the time being; see Sects. 3.6 and 4.2.1 below). Table 1 contains relevant parameters for triplets interesting for coronal studies; they refer to the case of a plasma that is at the maximum formation temperature of the respective ion (for detailed tabulations, see Porquet et al. 2001). A systematic problem with He-like triplets is that the critical density N_c increases with the formation temperature of the ion, i.e., higher-Z ions measure only high densities at high T, while the lower-density analysis based on C V, N VI, O VII, and Ne IX is applicable only to cool plasma.

He-like triplets are usually bright in coronal spectra and have therefore been used extensively for density estimates (e.g., Mewe et al. 2001; Ness et al. 2001). Large samples of coronal stars were surveyed by Ness et al. (2004) and Testa et al. (2004a). Although density estimates are roughly in line with experience from the solar corona (at least as far as analysis of the O VII triplet forming at temperatures of ≈2 MK is concerned), several systematic features have become apparent. The following trends predominantly apply to O VII derived densities:

– Low-activity stars tend to show low densities (often represented by upper limits), i.e., $\log n_e < 10$ (Ness et al. 2001; Raassen et al. 2003b).
– Higher densities significantly measured by the O VII triplet, i.e., $\log n_e = 10 - 11$, are only reported from magnetically active stars, many of which are located on the main sequence. Examples include very active solar analogs, very young K dwarfs

such as AB Dor, or active M dwarfs (even higher densities have been reported for accreting TTS; see Sect. 3.2).
– For evolved active binaries (RS CVn binaries, contact binaries), both density ranges are relevant.

Higher-Z triplets are more difficult to interpret, in particular because the range of sensitivity shifts to higher density values that may exceed coronal values. These triplets are also subject to more problematic blending, which is in particular true for the Ne IX triplet that suffers from extensive blending by line of Fe, specifically Fe XIX (Ness et al. 2003a). Mewe et al. (2001) found $n_e > 3 \times 10^{12}$ cm^{-3} for Capella from an analysis of Mg XI and Si XIII, but the results disagree with measurements using lines of Fe XX–XXII (Mewe et al. 2001). Similarly, Osten et al. (2003), Argiroffi et al. (2003), and Maggio et al. (2004) found sharply increasing densities moving from cooler to hotter plasma, with densities reaching up to order 10^{12} cm^{-3}. But the trend reported by Osten et al. (2003) is contradicted by the analysis of Si XIII that indicates $n_e < 10^{11}$ cm^{-3} despite its similar formation temperature as Mg XI. The high-density results have been questioned altogether from detailed analyses of the Capella and II Peg spectra, for which upper limits to electron densities have been derived from Ne, Mg, and Si triplets (Canizares et al. 2000; Ayres et al. 2001a; Huenemoerder et al. 2001; Phillips et al. 2001).

The most detailed analyses of the higher-Z triplets are those by Ness et al. (2004) and Testa et al. (2004a). Ne IX density measurements are typically higher than those using O VII, covering the range of $\log n_e = 11 - 12$ despite the significant temperature overlap between the two ions (Ness et al. 2004). Unrecognized blends in the Ne IX triplet may still be problematic. Mg XI and Si XIII systematically yield even higher densities for various types of active stars. Testa et al. (2004a) report Mg-derived densities of a few times 10^{12} cm^{-3}, with a trend for stars with higher L_X/L_{bol} to show higher densities, a trend paralleling suggestions from O VII (see above) albeit for much higher densities. The situation is less clear for Si XIII as most measured f/i flux ratios *exceed* the theoretical upper limit.

Coronal densities from Fe lines Many transitions of Fe ions are sensitive to density as well (Brickhouse et al. 1995). Line ratios of Fe XIX–XXII in the EUV range have frequently been used for density estimates (Dupree et al. 1993; Schrijver et al. 1995; Sanz-Forcada et al. 2002), resulting in relatively high densities in magnetically active stars. Given the formation temperatures of the respective Fe ions, reported densities in the range of 10^{12} cm^{-3}–10^{13} cm^{-3} are, however, in agreement with densities inferred from Mg XI (see above).

For inactive and intermediately active stars such as Procyon, α Cen, ϵ Eri, or ξ Boo A, much lower densities, $n_e < 10^{10}$ cm^{-3}, are inferred from lower ionization stages of Fe (e.g., Fe X–XIV; Mewe et al. 1995; Schmitt et al. 1994, 1996; Schrijver and Haisch 1996; Laming et al. 1996; Laming and Drake 1999).

A number of conflicting measurements are worthwhile to mention, however. Measurements using CHANDRA spectroscopy have shown systematic deviations from earlier EUVE measurements, perhaps due to blending affecting EUVE spectroscopy (Mewe et al. 2001). For the active Algol, Ness et al. (2002) report rather low den-

sities of $\log n_e \lesssim 11.5$ from Fe XXI. Similarly, Phillips et al. (2001) concluded that Fe XXI line ratios indicate densities below the low-density limits for the respective ratios ($\log n_e < 12$). Ayres et al. (2001b) found contradicting results from various line ratios for the giant β Cet, suggesting that densities are in fact low. Further conflicting measurements of this kind have been summarized by Testa et al. (2004a), and a systematic consideration of Fe-based density measurements was presented by Ness et al. (2004). The latter authors found that *all* Fe line ratios are above the low-density limit, but by an approximately constant factor, suggesting that all densities are compatible with the low-density limit after potential correction for systematic but unrecognized blends or inaccuracies in the atomic databases.

The present situation is certainly unsatisfactory. Contradictory measurements based on different density diagnostics or extremely (perhaps implausibly) high densities inferred from some line ratios make a reconsideration of blending and the atomic databases necessary. Bias is also introduced by high low-density limits; any deviation of flux ratios into the density-sensitive range, perhaps by slight blending, by necessity results in "high densities" while lower densities are, by definition, inaccessible.

Coronal structure from density measurements Density measurements in conjunction with emission measure analysis provide an order-of-magnitude estimate of coronal volumes V (because $EM = n_e n_H V$ for a plasma with uniform density). Taken at face value, the very high densities sometimes inferred for hot plasma require compact sources and imply small surface-filling factors. For example, Mewe et al. (2001) estimated that the hotter plasma component in Capella is confined in magnetic loops with a semi-length of only $L \lesssim 5 \times 10^7$ cm, covering a fraction of $f \approx 10^{-6}$–10^{-4} of the total surface area. Confinement of such high-pressure plasma would then require coronal magnetic field strengths of order 1 kG (Brickhouse and Dupree 1998). In that case, the typical magnetic dissipation time is only a few seconds for $n_e \approx 10^{13}$ cm^{-3} if the energy is derived from the same magnetic fields, suggesting that the small, bright loops light up only briefly. In other words, the stellar corona would be made up of numerous ephemeral loop sources that cannot be treated as being in quasi-static equilibrium (van den Oord et al. 1997).

Both Ness et al. (2004) and Testa et al. (2004a) calculated coronal *filling factors* f for plasma emitting various He-like triplets. The total "available" volume, V_{avail}, for coronal loops of a given temperature depends on a corresponding "characteristic height" for which the height of a hydrostatic loop (Eq. 10) can be assumed. The volume-filling factor thus derived, V/V_{avail}, is surprisingly small for cool plasma detected in O VII and Ne IX, namely of order a few percent and increasing with increasing activity level. The emission supposedly originates in solar-like active regions that cover part of the surface, but never entirely fill the available volume. With increasing magnetic activity, a hotter component appears (recall the general correlation between average coronal temperature and activity level, Sect. 2.1). This component seems to fill in the volume between the cooler active regions and contributes the bulk part of the emission measure in very active stars although the high densities suggest very small loop structures and filling factors ($L \lesssim 10^{-2}\ R_*$ resp. $f \ll 1\%$ for AD Leo; Maggio et al. 2004). Hotter plasma could thus be a natural result of increased flaring in the interaction zones between cooler regions. This provides support for *flare-induced* coronal

heating in particular in magnetically active stars. The higher densities in the hotter plasma components are then also naturally explained as a consequence of flaring (see Sect. 2.4.5). Explicit support for this picture comes from f/i ratios in the active M dwarf AD Leo that vary between observations separated by more than a year, higher densities being inferred for the more active states; the overall flaring contribution may have changed between the two epochs, although a different configuration of active regions with different average electron densities cannot be excluded (Maggio and Ness 2005).

At this point, a word of caution is in order. There is no doubt (cf. the solar corona!) that coronal plasma comes in various structures covering a wide range of densities. Because the emissivity of a coronal plasma scales with n_e^2, any X-ray observation is biased toward detections of structures at high densities (and sufficiently large volumes). The observed f/i line flux ratios may therefore be a consequence of the *density distribution* and may not represent any existing, let alone dominant, electron density in the corona. Rather, they are dependent on the steepness of the density distribution, but because of the n_e^2 dependence, they do not even correspond to a linear average of the f/i ratio across all coronal volume elements. A calculated example is given in Güdel (2004).

2.3.4 Inferences from coronal opacities

Emission lines in coronal spectra may be suppressed by optical depth effects due to resonance scattering in the corona. This effect was discussed in the context of "anomalously faint" EUV lines (Schrijver et al. 1994, 1995), now mostly recognized to be a consequence of sub-solar element abundances. Resonance scattering requires optical depths in the line centers of $\tau \gtrsim 1$, and τ is essentially proportional to $n_e \ell / T^{1/2}$ (Mewe et al. 1995) where ℓ is the path length. For static coronal loops, this implies $\tau \propto T^{3/2}$ (Schrijver et al. 1994; e.g., along a loop or for a sample of nested loops in a coronal volume).

Optical depth effects due to scattering are marginal in stellar coronae; initial attempts to identify scattering losses in the Fe XVII λ15.01 were negative (Ness et al. 2001; Mewe et al. 2001; Phillips et al. 2001; Huenemoerder et al. 2001; Ness et al. 2002; Audard et al. 2003), regardless of the magnetic activity level of the considered stars. Larger survey work by Ness et al. (2003b) again reported no significant optical depth for strong Fe XVII lines and for f/r ratios in He-like triplets, after carefully correcting for effects due to line blending. Although Fe XVII line ratios, taken at face value, do suggest the presence of line opacities, the deviations turned out to be similar for *all* stars, suggesting absence of line scattering while the deviations should be ascribed to systematic problems in the atomic physics databases. Similar conclusions were reached in the work by Huenemoerder et al. (2001) and Osten et al. (2003) using the Lyman series for O VIII, Ne X, or Si XIV.

More recent survey work by Testa et al. (2004b, 2007) supports the above overall findings although significant (at the 4–5σ level) optical depths were reported for two RS CVn-type binaries and one active M dwarf based on Lyα/Lyβ line-flux ratios of O VIII and Ne X. Moreover, the optical depth was found to be variable in one of the binaries. The path length was estimated at $\ell \approx 2 \times 10^{-4} R_* – 4 \times 10^{-2} R_*$, with

very small corresponding surface-filling factors, $f \approx 3 \times 10^{-4}$–$2 \times 10^{-2}$. Although rather small, these scattering source sizes exceed the heights of corresponding hydrostatic loops estimated from measured densities and temperatures. Alternatively, active regions predominantly located close to the stellar limb may produce an effective, non-zero optical depth as well.

We note here that upper limits to optical depth by resonance scattering were also used to assess upper limits to source sizes based on simple escape probability estimates (e.g., Phillips et al. 2001; Mewe et al. 2001), but caution that, as detailed by Testa et al. (2007), due to potential scattering of photons *into* the line of sight these estimates in fact provide upper limits to lower limits, i.e., no constraint. We should also emphasize that the absence of optical depth effects due to resonance scattering does not imply the absence of scattering in individual stellar active regions. The question is simply whether there is a net loss or gain of scattered photons along the line of sight, and for most coronal sources such an effect is not present for the (disk-integrated) emission.

2.3.5 Summary: trends and limitations

Despite a panoply of methods and numerous observed examples, it appears difficult to conclude on how stellar coronae are structured. There is mixed evidence for compact coronae, coronae predominantly located at the pole but also distributed coronae covering lower latitudes. Filling factors appear to be surprisingly small even in saturated stars, as derived from rotational modulation but also from spectroscopic modeling, in particular based on measurements that indicate very high densities. Larger structures may be inferred from X-ray flares (see Güdel 2004 for a summary).

We should however keep in mind that strong bias is expected from X-ray observations. There is little doubt—judging from the solar example—that coronae are considerably structured and come in packets with largely differing temperatures, size scales, and densities. Because the X-ray emissivity of a piece of volume scales with n_e^2, the observed X-ray light is inevitably dominated by dense regions that occupy sufficiently large volumes. Regions of very low density may remain undetected despite large volumes (as an example we mention the solar wind!).

Keeping with our definition of coronae as the ensemble of closed stellar magnetic fields containing heated gas and plasma or accelerated, high-energy particles, X-ray observations miss those portions of the corona into which hot plasma has not been evaporated, and it is likely to miss very extended structures. The latter are favorable places for high-energy electrons, and radio interferometry has indeed shown extended radio coronae reaching out to several stellar radii (e.g., Mutel et al. 1985).

2.4 X-ray flares

2.4.1 Introduction

A flare is a manifestation of a sudden release of magnetic energy in the solar or in a stellar corona. Observationally, flares reveal themselves across the electromagnetic spectrum, usually sowing a relatively rapid (minutes to hours) increase of radiation up

to the "flare peak" that may occur at somewhat different times in different wavelength bands, followed by a more gradual decay (lasting up to several hours). Solar X-ray flare classification schemes (Pallavicini et al. 1977) distinguish between *compact* flares in which a small number of magnetic loops lighten up on time scales of minutes, and *long-duration* (also "2-Ribbon") flares evolving on time scales of up to several hours. The latter class involves complex loop arcades anchored in two roughly parallel chromospheric Hα ribbons. These ribbons define the footpoint regions of the loop arcade. Such flares are energized by continuous reconnection of initially open magnetic fields above a neutral line at progressively larger heights, so that nested magnetic "loops" lighten up sequentially, and possibly also at different times along the entire arcade. The largest solar flares are usually of this type.

Transferring solar flare classification schemes to the stellar case is problematic; most stellar flares reported in the literature reveal extreme luminosities and radiative energies, some exceeding even the largest solar flares by several orders of magnitude. This suggests, together with the often reported time scales in excess of 1 h, that most stellar flares interpreted in the literature belong to the class of "2-Ribbon" or arcade flares involving considerable magnetic complexity. We caution, however, that additional flare types not known on the Sun may exist, such as flares in magnetic fields connecting the components of close binary systems, flares occurring in dense magnetic fields concentrated at the stellar poles, reconnection events on a global scale in large stellar "magnetospheres", or flares occurring in magnetic fields connecting a young star and its circumstellar disk.

In a standard model developed for solar flares, a flare event begins with a magnetic instability that eventually leads to magnetic reconnection in tangled magnetic fields in the corona. In the reconnection region, heating, particle acceleration, and some bulk mass acceleration takes place. The energized particles (e.g., electrons) travel along closed magnetic fields toward the stellar surface; as they reach denser layers in the chromosphere, they deposit their energy by collisions, heating the ambient plasma explosively to millions of K. The ensuing overpressure drives the hot plasma into coronal loops, at which point the "X-ray flare" becomes manifest.

Clearly, understanding the physical processes that lead to a flare, and in particular interpreting the microphysics of plasma heating, is mostly a task for the solar coronal physics domain. Nevertheless, stellar flare observations have largely extended the parameter range of flares, have added new features not seen in solar flares, and have helped understand the structure of stellar magnetic fields in various systems. Most of the information required for an interpretation of coronal flares is extracted from "light curve analysis", most importantly including the evolution of the characteristic temperatures that relate to heating and cooling processes in the plasma. A summary of the methodology has been given in Güdel (2004) and will not be addressed further here. High-resolution spectroscopy, ideally obtained in a time-resolved manner, adds important information on stellar flares; specifically, it provides information for which spatially resolved imaging would otherwise be needed (as in the solar case), namely clues on densities in the flaring hot plasma, opacities, and signatures of fluorescence that all provide information on the size of flaring regions. Furthermore, line shifts may be sufficiently large to measure plasma flows in flares.

2.4.2 An overview of stellar flares

A vast amount of literature on flares is available from the past three decades of stellar X-ray astronomy. A collection of results from flare interpretation studies until 2004 is given in tabular form in Güdel (2004). Here, we summarize the basic findings.

Increased temperatures during flares are a consequence of efficient heating mechanisms. Spectral observations of large stellar flares have consistently shown electron temperatures up to 100 MK, in some cases even more (Tsuboi et al. 1998; Favata and Schmitt 1999; Osten et al. 2005, 2007), much beyond typical solar-flare peak temperatures (20–30 MK). Somewhat unexpectedly, the flare peak temperature, T_p, correlates with the peak emission measure, $\mathrm{EM_p}$ (or, by implication, the peak X-ray luminosity), roughly as

$$\mathrm{EM_p} \propto T_\mathrm{p}^{4.30\pm0.35} \tag{12}$$

(Güdel 2004) although observational bias may influence the precise power-law index. For solar flares, a similar trend holds with a normalization (EM) offset between solar and stellar flares—again perhaps involving observational bias (Aschwanden et al. 2008; Fig. 5). The $\mathrm{EM_p}$–T_p relation was interpreted based on MHD flare modeling (Shibata and Yokoyama 1999, 2002), with the result that larger flares require larger flaring sources (of order 10^{11} cm for the most active stars) while magnetic field strengths ($B \approx 10$–150 G) should be comparable to solar flare values.

Following the standard flare scenario exposed above, we should expect that a flare reveals itself first in the radio regime through gyrosynchrotron emission from the injected, accelerated electron population, and also in the optical/UV as a result of prompt emission from the heated chromospheric region at the loop footpoints. Further, as the electrons impact on the denser layers, they promptly emit non-thermal hard X-rays (HXR, >10 keV) that have indeed been of prime interest in solar flare research. These initial emission bursts characterize and define the *impulsive phase* of the flare during which the principal energy is released. The more extended phase of energy conversion, mass motion, and plasma cooling characterizes the *gradual phase*. In particular, soft X-ray emission is a consequence of plasma accumulation in the coronal loops, which roughly increases with the integral of the deposited energy.[2] A rough correlation is therefore expected between the time behavior of the radio, optical/UV, and hard X-rays on the one hand and soft X-rays on the other hand, such that the former bursts resemble the time derivative of the increasing soft X-ray light curve, $L_\mathrm{R,O,UV,HXR}(t) \propto \mathrm{d}L_\mathrm{X}(t)/\mathrm{d}t$, a relation known as the "Neupert Effect" (after Neupert 1968).

The Neupert effect has been observed in several stellar flares (e.g., Hawley et al. 1995; Güdel et al. 2002; Osten et al. 2004, 2007; Smith et al. 2005; Mitra-Kraev et al. 2005; see Fig. 8 in Sect. 2.4.5 below), in cases with emission characteristics very

[2] Schmitt et al. (2008) report the case of a strong flare on the M dwarf CN Leo in which an initial thermal soft-Xray pulse was observed on time scales of a few seconds during the impulsive flare phase, coincident with the optical flare peak. This radiation may originate from the initial plasma heating at the bottom of the magnetic loops, at a time when evaporation only starts to fill the loops.

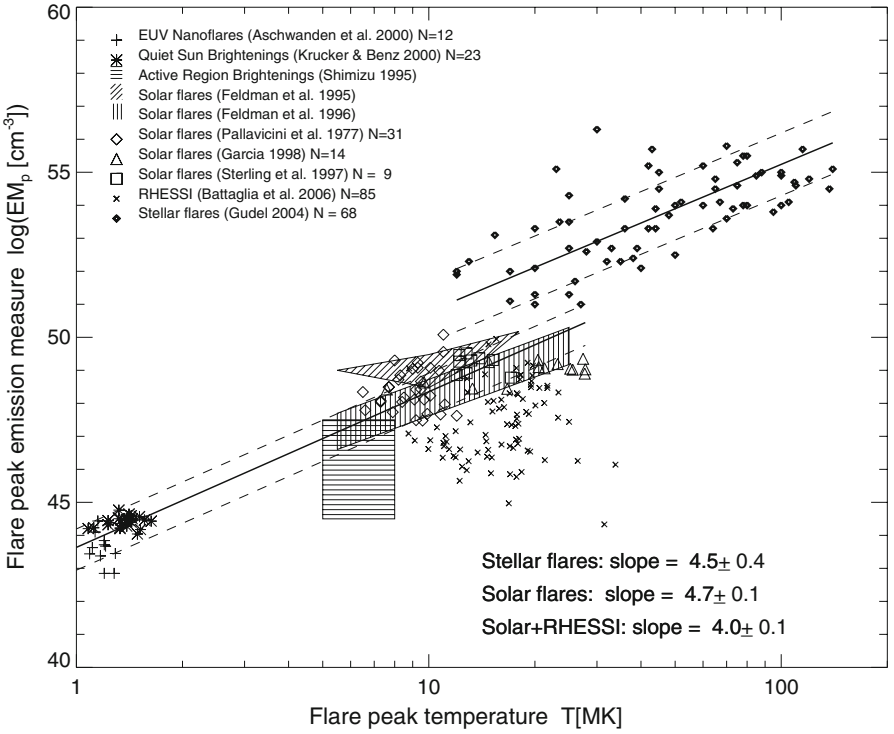

Fig. 5 Flare peak emission measure as a function of flare peak temperature for solar and stellar flares. Note the similar trends for solar and stellar flares although there is an offset between the regression lines (from Aschwanden et al. 2008, reproduced by permission of the AAS)

similar to the standard case of solar flares. Such observations testify to the chromospheric evaporation scenario in many classes of stars. Equally important is the lack of correlated behavior—also observed in an appreciable fraction of solar flares—which provides important clues about "non-standard" behavior. Examples of X-ray flares without accompanying radio bursts or radio bursts peaking at the time of the X-rays or later were presented by Smith et al. (2005). In a most outstanding case, described by Osten et al. (2005), a sequence of very strong X-ray, optical, and radio flares occurring on an M dwarf show a complete breakdown of correlated behavior. While the presence of X-ray flares without accompanying signatures of high-energy electrons can reasonably be understood (e.g., due to flares occurring in high-density environments in which most of the energy is channeled into direct heating), the reverse case, radio and correlated U-band flares without any indication of coronal heating, is rather puzzling; this is especially true given that the non-thermal energy must eventually thermalize, and the thermal plasma is located close to or between the non-thermal coronal radio source and the footpoint U-band source. Possible explanations include an unusually low-density environment, or heating occurring in the lower chromosphere or photosphere after deep penetration of the accelerated electrons without appreciable

evaporation at coronal temperatures (Osten et al. 2005), but a full understanding of the energy transformation in such flares is still missing.

Last, we mention the fundamental role that flares may play in the heating of entire stellar coronae. The suggestion that stochastically occurring flares may be largely responsible for coronal heating is known as the "microflare" or "nanoflare" hypothesis in solar physics (Parker 1988). Observationally, solar flares are distributed in energy following a power law, $\mathrm{d}N/\mathrm{d}E = kE^{-\alpha}$ where $\mathrm{d}N$ is the number of flares per unit time with a total energy in the interval $[E, E + \mathrm{d}E]$, and k is a constant. If $\alpha \geq 2$, then the energy integration (for a given time interval) diverges for $E_{\min} \rightarrow 0$, i.e., a lower energy cutoff is required, and depending on its value, an arbitrarily large amount of energy could be related to flares. Solar studies indicate α values of 1.6–1.8 for ordinary solar flares (Crosby et al. 1993), but some recent studies of low-level flaring suggest $\alpha = 2.0$–2.6 (Krucker and Benz 1998; Parnell and Jupp 2000). Stellar studies have provided interesting evidence for $\alpha > 2$ as well, for various classes of stars including TTS and G–M-type dwarf stars (Audard et al. 2000; Kashyap et al. 2002; Güdel et al. 2003; Stelzer et al. 2007; Wargelin et al. 2008). There is considerable further evidence that flares contribute fundamentally to coronal heating, such as correlations between average X-ray emission on the one hand and the observed (optical or X-ray) flare rate or UV emission on the other hand. Continuous flaring activity in light curves, in some cases with little evidence for a residual, truly constant baseline level, add to the picture. Evidence reported in the literature has been more comprehensively summarized in Güdel (2004).

2.4.3 Non-thermal hard X-ray flares?

The X-ray spectrum of solar flares beyond approximately 15–20 keV is dominated by *non-thermal* hard X-rays. These photons are emitted when a non-thermal, high-energy population of electrons initially accelerated in the coronal reconnection region collides in the denser chromosphere and produce "thick-target" bremsstrahlung. The spectrum is typically a power law, pointing to a power-law distribution of the accelerated electrons (Brown 1971). Detection of such emission in magnetically active stars would be of utmost importance as it would provide information on the energetics of the initial energy release, the particle acceleration process in magnetic field configurations different from the solar case, the relative importance of particle acceleration and direct coronal heating, and possibly travel times and therefore information on the size of flaring structures. The presence of high-energy electron populations is not in doubt: they are regularly detected from their non-thermal gyrosynchrotron radiation at radio wavelengths.

Detection of non-thermal hard X-rays is hampered by the low expected fluxes, but also by the trend that large flares produce very hot plasma components that dominate the bremsstrahlung spectrum up to very high photon energies (Eq. 12). This latter effect has clearly been demonstrated in observations successfully recording X-ray photons up to about 100 keV from large stellar flares (Favata and Schmitt 1999; Rodonò et al. 1999; Franciosini et al. 2001), the extended X-ray spectrum being compatible with an extrapolation of the thermal soft X-ray spectrum. The most promising case has been reported from a very large flare occurring on the RS CVn binary II Peg in which

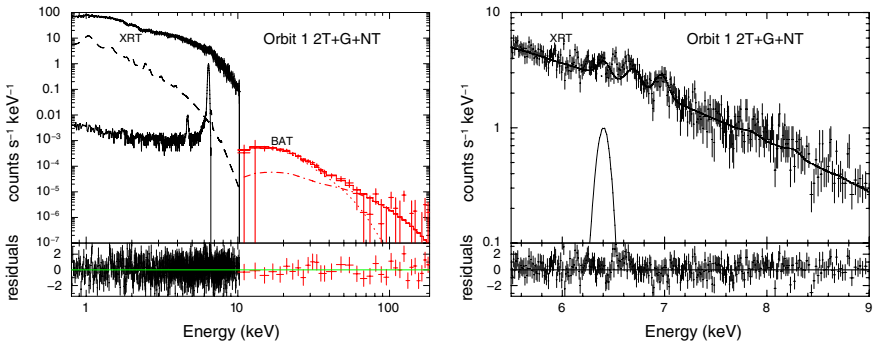

Fig. 6 **a** The observed spectrum of a large flare on the RS CVn binary II Peg is shown with a spectral fit (consisting of two thermal components, a Gaussian for the 6.4 keV Fe Kα line, and a power law for the highest energies). The spectrum was obtained by different detectors (above and below $\approx$10 keV). The individual contributions by the model components are shown *dashed* and *dotted*, or by a *thin solid line* (6.4 keV feature). Fit residuals are shown in the *bottom panel*. **b** Extract from **a**, showing the region around the 6.4 keV Kα feature and the 6.7 keV Fe XXV complex (from Osten et al. 2007, reproduced by permission of the AAS)

activity was recorded up to 100 keV during the entire flare episode (Osten et al. 2007; Fig. 6). Although the spectrum could be interpreted with bremsstrahlung from a very hot, $\approx$300 MK component, Osten et al. (2007) favored a non-thermal interpretation, arguing that conductive losses would be excessive for a thermal component; also, the concurrent Fe Kα 6.4 keV emission recorded during the flare may be the result from non-thermal electron impact ionization rather than from photoionization fluorescence (Sect. 2.4.4), given the high hydrogen column densities required. However, while suggestive, these arguments remain somewhat inconclusive; first, conductive losses across extreme temperature gradients cannot exceed the free-streaming electron limit at which conduction saturates. Second, the hard component persists into the flare decay phase, at high levels, unlike in solar flares. And third, recent detailed fluorescence calculations suggest that the observed Fe Kα feature can in fact be explained as arising from photoionization, while the impact ionization mechanism is inefficient (Drake et al. 2008b; Ercolano et al. 2008; Testa et al. 2008a). Unequivocal detection of non-thermal hard X-rays from stellar coronae remains an important goal, in particular for future detectors providing high sensitivity and low background up to at least 100 keV.

2.4.4 Fluorescence and resonance scattering during stellar flares

Photoionization of cool material by X-ray photons above the Fe K edge at 7.11 keV produces a prominent line feature at 6.4 keV (Fe Kα feature; see Sect. 3.9 for further details). This feature is usually too faint to be detected in any stellar X-ray spectrum; exceptions include a few TTS for which fluorescence on the circumstellar disk due to irradiation by stellar X-rays has been proposed (Sect. 3.9). In more evolved stars, 6.4 keV Kα emission would originate from the stellar *photosphere* but has so far been detected in only two cases. Prominent Fe Kα emission was recorded from a giant flare

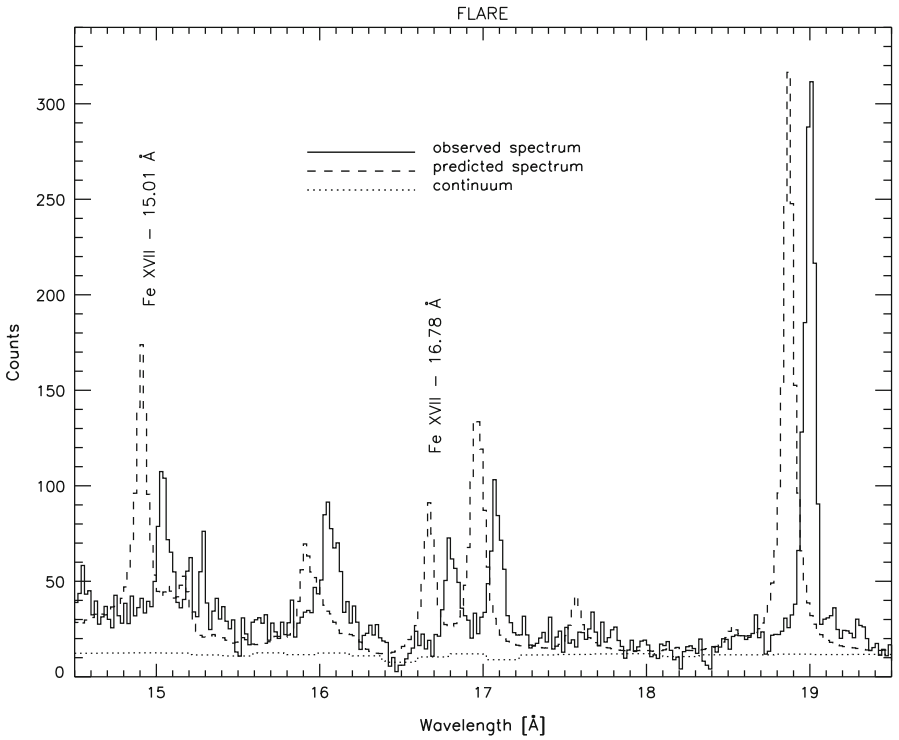

Fig. 7 Evidence for optical depth effects due to resonance scattering. The *plot* shows the observed spectrum (*solid*), the predicted spectrum (*dashed*, slightly shifted in wavelength for clarity), and the continuum (*dotted*). Although there are discrepancies for several lines, the model overprediction of the 15.01 Å line is significantly larger than during quiescence (from Matranga et al. 2005, reproduced by permission of the AAS)

on the RS CVn binary II Peg (Osten et al. 2007; Fig. 6b) although a model based on electron impact ionization was put forward as discussed earlier (Sect. 2.4.3). More recently, Testa et al. (2008a) presented evidence for photospheric fluorescence in the single G-type giant HR 9024, using detailed fluorescence calculations to estimate a source height of $\lesssim 0.3 R_*$ ($R_* = 13.6 R_\odot$).

Resonance scattering (Sect. 2.3.4) is another potential method to measure the size of flaring coronal structures. A suppression of the strong Fe XVII λ15.01 line compared to the Fe XVII λ16.78 line was recorded during a flare on AB Dor (Fig. 7) and interpreted in terms of an optical depth of 0.4 in the line center, implying a path length of order 8,000 km (Matranga et al. 2005).

2.4.5 Flare densities: evidence for evaporation

According to the standard flare scenario, densities in flaring loops should largely increase as a consequence of chromospheric evaporation. This is the essential cause of the large emission measure increase in the flaring corona. Spectroscopic density

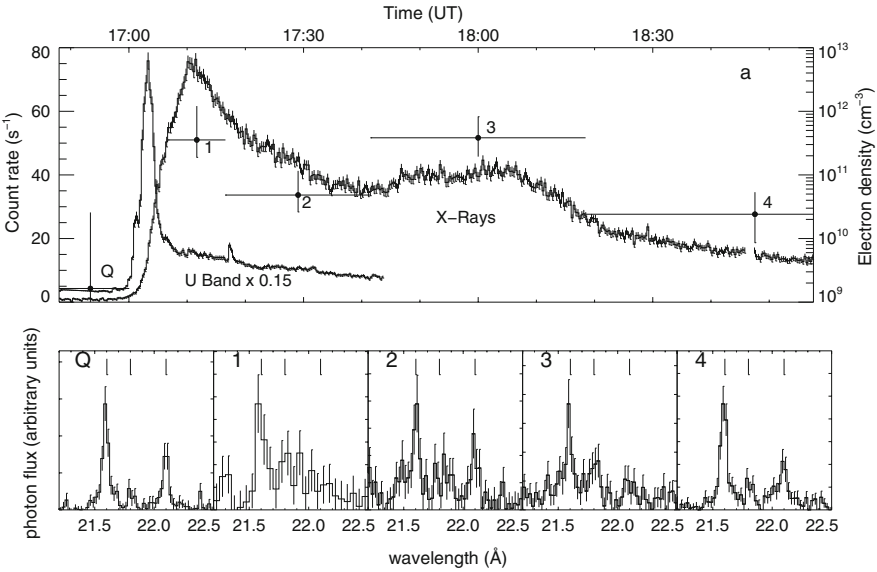

Fig. 8 Evolution of a large flare on Proxima Centauri. The *upper panel* shows the X-ray light curve together with the short pulse in the U band peaking at about 17:05 UT. The *large crosses* show electron densities during the intervals defined by the horizontal arms, derived from the O VII line triplet fluxes (the density scale is given on the right y-axis). The triplets for the five intervals are shown in the *bottom panel*, marked "Q" for quiescence and "1"–"4" for the four flare episodes. The three *marks* in the upper parts of the figures show the locations of the resonance, intercombination, and forbidden lines (from *left* to *right*) (adapted from Güdel et al. 2002)

measurements in *solar* flares using He-like triplets (Sect. 2.3.3) confirm this picture, suggesting density increases to several times 10^{12} cm^{-3} (McKenzie et al. 1980; Doschek et al. 1981; Phillips et al. 1996; Landi et al. 2003).

Stellar evidence is still limited given the high signal-to-noise ratio required for short observing intervals. First significant spectral evidence for strong density increases were reported for a large flare on Proxima Centauri (Güdel et al. 2002, 2004), both for the O VII and (more tentatively) for the Ne IX triplet. The forbidden line in the O VII triplet nearly disappeared during the flare peaks, while a strong intercombination line showed up (Fig. 8). The derived densities rapidly increased from a pre-flare level of $n_e < 10^{10}$ to $\approx 4 \times 10^{11}$ cm^{-3} at flare peak, then again rapidly decayed to $\approx 2 \times 10^{10}$ cm^{-3}, to increase again during a secondary peak, followed by a gradual decay. The instantaneous mass involved in the cool, O VII emitting source was estimated at $\approx 10^{15}$ g, suggesting similar (instantaneous) potential and thermal energies in the cool plasma, both of which are much smaller than the total radiated X-ray energy. It is therefore probable that the cool plasma is continuously replenished by the large amount of material that is initially heated to higher temperatures and subsequently cools to O VII forming temperatures and below. The measured densities agree well with estimates from hydrodynamic simulations (Reale et al. 2004) and, together with light curve analysis, provide convincing evidence for the operation of chromospheric evaporation in stellar flares.

Marginal signatures of increased densities during flares have been suggested from He-like triplet flux ratios for several further stars, in particular for YY Gem (Stelzer et al. 2002), σ^2 CrB (Osten et al. 2003), AD Leo (van den Besselaar et al. 2003), AT Mic (Raassen et al. 2003a), AU Mic (Magee et al. 2003), and CN Leo (Fuhrmeister et al. 2007).

2.5 The composition of stellar coronae

2.5.1 The FIP and IFIP effects

Studies of element abundances in stars are of fundamental interest as they contribute to our understanding of galactic chemistry and its evolution as well as to refined models of stellar interiors. The composition of material available in young stellar environments is of course also relevant for the planet-formation process.

The composition of stellar material could change as it is driven from the surface into the corona or the stellar wind, owing to various fractionation processes. Specifically, elements with a low first ionization potential ("low-FIP" elements Mg, Si, Ca, Fe, Ni) are predominantly ionized at chromospheric levels, while high-FIP elements (C, N, O, Ne, Ar, and marginally also S) are predominantly neutral. Ions and neutrals could then be affected differently by electric and magnetic fields.

It is well known that the composition of the solar corona and the solar wind is indeed at variance with the photospheric mixture; low-FIP elements are enhanced in the corona and the wind by factors of a few, whereas high-FIP elements show photospheric abundances (this is the essence of the "FIP effect"; Feldman 1992). There are considerable variations between different solar coronal features, e.g., active regions, quiet-Sun regions, old magnetic loop systems, or flares. A discussion of the physics involved in this fractionation is beyond the scope of this review, and in fact a universally accepted model does not yet exist; see, e.g., Hénoux (1995) and Drake (2003a) for a few selected model considerations.

Although a solar-like FIP effect could be identified in a couple of nearby stars based on EUVE observations (Laming et al. 1996; Laming and Drake 1999; Drake et al. 1997), early observations of magnetically active stars started painting a different, and confusing, picture when abundances were compared with standard solar photospheric abundances (assumed to be similar to the respective stellar composition). In many low-resolution spectra, unusually weak line complexes required significantly subsolar abundances (e.g., White et al. 1994; Antunes et al. 1994; Gotthelf et al. 1994 and many others) also confirmed by EUVE observations (e.g., Stern et al. 1995).

A proper derivation of abundances requires well-measured fluxes of lines from different elements, and this derivation is obviously tangled with the determination of the emission measure distribution. It is therefore little surprising that at least partial clarification came only with the introduction of high-resolution X-ray spectroscopy from XMM-*Newton* and CHANDRA. High-resolution X-ray spectra of magnetically active stars revealed a new trend that runs opposite to the solar FIP effect and that has become known as the "inverse FIP (IFIP) effect". Coronae expressing an IFIP effect show low-FIP abundances systematically depleted with respect to high-FIP elements

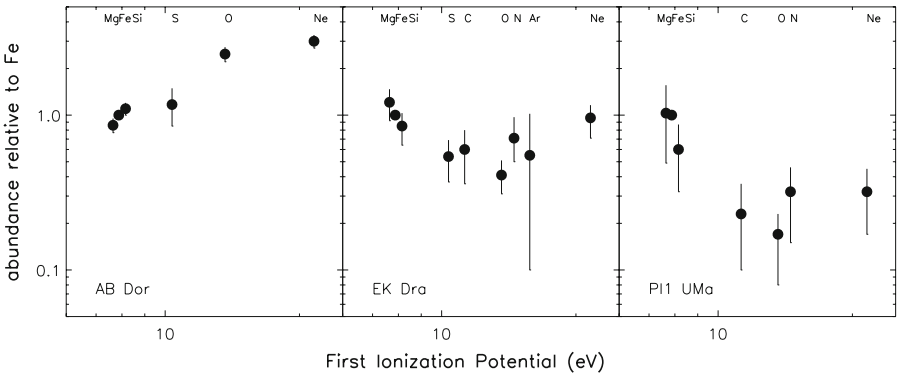

Fig. 9 Coronal abundances as a function of FIP, normalized to the coronal abundance of Fe. **a** AB Dor, an example for an inverse-FIP effect (data from García-Alvarez et al. 2005). **b** EK Dra, an intermediate case, showing increasing abundances toward the lowest and highest FIP (data from Telleschi et al. 2005). **c** π^1 UMa, an intermediately active star showing a solar-like FIP effect (data from Telleschi et al. 2005)

(Brinkman et al. 2001; see example in Fig. 9). As a consequence of this anomaly, the ratio between the abundances of Ne (highest FIP) and Fe (low FIP) is unusually large, of order 10 in some cases, compared to solar photospheric conditions (see also Drake et al. 2001; Audard et al. 2001). The IFIP effect has been widely confirmed for many active stars or binaries (e.g., Huenemoerder et al. 2001, 2003; García-Alvarez et al. 2005). With respect to the hydrogen abundance, most elements in active stars remain, however, depleted.

The FIP and IFIP effects in fact represent only two extremes in a bigger picture related to coronal evolution. With decreasing activity (e.g., as parameterized by the L_X/L_{bol} ratio, or the average coronal temperature), the IFIP effect weakens until the abundance distribution becomes flat (Audard et al. 2003; Ball et al. 2005), and eventually turns into solar-like FIP trend for less active stars with $\log L_X/L_{bol} \lesssim -4$ or an average coronal temperature $\lesssim$7–10 MK (Telleschi et al. 2005; Güdel 2004; Fig. 9). At this critical activity level, we also observe that the dominant, very hot plasma component disappears. This trend is best seen in the Ne/Fe abundance ratio (high-FIP vs. low-FIP) that decreases by an order of magnitude from the most active to the least active coronae (Fig. 10a). On the high-activity side, the trends continue into the "supersaturation regime" (Sect. 2.1) of the fastest rotators, where L_X/L_{bol} converges to $\approx 10^{-3}$ and becomes unrelated to rotation; for these stars, the Fe abundance continues to drop sharply, while the O abundance continues to increase, possibly reaching a saturation level for the most active stars (García-Alvarez et al. 2008).

While these trends have been well studied in main-sequence stars and subgiant RS CVn binaries, similar trends apply to giant stars. A FIP effect is seen in giants evolving through the Hertzsprung gap and into the red giant phase (García-Alvarez et al. 2006), a transformation during which stars develop a deep convection zone anew, regenerate magnetic activity and become subject to rapid braking. In contrast, strong enhancements of Ne but low abundances of low-FIP elements characterize the class of extremely active, rapidly rotating FK Com-type giants and active giants in tidally locked binaries (Gondoin et al. 2002; Gondoin 2003; Audard et al. 2004).

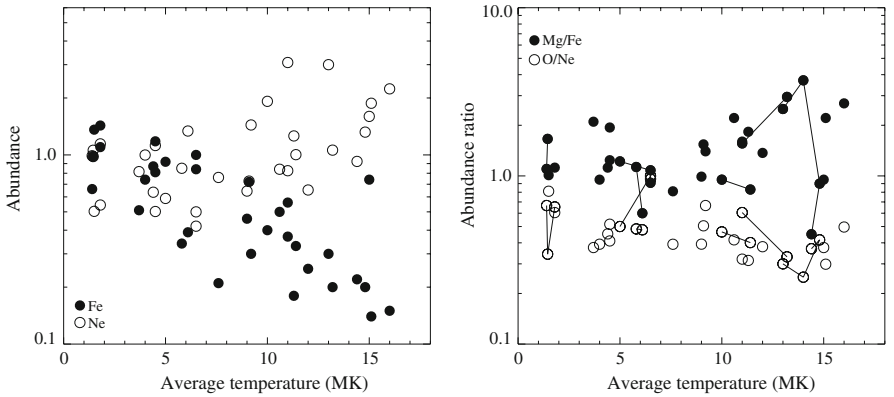

Fig. 10 **a** Abundances of Fe and Ne, normalized to the solar photospheric values, for a sample of stars at different activity levels as characterized by the average coronal temperature. **b** Abundance ratios of Me/Fe (both low-FIP elements) and O/Ne (both high-FIP elements), with respect to the solar photospheric mixture. *Lines* connect different measurements for the same star (from Güdel 2004)

Furthermore, the strength of the IFIP effect is also a function of the spectral type or $T_{\rm eff}$ of the star. As noted by Telleschi et al. (2007b) based on studies of high-resolution X-ray spectra, the IFIP trend is much more pronounced in active K and M type stars than in G stars, the Fe/O and Fe/Ne abundance ratios indicating much stronger depletion of Fe in later-type active stars. This trend is evident for young main-sequence stars and also for TTS regardless of whether they are accreting or not. For TTS, the spectral-type dependent strength of the IFIP effect has been confirmed from low-resolution spectroscopy (Scelsi et al. 2007).

Variations of these general abundance features have been noted. In some cases, the lowest-FIP elements (such as Al, Na, and Ca, sometimes others) seem to show abundances in excess of the IFIP trend in active stars, resulting in an abundance distribution with a minimum around FIP $\approx$10 eV and increasing trends to both lower and higher FIP (Sanz-Forcada et al. 2003; Argiroffi et al. 2004; Scelsi et al. 2005; Maggio et al. 2007; see Fig. 9). Some of these element abundances are extremely difficult to assess, and conflicting results have been reported (see, e.g., García-Alvarez et al. 2005).

Caution must be applied when interpreting stellar coronal abundances as derived from high-resolution spectra. First, as we know from the Sun, coronal abundances vary from region to region, and they also evolve in time. A stellar spectrum represents a snapshot of the integrated corona, averaging out all variations that might be present. Abundance measurements, therefore, most likely represent weighted means, and the formal uncertainties do not include the true variation in location and time. Extreme precision in the abundance tabulations may indeed be useless—the important information is in overall trends in stellar samples.

Significant differences have also been found among stars that share most of their fundamental properties; the primary of the intermediately active K star binary 70 Oph shows a distinct solar-like FIP effect, while such bias is absent in the otherwise very similar secondary (Wood and Linsky 2006). On the other hand, very similar coronal thermal and abundance properties can be found in stars with similar properties but

different evolutionary histories; examples include two rapidly rotating K stars, the younger of which (AB Dor) still keeps its primordial angular momentum while the older (V471 Tau) is subject to tidal spin-up due to a companion star (García-Alvarez et al. 2005); and finally, the post-main-sequence active binaries Algol and HR 1099 contain very similar K-type subgiants revealing very similar X-ray spectra, a similar coronal thermal structure, and similar coronal abundance patterns (except for mass-loss related abundances of C and N in Algol) despite their fundamentally different evolutionary histories (Drake 2003b).

Caution is in order also because the coronal material is processed gas from the stellar photosphere, and appropriate *stellar photospheric abundances* should therefore be taken as a reference. For most stars of interest such measurements are not available, or are difficult to obtain due to, e.g., rapid rotation. Do the FIP and IFIP trends survive once the coronal measurements are related to the *stellar* photospheric composition rather than the standard solar mixture? Some reports suggest they do not. Studies of a few individual examples with well-measured photospheric abundances (Drake et al. 1995; Raassen et al. 2002; Sanz-Forcada et al. 2004) as well as a larger sample of stars in the Orion Nebula (Maggio et al. 2007) or a sample of M dwarfs (with relatively poorly known photospheric metallicities; Robrade and Schmitt 2005) indicate that the coronal abundances reflect the photospheric mix, or at least the global photospheric metallicity, of the respective stars. However, while suggestive, these observations must be contrasted with cases for which non-photospheric coronal abundances are undisputed. Specifically, IFIP and FIP trends have been identified in nearby stars with well-measured near-solar photospheric abundances such as AB Dor or several solar analogs (Sanz-Forcada et al. 2003; Telleschi et al. 2005; García-Alvarez et al. 2005); further, the similarity of the FIP or IFIP effects in stars with similar activity levels, or the trends depending on activity would be difficult to explain as being due to the photospheric mixture. Younger (and therefore more active) stars would be expected to be more enhanced in metals, contrary to the observed trends. Also, the FIP and IFIP effects would reflect a photospheric anomaly of apparently most stars when compared with the Sun. But it is the Sun itself that proves otherwise: the solar FIP effect is a true coronal property, suggesting that equivalent trends observed in stars are, by analogy, coronal in origin as well. Solar and stellar flares in which abundances change systematically compared to quiescence support this picture further, suggesting genuine FIP-related abundance biases in stellar coronae (see Sect. 2.5.3).

Given the somewhat contradictory findings, it should then not be surprising that there is also no fully accepted physical model explaining all types of FIP bias coherently. For the normal FIP effect, solar physics has provided several valuable models. Ideas proposed specifically for the stellar case involve stratification of the atmosphere, with different scale heights for ions of different mass and charge (Mewe et al. 1997); enrichment of the coronal plasma by some type of "anomalous flares" also seen on the Sun (e.g., Ne-rich flares; Brinkman et al. 2001); electric currents that affect diffusion of low-FIP elements into the corona (Telleschi et al. 2005); or a recent model based on a resonance between chromospheric Alfvén waves and a coronal loop, explaining either a FIP or an IFIP effect (Laming 2004). Given the present uncertainties, we do not elaborate further on any of these models in the stellar context.

2.5.2 The Ne/O abundance ratio: an indicator of magnetic activity?

Not only stellar photospheric abundances remain uncertain for most stars commonly observed in X-rays, but tabulations of the solar photospheric composition themselves have seen various revisions in the recent past. The solar composition is a determining factor for the depth of the solar convective zone, and the abundances given by Grevesse and Sauval (1998), widely used in the stellar community, have led to an excellent agreement with the "standard solar model" describing the solar interior. The latest revision, correcting solar C, N, and O abundances downward (Asplund et al. 2005b), however led to serious disagreement with the observed helioseismology results (Bahcall et al. 2005). Regardless of these revisions, the absolute solar Ne/O abundance ratio remained at similar levels of 0.15–0.18.

The helioseismology problem could be solved by adopting a solar photospheric Ne abundance higher by a factor of about 3–4, or somewhat less if slight re-adjustments are also made for CNO (Antia and Basu 2005). There is freedom to do so as the photospheric Ne abundance is not really well known, given the absence of strong photospheric Ne lines in the optical spectrum.

Telleschi et al. (2005) were the first to point out that the systematically non-solar coronal Ne/O abundance ratios measured in several solar-analog stars (offset by similar factors) may call for a revision of the adopted solar photospheric Ne abundance, thus at the same time solving the solar helioseismology problem. Although X-rays measure *coronal* abundances, the derived stellar coronal Ne/O ratios indeed seem to be consistently high (by a factor of 2–3) for stars of various activity levels when compared with the adopted solar photospheric value; given that both O and Ne are high-FIP elements, the assumption here is that the coronal abundance ratio faithfully reflects the photospheric composition. This was further elaborated in detail by Drake and Testa (2005) who suggested a factor of 2.7 upward revision of the adopted solar Ne abundance. However, as part of a subsequent debate, analysis of solar active region X-ray spectra and of EUV spectra from transition-region levels (Schmelz et al. 2005; Young 2005) both reported robust Ne/O abundance ratios in agreement with the "standard" ratios, rejecting an upward correction of Ne.

A major problem may, in fact, be due to selection effects, as initially discussed by Asplund et al. (2005a). Most of the stars in the sample studied by Drake and Testa (2005) are magnetically active stars with coronae unlike that of the Sun. The only stars considered with activity indicators L_X/L_{bol} in the solar range were subgiants or giants; in one case (Procyon) different Ne/O abundance ratios, some in agreement with the solar value, can be found in the published literature, and two further reports on α Cen and β Com suggest values close to the solar mix. Asplund et al. (2005a) therefore proposed that the Ne/O ratio is *activity dependent*, high values referring to magnetically active stars while lower, solar-like values refer to inactive, "solar-like" stars. This echoes suggestions already made by Brinkman et al. (2001) for the high Ne abundance seen in a very active RS CVn-type binary to be possibly due to flaring activity. The dependence of the Ne/O abundance ratio on activity is in fact fully recovered in a statistical compilation presented in Güdel (2004) (Fig. 10b). These suggestions have, meanwhile, been confirmed from high-resolution spectroscopy of low-activity stars in the solar neighborhood (including the above objects), indicating

an abundance ratio of Ne/O $\approx 0.2 \pm 0.05$ for the Sun and weakly active stars, increasing to Ne/O ≈0.4–0.5 for magnetically active stars (Liefke and Schmitt 2006; Robrade et al. 2008).

The solar Ne/O ratio is thus in line with coronal abundances of inactive stars, i.e., the ratio is low as adopted by both the older and revised solar abundance lists. A selective increase of the solar Ne abundance to reconcile measurements of solar composition with helioseismology results seems to be ruled out. The discrepancy with the solar model may require other modifications yet to be identified.

2.5.3 Abundance changes in flares

The chromospheric evaporation scenario for flares predicts that bulk mass motions emerging from the chromosphere fill coronal loops. One would therefore anticipate that any FIP or IFIP effect becomes suppressed during large flares, as the corona is replenished with material of chromospheric/photospheric origin. This is indeed what has been derived from X-ray spectroscopy of stellar flares. Given the commonly observed IFIP trend outside flares in active stars, flares tend to enhance low-FIP elements more than high-FIP elements, with abundances eventually approaching the photospheric composition (e.g., Osten et al. 2000; Audard et al. 2001), but such FIP-related abundance changes are not always observed (Osten et al. 2003; Güdel et al. 2004; Nordon et al. 2006).

The systematics in FIP-related abundance changes in flares was clarified considerably by Nordon and Behar (2007) and Nordon and Behar (2008) who spectroscopically studied 14 flares observed with XMM-*Newton* and CHANDRA. The analysis was performed *relative* to the quiescent emission, i.e., trends are *independent of the mostly unknown photospheric abundances.* The majority of the flares indeed showed a "relative" solar-like FIP effect (with respect to quiescence), although relative IFIP effects and absence of relative changes were observed as well. The latter case can be explained by flares changing the total stellar emission measure only at high temperatures (above 10–20 MK; Fig 11), i.e., above limit of significant line formation in the 5–20 Å range. While flare-induced abundance changes may occur, they thus remain undetected as the observable lines are still generated by quiescent plasma.

More interestingly, a clear correlation is apparent between quiescent and flaring composition in the sense that quiescent coronae with a FIP effect typically show a relative IFIP bias during flares, and quiescent IFIP-biased coronae change to a FIP effect (Fig. 12). This relation leads to three significant conclusions: first, it confirms the chromospheric evaporation scenario that posits that fresh, unfractionated chromospheric/photospheric material is brought up into the corona; second, it suggests that the observed coronal (I)FIP biases are genuine and are not a consequence of the photospheric composition. And third, if active stellar coronae are generated by a large number of small-scale flares (Sect. 2.4.2), then these should enrich the corona with FIP-biased material, different from individual large flares that reveal an opposite trend.

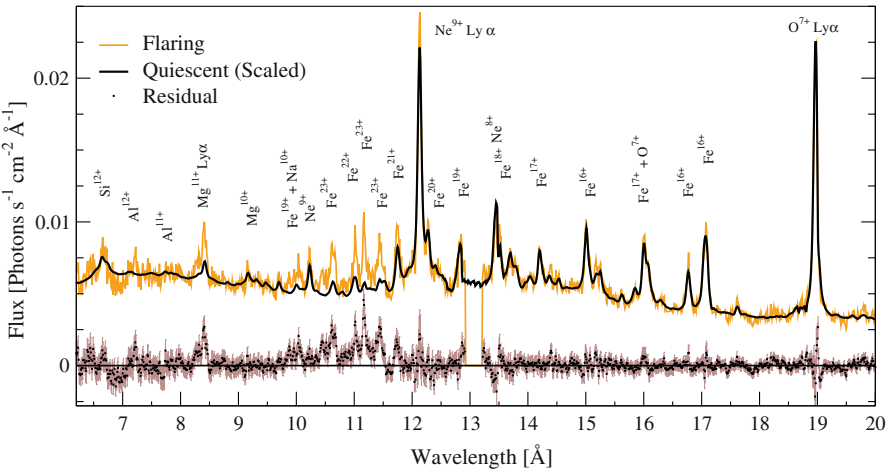

Fig. 11 Comparison of a spectrum taken during a large flare on the RS CVn-type binary σ Gem (*orange*) with a spectrum taken during the quiescent stage (*black*). An ad hoc continuum has been added to the quiescent spectrum to match the flare spectrum (because of the broad-band nature of the bremsstrahlung continuum). The lowest spectrum shows the residuals "flare-quiescent". Note that only short-wavelength lines forming at high temperatures react to the flare (from Nordon et al. 2006)

3 X-rays from young stellar objects and their environments

3.1 From protostars to T Tauri stars: coronal properties

X-ray observations of young, forming stars are ideal to address the question on the first appearance of stellar magnetic fields. It is presently unknown whether such fields would preferentially be fossil or are generated by emerging internal dynamos.

A rather comprehensive picture of the X-ray characteristics is available for the latest stages of the star formation process, the T Tauri phase when stars are essentially formed but may still be moderately accreting from a circumstellar disk. Significant information has been collected from large recent surveys conducted with XMM-*Newton* and CHANDRA (Getman et al. 2005; Güdel et al. 2007a; Sciortino 2008), but also from case studies of individual, close TTS. In short, as judged from the temperature structure, flaring behavior, or rotational modulation, X-ray emission from TTS mostly originates from magnetic coronae, with characteristics comparable to more evolved active main-sequence stars. X-rays from CTTS saturate at a level of $\log(L_X/L_{bol}) \approx -3.5$, again similar to main-sequence stars. Because for a typical pre-main sequence association L_{bol} roughly correlates with stellar mass M_*, one also finds a distinct correlation between L_X and M_*, $L_X \propto M_*^{1.7\pm0.1}$ (Telleschi et al. 2007a). Flaring is common in TTS (Stelzer et al. 2007), the most energetic examples reaching temperatures of $\approx 10^8$ K (Imanishi et al. 2001).

Our view of X-ray production in younger phases, protostars of Class I (in which most of the final mass has been accreted) and Class 0 (in which the bulk of the final mass is still to be accreted) is much less complete owing to strong X-ray attenuation by the circumstellar material. Non-thermal radio emission from Class I protostars sug-

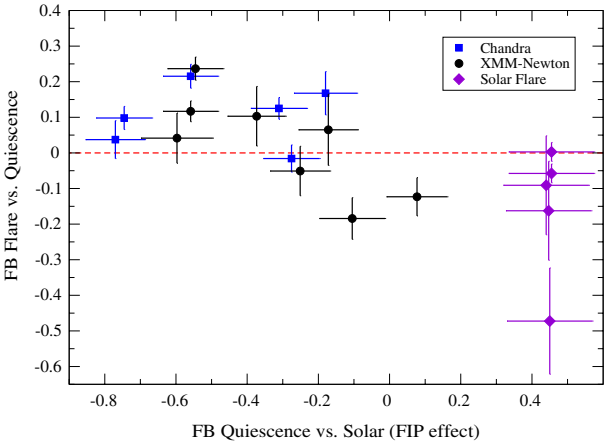

Fig. 12 The abscissa gives the logarithm of the *quiescent* abundance ratio between low-FIP elements and high-FIP elements normalized to solar photospheric values; high values indicate quiescent coronae with a solar-like FIP effect, low values coronae with an IFIP effect. The ordinate gives a similar ratio for *flares* normalized to quiescence. Here, high values indicate a *relative* FIP effect during the flare, and low values a relative IFIP effect. *Points to the right* refer to solar flares. Note the anticorrelation, indicating that flares in FIP-effect coronae show a relative IFIP effect and vice versa (from Nordon and Behar 2008)

gests the presence not only of magnetic fields but also accelerated particles in a stellar corona (e.g., Smith et al. 2003).

Class I protostars have amply been detected in X-rays by XMM-*Newton* and CHANDRA although sample statistics are biased by the X-ray attenuation, favoring detection of the most luminous and the hardest sources. Overall, X-ray characteristics are very similar to TTS, confirming that magnetic coronae are present at these earlier stages. A comprehensive study is available for stars in the Orion region (Prisinzano et al. 2008). Here, the X-ray luminosities increase from protostars to TTS by about an order of magnitude, although the situation is unknown below 1–2 keV. No significant trend is found for the electron temperatures, which are similarly high ($\approx$1–3 keV) for all detected classes. Again, flaring is common in Class I protostars (Imanishi et al. 2001).

For Class 0 objects, a few promising candidates but no definitive cases have been identified (e.g., Hamaguchi et al. 2005). Giardino et al. (2007a) reported several non-detections of nearby Class 0 objects, with a "stacked Class 0 data set" corresponding to 540 ks of Chandra ACIS-I exposure time still giving no indication for a detection. In the absence of detailed information on the absorbing gas column densities or the intrinsic spectral properties, an interpretation within an evolutionary scenario remains difficult.

3.2 X-rays from high-density accretion shocks?

Accretion streams falling from circumstellar disks toward the central stars reach a maximum velocity corresponding to the free-fall velocity,

$$v_{\rm ff} = \left(\frac{2GM_*}{R}\right)^{1/2} \approx 620 \left(\frac{M}{M_\odot}\right)^{1/2} \left(\frac{R}{R_\odot}\right)^{-1/2} \left[\text{km s}^{-1}\right]. \quad (13)$$

This velocity is an upper limit as the material starts only at the inner border of the circumstellar disk, probably following curved magnetic field lines down toward the star; a more realistic terminal speed is $v_{\rm m} \approx 0.8 v_{\rm ff}$ (Calvet and Gullbring 1998). Upon braking at the stellar surface, a shock develops which, according to the strong-shock theory, reaches a temperature of

$$T_{\rm s} = \frac{3}{16k} m_{\rm p} \mu v_{\rm m}^2 \approx 3.5 \times 10^6 \frac{M}{M_\odot} \left(\frac{R}{R_\odot}\right)^{-1} \text{[K]} \quad (14)$$

(where $m_{\rm p}$ is the proton mass and μ is the mean molecular weight, i.e., $\mu \approx 0.62$ for ionized gas). For typical TTS, $M = (0.1\text{–}1) M_\odot$, $R = (0.5\text{–}2) R_\odot$, and $M/R \approx (0.1\text{–}1) M_\odot/R_\odot$ and therefore $T_{\rm s} \approx (0.4\text{–}4) \times 10^6$ MK. Such electron temperatures should therefore produce soft X-ray radiation (Ulrich 1976). The bulk of the ensuing X-rays is probably absorbed in the shock, contributing to its heating, although part of the X-rays may escape and heat the pre-shock gas (Calvet and Gullbring 1998).

The pre-shock electron density, n_1, can be estimated from the mass accretion rate, $\dot{M}_{\rm acc}$, and the surface-filling factor of the accretion streams, f: using the strong-shock condition for the post-shock density, $n_2 = 4 n_1$, together with $\dot{M}_{\rm acc} \approx 4\pi R_*^2 f v_{\rm m} n_1 m_{\rm p}$ one finds

$$n_2 \approx \frac{4 \times 10^{11}}{f} \left(\frac{\dot{M}_{\rm acc}}{10^{-8}\ M_\odot\ \text{year}^{-1}}\right) \left(\frac{R_*}{R_\odot}\right)^{-3/2} \left(\frac{M_*}{M_\odot}\right)^{-1/2} \left[\text{cm}^{-3}\right] \quad (15)$$

which, for typical stellar parameters, accretion rates, and filling factors $f \approx 0.001\text{–}0.1$ (Calvet and Gullbring 1998), predicts densities of order 10^{11}–10^{13} cm^{-1}. Given the expected shock temperatures and electron densities, X-ray grating spectroscopy of the density-sensitive He-like C V, N VI, O VII, and Ne IX line triplets should be ideal to detect accretion shocks. We emphasize that in Eq. 15, the shock density is proportional to $\dot{M}_{\rm acc}/f$, i.e., strongly dependent on the magnetic structure and the accretion rate, but it also depends on the fundamental stellar properties via $R_*^{-3/2} M_*^{-1/2}$ (Telleschi et al. 2007b; Robrade and Schmitt 2007).

The first suggestion for this mechanism to be at work was made by Kastner et al. (2002), based on grating spectroscopy of the nearby CTTS TW Hya. TW Hya's spectrum shows an unusually high f/i ratio for the Ne IX triplet, pointing to $n_{\rm e} \approx 10^{13}$ cm^{-3}. Also, and again at variance with the typical coronal properties of CTTS, the X-ray emitting plasma of TW Hya is dominated by a cool component, with a temperature of only $T \approx 2\text{–}3$ MK. Similarly high electron densities are suggested from the O VII triplet (Stelzer and Schmitt 2004), and supporting albeit tentative evidence is also found from ratios of Fe XVII line fluxes (Ness and Schmitt 2005). Simple 1-D plane-parallel shock models, including ionization and recombination physics can successfully explain the observed temperatures and densities, resulting in rather compact accretion spots with a filling factor of ≈0.3%, requiring a mass accretion rate responsible for the X-ray production of $2 \times 10^{-10}\ M_\odot$ year^{-1} (Günther et al. 2007).

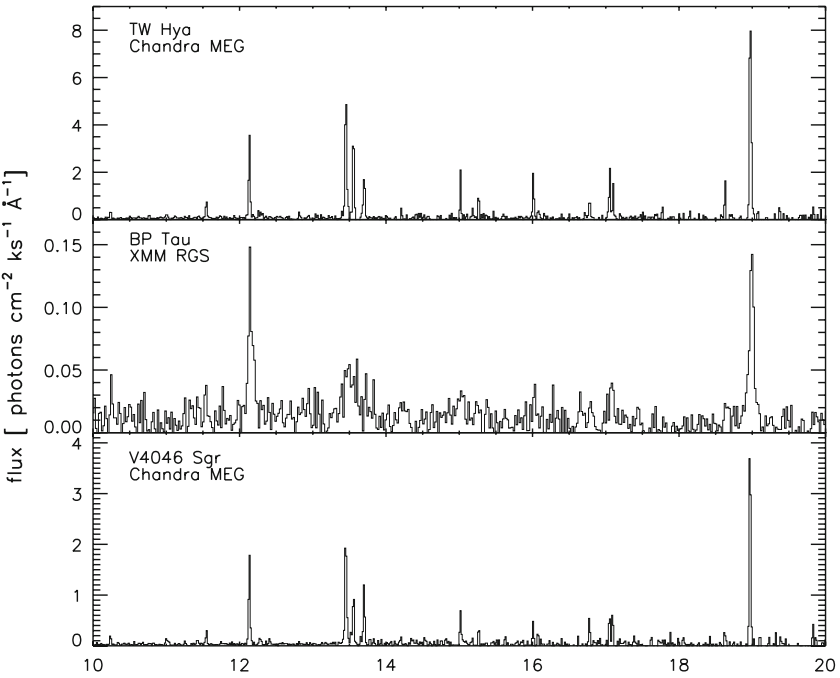

Fig. 13 Three spectra from CTTS (from *top* to *bottom*, TW Hya, BP Tau, and V4046 Sgr). Note the strong intercombination lines of Ne IX (the *middle line* in the line triplet at 13.4–13.7 Å) (from Günther et al. 2006)

Several further CTTS have been observed with X-ray gratings, although the moderate spectral flux of CCTS and the modest effective areas of detectors presently available have kept the number of well exposed spectra small (see examples in Fig. 13). In most cases, high densities are present as judged from the O VII and Ne IX triplets, but all spectra are dominated by a hot, coronal component with the exception of TW Hya. X-ray emission from CTTS may thus have at least two origins, namely magnetic coronae and accretion flows. Table 2 summarizes published observations of O VII triplets in CTTS (and Herbig stars, see Sect. 3.6) together with derived electron densities.

3.3 The "X-Ray Soft Excess" of classical T Tauri stars

Although TW Hya's soft spectrum remains exceptional among CTTS, lines forming at temperatures of only a few MK reveal another anomaly for seemingly *all* CTTS, illustrated in Fig. 14. This figure compares XMM-*Newton* RGS spectra of the active binary HR 1099 (X-rays mostly from a K-type subgiant), the weakly absorbed WTTS V410 Tau, the CTTS T Tau N, and the old F subgiant Procyon. HR 1099 and V410 Tau show the typical signatures of a hot, active corona such as a strong continuum, strong lines of Ne X and highly-ionized Fe but little flux in the O VII line triplet. In contrast, lines of C, N, and O dominate the soft spectrum of Procyon, the O VII triplet exceeding the O VIII Lyα line in flux. T Tau reveals a "hybrid spectrum": we see signatures of a

Table 2 Density measurements in CTTS and Herbig stars based on O VII triplet line fluxes

Star	Spectral type	Mass ($M_\odot$)	O VII[a] $\mathcal{R} = f/i$	Electron density (cm^{-3})	Reference
Hen 6-300	M (3 + 3.5)	…	1.0 (0.5)	6×10^{10}	Huenemoerder et al. (2007)
TW Hya	K8	0.7[b]	0.054 (0.045)	1.3×10^{12}	Robrade and Schmitt (2006)
RU Lup	K	0.8	0.26 (0.23)	4.4×10^{11}	Robrade and Schmitt (2007)
BP Tau	K5-7	0.75[c]	0.37 (0.16)	3×10^{11}	Schmitt et al. (2005)
V4046 Sgr	K5+K7	0.86 + 0.69	0.33 (0.28)	3×10^{11}	Günther et al. (2006)
CR Cha	K2	…	0.64 (0.44)	1.6×10^{11}	Robrade and Schmitt (2006)
MP Mus	K1	1.2[b]	0.28 (0.13)	5×10^{11}	Argiroffi et al. (2007)
T Tau	K0	2.4[c]	4.0	$\lesssim 8\times10^{10}$	Güdel et al. (2007b)
HD 104237	A (7.5–8)	2.25	$1.8^{+2}_{-0.9}$ [a]	6×10^{11}	Testa et al. (2008a)
HD 163296	A1	2.3	4.6;>2.6	$\lesssim 2.5\times10^{10}$	Günther and Schmitt (2009)
AB Aur	A0	2.7	≈4	$\lesssim 1.3\times10^{11}$	Telleschi et al. (2007c)

Values generally from references given in last column and further references therein
[a] Errors in parentheses; $\mathcal{R}$ for HD 104237 refers to the Ne IX triplet, O VII being too weak for detection
[b] Values from Robrade and Schmitt (2007)
[c] Values from Güdel et al. (2007a)

very active corona shortward of 19 Å but also an unusually strong O VII triplet. Because T Tau's N_H is large (in contrast to N_H of the other stars), the intrinsic behavior of the O VII line becomes only evident after correction for absorption: *The* O VII *lines are in fact the strongest lines in the intrinsic X-ray spectrum,* reminiscent of the situation in the inactive Procyon.

While the O VII line triplet remains undetected in almost all WTTS grating spectra despite the usually low absorption column densities toward WTTS, the same triplet is frequently detected as an unusually strong feature in CTTS with their typically larger column density. This reflects quantitatively in an anomalously large flux ratio, S, between the intrinsic (unabsorbed) O VII resonance (r) line and the O VIII Lyα line, defining the *X-ray soft excess* in classical TTS (Güdel 2006; Telleschi et al. 2007b; Güdel et al. 2007c; Güdel and Telleschi 2007).

Figure 15a shows the S ratio as a function of L_X, comparing CTTS and WTTS with a larger MS sample (from Ness et al. 2004) and MS solar analogs (from Telleschi et al. 2005). The trend for MS stars (black crosses and triangles, cf. Eq. 4, Sect. 2.1) is evident: as the coronae get hotter toward higher L_X, the ratio of O VII r/O VIII Lyα line luminosities decreases. This trend is followed by the sample of WTTS, while CTTS show a systematic excess. Interestingly, the excess emission itself seems to correlate with the stellar (coronal) X-ray luminosity diagnosed by the O VIII Lyα flux (Fig. 15b). The soft excess appears to *depend on stellar coronal activity while it requires accretion.*

The origin of the additional cool plasma is thus likely to be related to the (magnetic) accretion process. One possibility is shock-heated plasma at the accretion funnel footpoints as discussed in Sect. 3.2. Alternatively, the cool, infalling material may partly

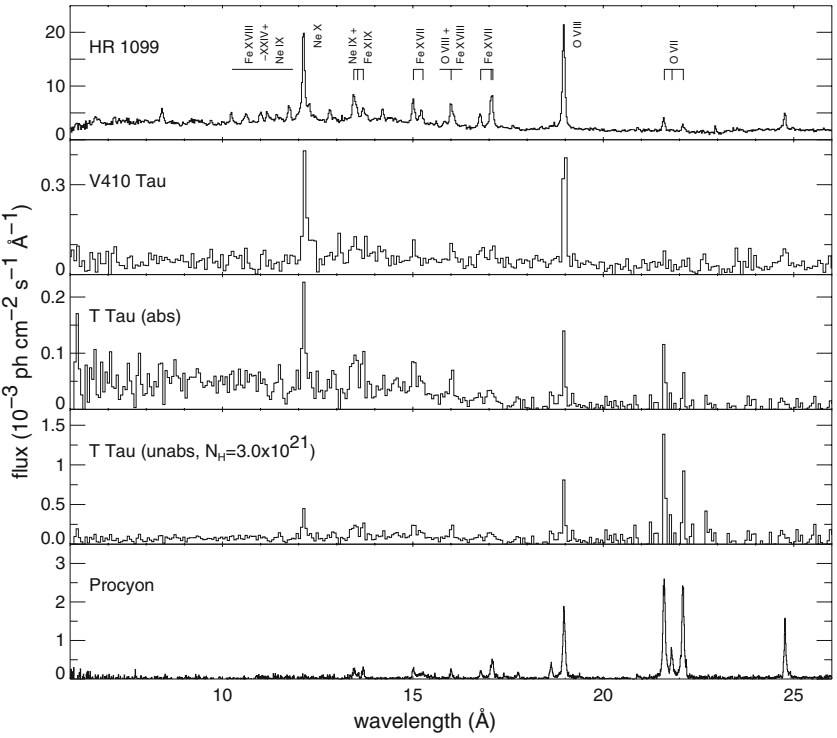

Fig. 14 Comparison of fluxed XMM-*Newton* RGS X-ray photon spectra of (from *top* to *bottom*) the active binary HR 1099, the WTTS V410 Tau, the CTTS T Tau, the T Tau spectrum modeled after removal of absorption (using $N_{\rm H} = 3 \times 10^{21}$ cm^{-2}), and the inactive MS star Procyon. Note the strong O VII line triplet in T Tau, while the same lines are absent in the spectrum of the WTTS V410 Tau (adapted from Güdel and Telleschi 2007)

cool pre-existing heated coronal plasma, or reduce the efficiency of coronal heating in the regions of infall (Preibisch et al. 2005; Telleschi et al. 2007b), which could explain the correlation between the soft excess and the coronal luminosity. Such a model would at the same time explain why CTTS are X-ray weaker than WTTS (Preibisch et al. 2005; Telleschi et al. 2007a). In any case, it seems clear that the soft excess described here argues in favor of a substantial influence of accretion on the X-ray production in pre-main sequence stars.

3.4 Abundance anomalies as tracers of the circumstellar environment?

Initial studies of a few accreting T Tau stars, in particular the old (≈10 Myr) TW Hya, showed an abundance pattern in the X-ray source similar to the IFIP effect although the Ne/Fe abundance ratio is unusually high, of order 10 with respect to the solar photospheric ratio, and the N/O and N/Fe ratios are enhanced by a factor of ≈3.

These anomalous abundance ratios have been suggested (Stelzer and Schmitt 2004; Drake et al. 2005) to reflect depletion of Fe and O in the accretion disk where almost

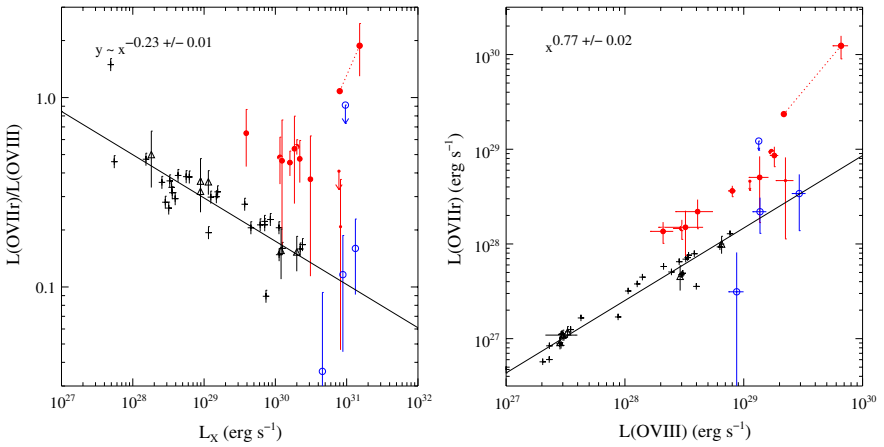

Fig. 15 **a** The ratio between O VII r and O VIII Lyα luminosities versus L_X. *Crosses* mark MS stars (from Ness et al. 2004), *triangles* solar analogs (from Telleschi et al. 2005), *filled* (*red*) *circles* CTTS, and *open* (*blue*) *circles* WTTS. The *solid line* is a power-law fit to the MS stars with $L_X > 10^{27}$ erg s^{-1} (the relation between the variables is given in the *upper left* corner). **b** Correlation between L(O VII r) and L(O VIII). Symbols are as in **a** (adapted from Güdel and Telleschi 2007)

all elements condense into grains except for N and Ne that remain in the gas phase. If accretion occurs predominantly from the gas phase in the higher layers of the disk while the grains grow and/or settle at the disk midplane, then the observed abundance anomaly may be a consequence.

Enlarging the sample of surveyed stars has made this picture less clear, however. Several CTTS *and non-accreting WTTS* have revealed large Ne/Fe ratios (≈4 or higher, Kastner et al. 2004a; Argiroffi et al. 2005, 2007; Telleschi et al. 2005, 2007b; Günther et al. 2006), suggesting that accretion is not the determining factor for the abundance ratio. Similar ratios are also found for evolved RS CVn binaries (Audard et al. 2003) for which the high Ne/Fe is a consequence of the inverse FIP effect (Sect. 2.5). On the other hand, the *accreting* CTTS SU Aur reveals a low Ne/Fe abundance ratio of order unity (Robrade and Schmitt 2006; Telleschi et al. 2007b), similar to several other massive CTTS (Telleschi et al. 2007b).

Partial clarification of the systematics has been presented by Telleschi et al. (2007b) who found that the abundance trends, and in particular the Ne/Fe abundance ratios, do not depend on the accretion status but seem to be a function of spectral type or surface $T_{\rm eff}$, the later-type magnetically active stars showing a stronger IFIP effect (larger Ne/Fe abundance ratios). The same trend is also seen in disk-less zero-age main-sequence stars. Further, the same statistical study showed that the Ne/O abundance ratio is, within statistical uncertainties, indistinguishable between WTTS and CTTS (excluding TW Hya, see below), arguing against accretion of selectively depleted disk material in these objects.

Anomalously high Ne/O abundance ratios remain, however, for TW Hya (Stelzer and Schmitt 2004) and V4046 Sgr (Günther et al. 2006) when compared to the typical level seen in magnetically active stars or TTS. Drake et al. (2005) proposed that the selective removal of some elements (e.g., O) from the accretion streams should occur

only in old accretion disks such as that of TW Hya where coagulation of dust to larger bodies is ongoing, whereas younger T Tauri stars still accrete the entire gas and dust mix of the inner disk. However, the old CTTS MP Mus does not show any anomaly in the Ne/O abundance ratio (Argiroffi et al. 2007). Larger samples are needed for clarification.

3.5 Summary: accretion-induced X-rays in T Tauri stars

The present status of the search for accretion-induced X-ray emission and current open problems can be summarized as follows:

- Densities higher than typical for non-flaring coronal plasma, i.e., $n_e \geq 10^{11}$ cm^{-3}, are seen in the majority of CTTS. A clear exception is T Tau.
- Densities scatter over a wide range; this may be the result of a variety of accretion parameters (Günther et al. 2007; Robrade and Schmitt 2007).
- While TW Hya's X-ray emission is dominated by an unusually soft component, essentially all other CTTS are dominated by much hotter plasma, with principal electron temperatures mostly in the 5–30 MK range, similar to coronal temperatures of magnetically active, young main-sequence stars. The presence of flares is also indicative of coronal emission dominating the X-ray spectrum.
- A "soft excess", i.e., anomalously high fluxes observed in lines forming at low temperatures, e.g., the O VII line triplet, is seen only in accreting TTS and is therefore likely to be related, in some way, to accretion. However, a correlation with the coronal luminosity points toward a relation with coronal heating as well. The two relations can be reconciled if the soft excess is due to an interaction of the accretion streams with the coronal magnetic field (Güdel and Telleschi 2007).
- While TW Hya's anomalously high Ne abundance (Drake and Testa 2005) and the low abundances of refractory elements (such as Fe or O, Stelzer and Schmitt 2004) may be suggestive of heated accretion streams from a circumstellar disk, other CTTS do not generally show abundance anomalies of this kind. Low abundances of low-FIP elements are a general characteristic of magnetically active stars regardless of accretion. And finally, element abundances appear to be a function of spectral type or photospheric effective temperature in CTTS, WTTS, and young main-sequence stars while accretion does not matter (Telleschi et al. 2007b).
- If accretion streams are non-steady, correlated X-ray and optical/ultraviolet time variability should be seen during "accretion events" when the mass accretion rate increases for a short time. Despite detailed searches in long time series of many CTTS, no such correlated events have been detected on time scales of minutes to hours (Audard et al. 2007) or hours to days (Stassun et al. 2006).

Accretion-induced X-ray radiation is clearly a promising mechanism deserving detailed further study and theoretical modeling. Observationally, the sample accessible to grating observations remains very small, however.

3.6 X-rays from Herbig stars

Herbig Ae/Be stars are defined after Herbig (1960) as young intermediate-mass ($\approx$2–10 $M_\odot$) stars predominantly located near star-forming regions. They reveal emission lines in their optical spectra, and their location in the Hertzsprung–Russell diagram proves that they are pre-main sequence stars. Herbig stars are therefore considered to be the intermediate-mass analogs of TTS. This analogy extends to infrared emission indicative of circumstellar disks.

Like their main-sequence descendants, B and A-type stars, Herbig stars are supposed to have radiative interiors, lacking the convective envelopes responsible for the $\alpha\omega$ magnetic dynamo in late-type stars. Fossil magnetic fields left over from the star formation process may still be trapped in the stellar interior. Transient convection may, however, be present during a short phase of the deuterium-burning phase in a shell (Palla and Stahler 1993). A dynamo powered by rotational shear energy may also produce some surface magnetic fields (Tout and Pringle 1995). Magnetic fields have, indeed, been detected on some Herbig stars with longitudinal field strengths of up to a few 100 G (e.g., Donati et al. 1997; Hubrig et al. 2004; Wade et al. 2005).

X-ray observations provide premium diagnostics for magnetic fields in Herbig stars and their interaction with stellar winds and circumstellar material. Surveys conducted with low-resolution spectrometers remain, however, ambiguous. Many Herbig stars are X-ray sources (Damiani et al. 1994; Zinnecker and Preibisch 1994; Hamaguchi et al. 2005), with $L_{\rm X}/L_{\rm bol} \approx 10^{-7}$–$10^{-4}$, i.e., ratios between those of TTS (10^{-4}–10^{-3}) and O stars ($\approx 10^{-7}$). This finding may suggest that undetected low-mass companions are at the origin of the X-rays (e.g., Skinner et al. 2004; the "companion hypothesis"). The companion hypothesis is still favored for statistical samples of Herbig stars including multiple systems studied with *Chandra's* high spatial resolution (Skinner et al. 2004; Stelzer et al. 2006, 2009).

The X-ray spectra of Herbig stars are clearly thermal; intermediate-resolution CCD spectra show the usual indications of emission lines, partly formed at rather high temperatures (Skinner et al. 2004). High electron temperatures (>10 MK) derived from spectral fits as well as flares observed in light curves further support the companion hypothesis for Herbig star samples, as both features are common to TTS (Giardino et al. 2004; Skinner et al. 2004; Hamaguchi et al. 2005; Stelzer et al. 2006). On the other hand, $L_{\rm X}$ correlates with wind properties such as wind velocity or wind momentum flux (but not with rotation parameters of the Herbig stars), perhaps pointing to shocks in unstable winds as a source of X-rays (Damiani et al. 1994; Zinnecker and Preibisch 1994).

High-resolution X-ray spectroscopy has now started revealing new clues about the origin of X-rays from Herbig stars. The first such spectrum, reported by Telleschi et al. (2007c) from AB Aur (Fig. 16), is at variance with X-ray spectra from CTTS in three respects: first, X-rays from AB Aur are unusually soft (compared to general Herbig X-ray samples or TTS); electron temperatures are found in the range of 2–7 MK. Second, the X-ray flux is modulated in time with a period consistent with periods measured in optical/UV lines originating from the stellar wind. And third, the O VII line triplet indicates a high f/i flux ratio (Sect. 2.3.3) in contrast to the usually low values seen in CTTS.

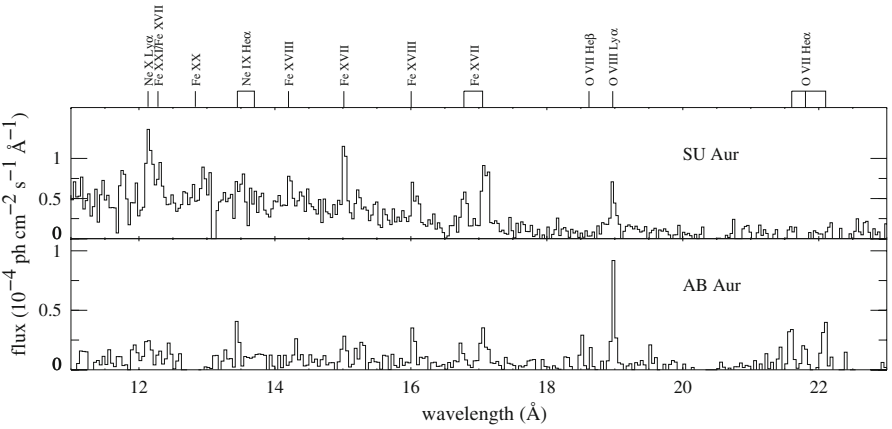

Fig. 16 XMM-*Newton* grating spectrum of the Herbig star AB Aur (*lower panel*) compared with the spectrum of the classical T Tauri star SU Aur (*upper panel*). Note the softer appearance of the AB Aur spectrum (e.g., absence of a strong continuum) and also the O VII triplet at 22 Å indicating low densities *and* the absence of a strong UV radiation field in the X-ray source (adapted from Telleschi et al. 2007c)

In the case of sufficiently hot stars ($T_{\rm eff} \gtrsim 10^4$ K), the f/i ratio of the X-ray source not only depends on the electron density (Sect. 2.3.3) but also on the ambient UV radiation field. In that case,

$$\mathscr{R} = \frac{f}{i} = \frac{\mathscr{R}_0}{1 + \phi/\phi_c + n_{\rm e}/N_{\rm c}}, \tag{16}$$

where $\mathscr{R}_0$ is the limiting flux ratio at low densities and negligible radiation fields, $N_{\rm c}$ is the critical density at which $\mathscr{R}$ drops to $\mathscr{R}_0/2$ (for negligible radiation fields), and ϕ_c is the critical photoexcitation rate for the $^3S_1 - ^3P_{1,2}$ transition, while ϕ characterizes the ambient UV flux. The ratio ϕ/ϕ_c can be expressed using $T_{\rm eff}$ and fundamental atomic parameters (for applications to stellar spectra, see Ness et al. 2002 and, specifically for AB Aur, Telleschi et al. 2007c). A high f/i ratio thus not only requires the electron density to be low ($\lesssim 10^{11}$ cm^{-3}; Table 2) but also the emitting plasma to be located sufficiently far away from the strong photospheric UV source. Considering all X-ray properties of AB Aur, Telleschi et al. (2007c) suggested the presence of magnetically confined winds shocks. These shocks form in the equatorial plane where stellar winds collide after flowing along the closed magnetic field lines from different stellar hemispheres (see also Sect. 4.6). As this shock is located a few stellar radii away from the photosphere, a high f/i ratio is easily explained.

HD 104237 is another Herbig star observed with X-ray gratings (Testa et al. 2008b). This object is of slightly later spectral type (A7.5 Ve–A8 Ve) than the other Herbigs observed with gratings, implying that the photospheric radiation field is irrelevant for the f/i ratio of the He-like O VII, Ne IX, Mg XI, and Si XIII triplets. At first sight, both the low-resolution spectrum (Skinner et al. 2004) and the high-resolution grating spectrum (Testa et al. 2008b) indicate high temperatures similar to TTS, and indeed HD 104237 is accompanied by a close (0.15 AU), relatively massive K3-type com-

panion (see Testa et al. 2008b and references therein). However, an anomalously cool component in the spectrum and rotational modulation compatible with the measured rotation period of the Herbig star point to the latter as the source of the softer emission (Testa et al. 2008b), while much of the harder emission may originate from the K-type T Tauri companion. This interpretation fits well into the emerging picture of Herbig X-ray emission sketched above although the origin of the soft emission [magnetically confined winds, accretion shocks, jet shocks (see below), cool coronae induced by shear dynamos] needs further investigation.

The third Herbig star observed at high resolution in X-rays, HD 163296, had previously attracted attention as another unusually soft X-ray source (Swartz et al. 2005). Although the latter authors suggested that the soft emission is due to accretion shocks in analogy to the mechanism proposed for CTTS, grating spectra paint a different picture: again, the f/i flux ratio is high, requiring the X-ray source to be located at some distance from the stellar surface and to be of low density (Günther and Schmitt 2009; Table 2). Although a similar model as for AB Aur may be applicable, HD 163296 is distinguished by driving a prominent jet marginally indicated in an image taken by CHANDRA (Swartz et al. 2005). A possible model, therefore, involves shock heating in jets, requiring an initial ejection velocity of 750 km s^{-1}, but shock heating at such velocities is required only for a fraction of ≈1% of the outflowing mass (Günther and Schmitt 2009).

3.7 Two-absorber X-ray spectra: evidence for X-ray jets

Shocks in outflows and jets may produce X-ray emission. Terminal shocks between jets and the interstellar medium, forming "Herbig-Haro (HH) objects", are obvious candidates. Sensitive imaging observations have indeed detected faint X-ray sources at the shock fronts of HH objects (e.g., Pravdo et al. 2001). Shocks may also form internally to the jet, close to the driving star. Such X-ray sources have been found close to the class I protostar L1551 IRS5 (Favata et al. 2002; Bally et al. 2003) and the classical T Tauri star DG Tau (Güdel et al. 2008). The faint low-resolution spectra are soft and indicate temperatures of a few million K, compatible with shock velocities of a few 100 km s^{-1}.

X-ray spectra of several very strongly accreting, jet-driving CTTS exhibit a new spectral phenomenology (Fig. 17, Table 3): These "Two-Absorber X-ray" (TAX) spectra reveal a cool component subject to very low absorption and a hot component subject to absorption about one order of magnitude higher. The temperature of the cool component, $T \approx 3$–6 MK, is atypical for T Tau stars.

The hard component of TAX sources requires an absorbing hydrogen column density $N_{\rm H} \gtrsim 10^{22}$ cm^{-2}, higher by typically an order of magnitude than predicted from the visual extinction $A_{\rm V}$ if standard gas-to-dust ratios are assumed (Güdel et al. 2007c and references therein). Because the hard component requires electron temperatures of tens of MK and occasionally shows flares, it is likely to be of coronal origin. The *excess absorption* can be generated by accretion streams falling down along the magnetic field lines and absorbing the X-rays from the underlying corona. The *excess absorption-to-extinction* (or equivalently, $N_{\rm H}/A_{\rm V}$) ratio then is an indicator of dust sublimation:

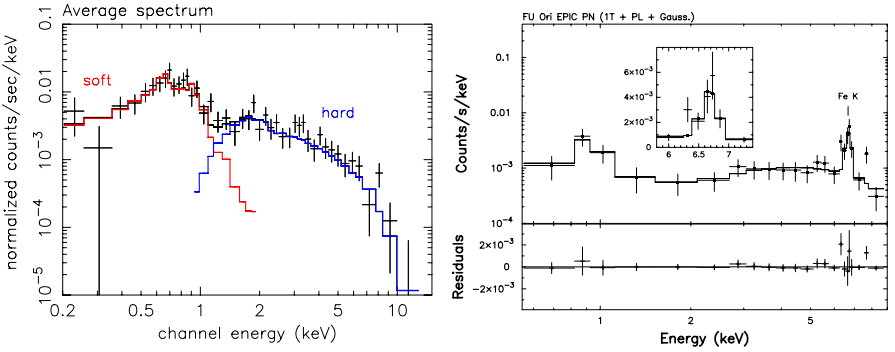

Fig. 17 **a** Spectrum of the Two-Absorber X-ray source DG Tau. The soft and the hard components are indicated. The *solid histograms* show model fits (adapted from Güdel et al. 2007c). **b** Spectrum of FU Ori. Note the essentially flat appearance between 0.6 and 7 keV, with two broad peaks related to two different spectral components absorbed by different gas columns (from Skinner et al. 2006b, reproduced by permission of the AAS)

the accreting gas streams are dust-depleted, which is to be expected given that dust is heated to sublimation temperatures (≈1,500 K) at distances of several stellar radii.

In contrast, $N_{\rm H}$ of the soft component is *lower* than suggested from the stellar $A_{\rm V}$. A likely origin of these very soft X-rays is *the base of the jet* (Güdel et al. 2007c), suggested by (i) the unusually soft emission compatible with the jet spectrum, (ii) the low $N_{\rm H}$ values, and (iii) the explicit evidence of jets in CHANDRA imaging (Güdel et al. 2008). Schneider and Schmitt (2008) supported this scenario by demonstrating that the soft component is very slightly offset from the harder, coronal component in the direction of the optical jet. We also note that some CCTS with jets show blueshifts in O VI and C III lines (forming at a few 10^5 K) as observed in *FUSE* spectra, again suggesting shock-heated hot material in jets (Günther and Schmitt 2008).

We should note here that one of the sources listed in Table 3, FU Ori, is an eruptive variable presently still in its outburst stage (which has lasted for several decades). This object is discussed in the context of eruptive variables below (Sect. 3.8).

3.8 X-rays from eruptive variables: coronae, accretion, and winds

A small class of eruptive pre-main sequence stars deserves to be mentioned for their peculiar X-ray spectral behavior, both during outbursts and during "quiescence". They are roughly classified into FU Orionis objects (FUors henceforth) and EX Lupi objects (EXors). For reviews, we refer to Herbig (1977) and Hartmann and Kenyon (1996).

The classical FUors show optical outbursts during which the systems' brightness increases by several magnitudes on time scales of 1–10 yrs, and then decays on time scales of 20–100 years. The presently favored model posits that the brightness rises owing to a strongly increasing accretion rate through the circumstellar disk (from 10^{-7} to 10^{-4} $M_\odot$ year^{-1}). FUor outbursts may represent a recurrent but transient

Table 3 TAX sources: X-ray parameters and general properties

Star	A_V (mag)	Soft component			Hard component		
		$N_{H,s}$ (10^{22} cm^{-2})	T_s (MK)	$L^a_{X,s}$ (10^{29} erg s^{-1})	$N_{H,h}$ (10^{22} cm^{-2})	T_h (MK)	$L^a_{X,h}$ (10^{29} erg s^{-1})
DG Tau	1.5–3	0.11	3.7	0.96	1.8	69	5.1
GV Tau	3–5	0.12	5.8	0.54	4.1	80	10.2
DP Tau	1.2–1.5	≈0	3.2	0.04	3.8	61	1.1
HN Tau		0.15	2.0, 6.6	1.46	1.1	62	3.5
CW Tau	2–3	…	…	…	…	…	…
FU Ori	1.8–2.4	0.42	7.8	2.7	8.4	83	53
Beehive		0.08	6.6	…	6.3	41	…

X-ray data and A_V for Taurus sources from Güdel et al. (2007a) and Güdel et al. (2007c); for FU Ori, see Skinner et al. (2006b), and for Beehive, see Kastner et al. (2005). Index "s" for soft component, "h" for hard component

[a] L_X for 0.1–10 keV range (for FU Ori, 0.5–7.0 keV), in units of 10^{29} erg s^{-1}

phase during the evolution of a T Tauri star. EXors show faster outbursts with time scales of a few months to a few years, smaller amplitudes (2–3 mag) and higher repetition rates.

The first FUor X-ray spectrum, observed from the prototype FU Ori itself, shows a phenomenology akin to the TAX spectra discussed for the jet sources (Sect. 3.7; Fig. 17b), but with notable deviations (Skinner et al. 2006b; Table 3). First, the cooler and less absorbed spectral component shows a temperature (≈8 MK) characteristic of *coronal* emission from TTS, with an absorption column density compatible with the optical extinction. An interpretation based on shocks in accretion flows or jets is thus unlikely, and jets have not been detected for this object although it does shed a very strong wind, with a mass loss rate of $\dot{M}_w \approx 10^{-5}\ M_\odot$ year^{-1}. The hard spectral component shows very high temperatures ($T \approx 65-83$ MK), but this is reminiscent of TAX sources. Possible models for the two-absorber phenomenology include patchy absorption in which emission from the cooler coronal component suffers less absorption, while the dominant hotter component may be hidden behind additional gas columns, e.g., dense accretion streams. Absorption by a strong, neutral wind is an alternative, although this model requires an inhomogeneous, e.g., non-spherical geometry to allow the soft emission to escape along a path with lower absorption.

The above X-ray peculiarity does not seem to be a defining property of FUors; X-ray emission from the FUor V1735 Cyg does neither show TAX phenomenology nor anomalous absorption but does reveal an extremely hard spectrum, reminiscent of the hard spectral component of FU Ori (Skinner et al. 2009). It is also unclear whether the spectral phenomenology is related with the outburst status of the stars; both FU Ori and V1735 Cyg have undergone outbursts, starting about 70 and 50 years ago (e.g., Skinner et al. 2009 and references therein), and the former is still in its declining phase.

Two objects, both probably belonging to the EXor group, have been observed from the early outburst phase into the late decay. The first, V1647 Ori, revealed a rapid rise in the X-ray flux by a factor of ≈30, closely tracking the optical and near-infrared light curves (Kastner et al. 2004b, 2006). The X-ray spectra revealed a hardening during the peak emission, followed by a softening during the decay. The absorbing column density did not change. Measured temperatures of order 6×10^7 K are much too high for accretion or outflow shocks; explosive magnetic reconnection in star-disk magnetic fields, induced by the strong rise of the disk-star accretion rate, is a possibility, and such events may be at the origin of ejected jet blobs (Kastner et al. 2004b). The picture of enhanced winds or outflows is supported by a gas-to-dust mass ratio enhanced by a factor of two during outburst, compared to standard interstellar ratios (Grosso et al. 2005).

A very different picture arose from the EXor-type eruption of V1118 Ori (Audard et al. 2005; Lorenzetti et al. 2006). While the optical and near-infrared brightness increased by 1–2 magnitudes on a time scale of 50 days, the X-rays varied slowly, by no more than a factor of two; however, the X-ray emission clearly *softened* during the outburst, suggesting that the hot plasma component disappeared during that episode. A possible model involves the disruption of the outer, hot magnetospheric or coronal magnetic loops by a disk that closed in as a consequence of the increased accretion rate (Audard et al. 2005).

3.9 X-rays from circumstellar environments: fluorescence

X-rays from TTS and protostars surrounded by circumstellar disks (and possibly molecular envelopes) inevitably interact with these environments. For the observer, this is most evident in increasingly large X-ray attenuation toward stars of earlier evolutionary stages. The responsible photoelectric absorption mechanism ionizes disk surfaces or envelopes quite efficiently (Glassgold et al. 1997), which has important consequences for chemistry, heating, or accretion mechanisms.

Here, we discuss direct evidence for disk ionization from fluorescent emission by "cold" (weakly ionized) iron. In brief, energetic photons emitted by a hot coronal source eventually hitting weakly ionized or neutral surfaces may eject an $1s$ electron from Fe atoms or ions. This process is followed by fluorescent transitions, the most efficient of which is the $2s$–$1p$ Fe Kα doublet at 6.4 keV, requiring irradiating photons with energies above the corresponding photoionization edge at 7.11 keV. The transition is known from X-ray observations of solar flares, in which case fluorescence is attributed to X-ray irradiation of the solar photosphere (Bai 1979). The physics of fluorescent emission is comparatively simple although radiative transfer calculations are required for accurate modeling (e.g., Drake et al. 2008b).

The same radiation can also be generated by impact ionization due to a non-thermal electron beam (Emslie et al. 1986), a mechanism that would be expected in particular during the early phases of a flare when high-energy electrons are abundant (Dennis 1985). Excitation by high-energy electrons is a rather inefficient process, however (Emslie et al. 1986; Ballantyne and Fabian 2003).

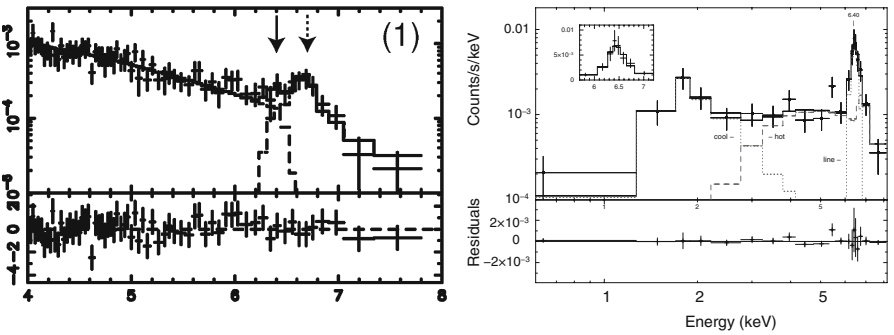

Fig. 18 **a** Evidence for an Fe fluorescence line at 6.4 keV (*left arrow*) next to the 6.7 keV feature of highly ionized Fe (*right arrow*); best-fit models including a narrow line at 6.4 keV, as well as the residuals (*bottom panel*) are also shown (from Tsujimoto et al. 2005, reproduced by permission of the AAS). **b** Spectrum of the deeply embedded infrared source NGC 2071 IRS-1; note the flat spectrum. The 6–7 keV region is entirely dominated by the 6.4 keV feature (from Skinner et al. 2007, reproduced by permission of the AAS)

Although fluorescent emission is prominent in accretion disks around compact objects, detection around normal stars is relatively recent. Observations of the 6.4 keV Fe Kα line require a spectral resolving power of ≈ 50 in order to separate the line from the adjacent, and often prominent, 6.7–7.0 keV Fe XXV–XXVI line complex from hot plasma. An unambiguous detection was reported by Imanishi et al. (2001) who found strong 6.4 keV line flux during a giant flare in the Class I protostar YLW 16A (in the ρ Oph dark cloud) and attributed it to irradiation of the circumstellar disk by X-rays from hot coronal flaring loops.

Detectable Fe fluorescence has remained an exception among CTTS or protostars, but a meaningful sample is now available (Tsujimoto et al. 2005; Fig 18a), with several unexpected features deserving further study. Specifically, strong fluorescence in the Class I protostar Elias 29 (in the ρ Oph region) appears to be quasi-steady rather than related to strong X-ray flares (Favata et al. 2005); even more perplexing, the 6.4 keV line is modulated on time scales of days regardless of the nearly constant stellar X-ray emission; it also does not react to the occurrence of appreciable X-ray flares in the light curve (Giardino et al. 2007b). The latter authors suggested that here we see 6.4 keV emission due to non-thermal electron impact in relatively dense, accreting magnetic loops. Given the high density, the electrons may not reach the stellar surface to produce evaporation and hence, an X-ray flare. The long time scale of this radiation is, however, still challenging to explain.

Occasionally, the fluorescence line dominates the 6–7 keV region entirely. An example is NGC 2071 IRS-1 in which a very broad and bright 6.4 keV feature (Fig. 18b) requires an absorbing column density of $\approx 10^{24}$ cm^{-2} for fluorescence, larger than the column density absorbing the rest of the spectrum (Skinner et al. 2007).

A connection with the initial energy release in a protostellar flare is seen in the case of the Class I star V1486 Ori in which strong 6.4 keV line flux is seen during the rise phase of a large soft X-ray flare (Czesla and Schmitt 2007; Fig. 19; the average quiescent + flare spectrum of this object is shown in Fig 18a). A relation with the electron beams usually accelerated in the initial "impulsive" phase of a (solar) flare is

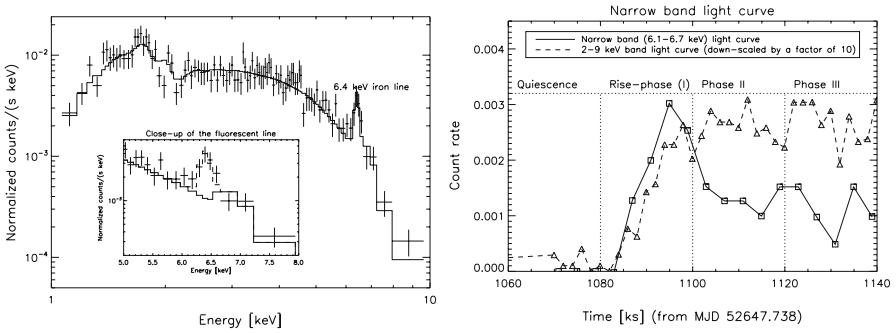

Fig. 19 **a** Medium-resolution spectrum of the flaring protostar V1486 Ori showing a 6.4 keV iron line with very little contribution from the 6.7 keV Fe XXV feature (see also *inset*). **b** The *solid light curve* refers to the 6.1–6.7 keV spectral range during the same flare, while the *dashed line* shows the integrated 2–9 keV light curve. Note that the ≈6.4 keV emission peaks early in the flare (from Czesla and Schmitt 2007)

suggestive, although this same flare phase commonly also produces the hardest thermal X-ray spectra. In any case, the extremely large equivalent width requires special conditions; detailed calculations by Drake et al. (2008b) suggest fluorescence by an X-ray flare partially obscured by the stellar limb.

4 X-rays from hot stars

In the Hertzsprung–Russell diagram, the top of the main sequence harbors stars with spectral types O and early B, which are the hottest objects of the stellar population (>20 kK). They also are the most luminous ($10^5\,L_\odot$) and the most massive ($M > 10\,M_\odot$) stellar objects. Early-type stars emit copious amounts of UV radiation which, through resonance scattering of these photons by metal ions, produce a strong outflow of material. Typically, the mass-loss rate of this stellar wind is about $10^{-6}\,M_\odot\,\mathrm{year}^{-1}$ (i.e., 10^8 times the average solar value!) while the terminal (i.e., final) wind velocity is about $2{,}000\,\mathrm{km\,s}^{-1}$. Though rare and short-lived (<10 Myr), hot stars have a profound impact on their host galaxies. Not only are they the main contributors to the ionizing flux, mechanical input, and chemical enrichment, but they can also be the precursors/progenitors of supernovae, neutron stars, stellar black holes and possibly gamma-ray bursts. Therefore, an improved understanding of these objects, notably through the analysis of their high-energy properties, can lead to a better knowledge of several galactic and extragalactic phenomena.

X-ray emission from hot stars was serendipitously discovered with the Einstein satellite 30 years ago (Harnden et al. 1979). One month after Einstein's launch, in mid-December 1978, calibration observations of Cyg X-3 revealed the presence of five additional sources to the North of that source. Dithering exposures showed that these moderately bright sources followed the motion of Cyg X-3, indicating that they were not due to contamination of the detector, as was first envisaged. A comparison with optical images finally unveiled the nature of these sources: bright O-type stars from the Cyg OB2 association. This discovery was soon confirmed by similar obser-

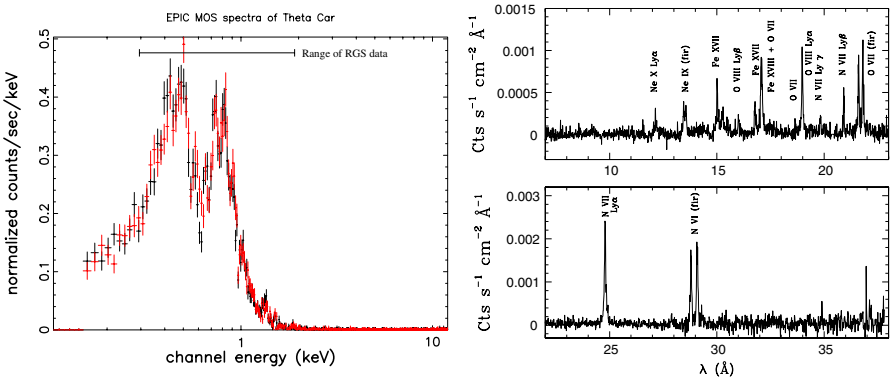

Fig. 20 Medium and high-resolution X-ray spectra of the massive system θ Car (B0.2V + late), as observed by XMM-*Newton*. The high-resolution spectrum distinctly shows lines from H-like and He-like ions, as well as lines associated with L shell transitions in iron ions (from Nazé and Rauw 2008)

vations in the Orion and Carina nebulae (Ku and Chanan 1979; Seward et al. 1979). The detection of high-energy emission associated with hot stars confirmed the expectations published in the same year by Cassinelli and Olson (1979), who showed that the "superionization" species (e.g., N V, O VI) observed in the UV spectra could be easily explained by the Auger effect in the presence of a significant X-ray flux.

Since then, hot stars have been regularly observed by the successive X-ray facilities: indeed, only X-rays can probe the energetic phenomena at work in these objects. However, the most critical information was only gained in the past 10 years thanks to the advent of new observatories, XMM-*Newton* and CHANDRA, which provided not only enhanced sensitivity but also the capability of high-resolution spectroscopy.

4.1 Global properties

4.1.1 Nature of the emission

Medium and high-resolution spectroscopy (see Figs. 20, 21) have now ascertained that the X-ray spectrum of hot stars, single as well as binaries, is composed of discrete lines from metals whose ionization stages correspond to a (relatively) narrow range of temperatures. These lines can be superimposed on a (weak) continuum bremsstrahlung emission. The X-ray spectrum thus appears mainly thermal in nature.

However, some hot, long-period binaries display non-thermal radio emission, which clearly reveals the presence of a population of relativistic electrons in the winds of these objects. Such relativistic electrons are probably accelerated by diffuse shock acceleration processes taking place near hydrodynamic shocks inside or (most probably) between stellar winds (for a review, see De Becker 2007). The possibility of a high-energy counterpart to this radio emission was investigated by Chen and White (1991). In this domain, inverse Compton scattering is expected to boost a small fraction of the ample supply of stellar UV photons to X-ray energies. To be detectable, such non-thermal X-ray emission needs to be sufficiently strong compared to the thermal

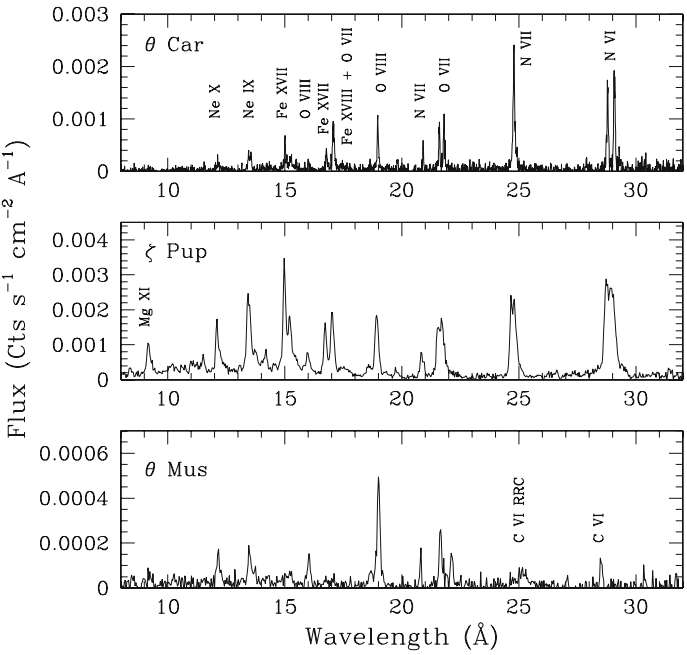

Fig. 21 High-resolution X-ray spectra of a B star (θ Car, *top*, adapted from Nazé and Rauw 2008), an O-star (ζ Pup, middle), and a WR star (θ Mus, *bottom*). (For the last two: data taken from the 2XMM database)

X-ray emission. This preferentially happens in short-period binaries, where the wind–wind interaction, and hence particle acceleration, takes place close to the stars and thus inside the radio photosphere, rather than in long-period binaries, where the interaction is located further away, outside the radio photosphere: the list of binary systems with non-thermal X-rays is thus expected to differ from that of non-thermal radio emitters (De Becker 2007). However, no convincing evidence has yet been found for the presence of non-thermal X-ray emission: only two candidates (HD 159176, De Becker et al. 2004, and FO15, Albacete Colombo and Micela 2005) present some weak indication of a possible non-thermal component in their spectra. In addition, the observed non-thermal emission of some binary systems still appears problematic, like, e.g., for Cyg OB2 #8A (Rauw 2008). Further work is thus needed to settle this question, and the answer may have to wait for the advent of more sensitive instruments, especially in the hard X-ray/soft gamma-ray range.

4.1.2 Temperatures

Except in the case of some peculiar objects (see Sects. 4.5, 4.6), the X-ray spectrum of single hot stars appears overall quite soft. Fits to medium-resolution spectra with optically-thin thermal plasma models in collisional ionization equilibrium (e.g., *mekal, apec*) always favor main components with temperatures less than 1 keV. For O stars, the best fits to good quality data can usually be achieved by the sum of two thermal

Table 4 $L_X - L_{bol}$ relations for O-type stars from the literature

Region	Relation	Energy band (keV)	Reference
RASS	$\log L_X = 1.08 \log L_{bol} - 11.89$	0.1–2.4	Berghöfer et al. (1997)
NGC 6231	$\log L_X = -6.912 \log L_{bol}$	0.5–10.0	Sana et al. (2006)
NGC 6231	$\log L_X = -7.011 \log L_{bol}$	0.5–1.0	Sana et al. (2006)
NGC 6231	$\log L_X = -7.578 \log L_{bol}$	1.0–2.5	Sana et al. (2006)
Cyg OB2	$\log L_X \sim -7 \log L_{bol}$	0.5–8.0	Albacete Colombo et al. (2007)
Carina OB1	$\log L_X = -6.58 \log L_{bol}$	0.4–10.0	Antokhin et al. (2008)
Carina OB1	$\log L_X = -6.82 \log L_{bol}$	0.4–1.0	Antokhin et al. (2008)
Carina OB1	$\log L_X = -7.18 \log L_{bol}$	1.0–2.5	Antokhin et al. (2008)

components at about 0.3 and 0.7–1 keV (e.g., the O stars in the NGC 6231 cluster, Sana et al. 2006, and in the Carina OB1 association, Antokhin et al. 2008).

High-resolution spectroscopic data of 15 OB stars were analyzed in a homogeneous way by Zhekov and Palla (2007) for the case of X-ray emitting regions distributed throughout the wind (see Sect. 4.2 for details). The distribution of the differential emission measure (DEM) as a function of temperature displays a broad peak centered on 0.1–0.4 keV (i.e., a few MK, see also a similar result obtained for 9 OB stars by Wojdowski and Schulz 2005), confirming the soft nature of the spectrum. A tail at high temperatures is sometimes present but is always of reduced strength compared to the low-temperature component. The only exceptions to this scheme are two magnetic objects (see Sect. 4.6) and the otherwise normal O-type star ζ Oph ($kT \sim$0.5–0.6 keV). In general, no absorbing column in addition to the interstellar contribution was needed in the fits, suggesting the absorption by the stellar wind to be quite small (Zhekov and Palla 2007, see also Sana et al. 2006).

4.1.3 L_X/L_{bol} relation

Already at the time of the discovery, Harnden et al. (1979) suggested that a correlation exists between the X-ray and optical luminosities. Such a relation was soon confirmed and slightly revised to a scaling law between unabsorbed X-ray and bolometric luminosities[3] of the form $L_X^{unabs} \sim 10^{-7} \times L_{bol}$ (see, e.g., Pallavicini et al. 1981). Sciortino et al. (1990) examined the possibility of correlations with other properties of these hot stars but could not find any evidence for relations with the rotation rate (contrary to late-type stars), the terminal wind velocity nor the mass-loss rate (though combinations of velocity and mass-loss rates gave good results, see below). More recently, Berghöfer et al. (1997) re-evaluated this scaling law using data from the ROSAT All-Sky Survey (RASS). Their relation (see Table 4) presents a large scatter (σ of 0.4 in logarithmic scale, or a factor 2.5) and flattens considerably below $L_{bol} \sim 10^{38}$ erg s^{-1}, i.e., for mid and late B stars.

[3] Indeed, for stars of similar spectral type and interstellar absorption, both relations are equivalent.

With the advent of XMM-*Newton* and CHANDRA, a more detailed investigation of this so-called "canonical" relation became possible. Rather than conducting a survey, the new studies rely on detailed observations of rich open clusters and associations, notably NGC 6231 (XMM-*Newton*, Sana et al. 2006), Carina OB1 (XMM-*Newton*, Antokhin et al. 2008), Westerlund 2 (CHANDRA, Nazé et al. 2008a), Cyg OB2 (CHANDRA, Albacete Colombo et al. 2007). The derived $L_X - L_{bol}$ relations are listed in Table 4. For NGC 6231 and Carina OB1, the stellar content and reddening are well known, enabling a precise evaluation of both the bolometric luminosity and the reddening correction to be applied to the observed X-ray flux. In both cases, the $L_X - L_{bol}$ relation appears much tighter (dispersion of only 40%) than in the RASS analysis. For Westerlund 2 and Cyg OB2, the optical properties are less constrained, naturally leading to a larger scatter. In the latter case, hints of a steeper relation were found for giant and supergiant stars compared to main-sequence objects (Albacete Colombo et al. 2007) but this needs to be confirmed.

The question arises about the actual origin of the difference between the RASS and XMM-*Newton* results. Part of the answer lies in the differences between the datasets, and differences in data handling. On the one hand, the RASS provides a large sample of hot stars, covering all spectral types, but generally with only approximate knowledge of the optical properties (spectral types taken from general catalogs, bolometric luminosities taken from typical values for the considered spectral types). The X-ray luminosities were derived from converting count rates using a single absorbing column and a single temperature matching the observed hardness ratios best. On the other hand, the chosen clusters provide a smaller sample but have undergone an intensive optical spectroscopic monitoring, leading to a better knowledge of their stellar content. In addition, the X-ray luminosities were derived from fits to the medium-resolution spectra. However, it remains to be seen whether the distinct data analyses are sufficient to explain all the differences in the scatter. One additional distinction between the datasets concerns the nature of the sample itself: clusters represent a homogeneous stellar population with respect to age, metallicity, and chemical composition, while the RASS analysis mixed stars from different clusters as well as field stars. The RASS scatter of the $L_X - L_{bol}$ relation could thus be partly real, and additional investigations, comparing more clusters, are needed. Notably, the study of high- or low-metallicity stellar populations would be of interest to better understand the X-ray emission as a whole. A first step in this direction was recently done by Chu et al. (in preparation). Their 300 ks observation of the LMC giant HII region N11 revealed an $L_X - L_{bol}$ relation some 0.5 dex higher than in NGC 6231. However, it is not yet clear if the observed OB stars are "normal", single objects or overluminous peculiar systems (see Sects. 4.5, 4.6).

It might also be worth noting that the $L_X - L_{bol}$ relation was investigated in different energy bands (Sana et al. 2006; Antokhin et al. 2008). The tight correlation exists in both soft (0.5–1 keV) and medium (1–2.5 keV) energy bands, but breaks down in the hard band (2.5–10 keV). While the scatter due to a poorer statistics (lower number of counts) cannot be excluded, it should be emphasized that the hard band is also more sensitive to additional, peculiar phenomena whose emission is expected to be harder, such as non-thermal emission, emission from magnetically-channeled winds

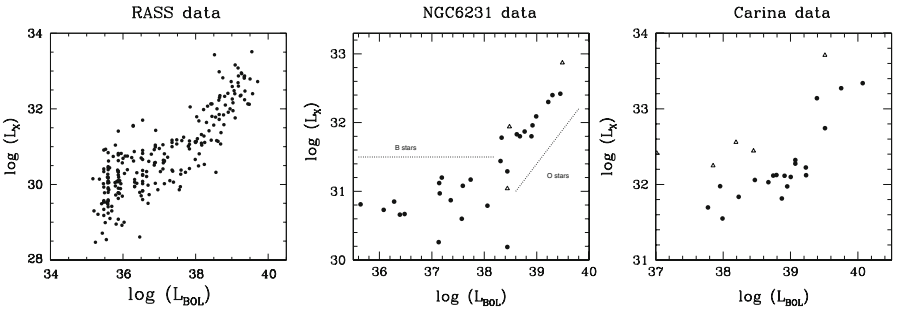

Fig. 22 $L_X - L_{bol}$ relations for OB stars in RASS, for OB stars in NGC 6231 and for O stars in Carina OB1. Peculiar objects or problematic objects are shown as *open symbols* (figures based on data from Berghöfer et al. 1997; Sana et al. 2006; Antokhin et al. 2008)

(see Sect. 4.6), etc. Indeed, even if such phenomena negligibly contribute to the overall level of X-ray emission, they could significantly affect the hard band.

Although a well established observational fact, the $L_X - L_{bol}$ relation is still not fully explained from the theoretical point-of-view. Qualitatively, it can of course be expected that the X-ray luminosity scales with the stellar wind properties (density, momentum or kinetic luminosity) if the X-ray emission arises in the wind (see Sect. 4.2). Since the wind is actually radiatively driven, these quantities should depend on the global level of light emission, i.e., on L_{bol}. However, the exact form of the scaling relation is difficult to predict. Owocki and Cohen (1999) made an attempt to explain the scaling law in the context of a distributed X-ray source. Considering that the volume filling factor varies as r^s, they found that L_X scales as $(\dot{M}/v_\infty)^{1+s}$ if the onset radius of the X-ray emission is below the radius of optical depth unity (optically thick case), and $(\dot{M}/v_\infty)^2$ otherwise. Adding the dependence of the wind parameters to the bolometric luminosity, one finally gets the observed scaling for s values of -0.25 or -0.40 in the optically thick case. For less dense winds (optically thin case), L_X should be proportional to $L_{bol}^{2.7 \text{ or } 3.5}$, i.e., the power law becomes steeper, as possibly observed for early B stars (Owocki and Cohen 1999, see, however, below). In this context, it may be interesting to note that recent high-resolution observations of ζ Ori seem to favor constant filling factors (i.e., $s = 0$ or $f \propto r^0$, Cohen et al. 2006).

Finally, recent studies have confirmed that the "canonical" $L_X - L_{bol}$ relation only applies for $L_{bol} > 10^{38}$ erg s^{-1}, i.e., down to B0–1 stars. It then breaks down at lower luminosities, with L_X/L_{bol} ratios two orders of magnitude smaller at B3 than at B1 (Cassinelli et al. 1994; Cohen et al. 1997). Some authors therefore questioned whether B stars should emit at all in the X-ray domain. Indeed, these stars lack both putative origins of X-ray emission (see Sect. 4.2): strong stellar winds, except maybe for the earliest subtypes, and developed coronae (because of the absence of a subsurface convective zone). However, when detected, the X-ray emission from B stars appears to be related to their bolometric luminosity, although with a shallower scaling law (see Fig. 22). This strongly suggests an intrinsic origin for the high-energy emission, and would request a revision of the current models. On the other hand, only a small fraction of these objects are detected: in the RASS, the detection fraction was less than 10% for B2 and later objects (Berghöfer et al. 1997); in NGC 6231, it is 24% for B0–B4 stars

but only 7% for B5 and later objects (Sana et al. 2006). Moreover, when detected, their spectra are often quite hard ($kT_2 > 1$ keV) and many X-ray sources associated with B stars present flares: these properties are more typical of pre main sequence (PMS) objects, suggesting that the detected X-ray emission from B stars actually corresponds to that of a less massive, otherwise hidden PMS companion.

4.1.4 A relation with spectral types?

High-resolution X-ray spectroscopy allowed Walborn (2008) to examine the metal lines in search of systematic effects related to the spectral classification, as are well known in the UV and optical domains. At first sight, the overall X-ray spectra seem to shift toward longer wavelengths for later types, and ratios of neighboring lines from the same element but at different ionization stages (e.g., Ne X/Ne IX, Mg XII/Mg XI, Si XIV/Si XIII) are seen to evolve or even reverse. These trends clearly call for confirmation using a larger sample but, if real, they would have to be explained by theoretical models.

4.2 Origin of the X-ray emission: insights from high-resolution spectroscopy

Different origins for the high-energy emission of hot stars were proposed in the first decades after its discovery. Observational tests are indeed crucial to distinguish between the models. Not surprisingly, the strongest constraints were derived only recently with the advent of high-resolution spectroscopy. The new results lead to modifications of the original models, which also affect other wavelength domains.

4.2.1 Proposed models and a priori predictions

The first proposed model to explain the X-ray emission from hot stars was a corona at the base of the wind, analogous to what exists in low-mass stars (see, e.g., Cassinelli and Olson 1979). However, several observational objections against such models were soon raised. First, while neutron stars in close high-mass X-ray binaries showed the presence of significant attenuation by the stellar wind of their companion, no strong absorption was found for the intrinsic X-ray emission of massive stars (Cassinelli and Swank 1983). This suggests that the source of the X-ray emission lies significantly above the photosphere, at several stellar radii. Second, the coronal [Fe XIV] λ 5,303Å line was never detected in hot stars spectra (Nordsieck et al. 1981; Baade and Lucy 1987). Finally, the line profiles from "superionized" species were incompatible with coronal models, unless the mass-loss rate was drastically reduced (Macfarlane et al. 1993).

An alternative scenario relies on the intrinsic instability of the line-driving mechanism (responsible for propulsing the stellar wind). Indeed, the velocity in an unstable wind is not the same everywhere: fast-moving parcels of material will overcome the slow-moving material, generating shocks between them. This causes the formation of dense shells which should be distributed throughout the whole wind. At first, strong forward shocks between the fast cloudlets and the ambient, slower ("shadowed") mate-

rial were considered as the most probable cause of the X-ray emission (Lucy and White 1980). Subsequent hydrodynamical simulations rather showed the presence of strong *reverse* shocks which decelerate the fast, low-density material (Owocki et al. 1988). However, the resulting X-ray emission from such rarefied material is expected to be quite low and cannot account for the level of X-ray flux observed in hot stars. Instead, Feldmeier et al. (1997) proposed that mutual collisions of dense, shock-compressed shells could lead to substantial X-ray emission (simulations yield values only a factor of 2–3 below the observations). In such a model, the X-ray emission arises from a few (always <5, generally 1 or 2) shocks present at a few stellar radii ($<10\,R_*$). Since these shocks fade and grow on short time scales, such models predict significant short-term variability, which is not observed. To reconcile the observations with their model, Feldmeier et al. (1997) further suggested wind fragmentation, so that individual X-ray fluctuations are smoothed out over the whole emitting volume, leading to a rather constant X-ray output. At the end of the twentieth century, this wind-shock scenario was the most favored model among X-ray astronomers.

To get a better insight into the properties of the X-ray emission region, high-resolution data were badly needed. Indeed, they provide crucial information. For example, the location of the X-ray emitting plasma can be derived from the analysis of line ratios. The most interesting lines to do so are triplets from He-like ions, which arise from transitions between the ground state and the first excited levels (see Fig. 4). The line associated with the $^1P_1 \rightarrow {}^1S_0$ transition is a resonance line (*r*), the one linked with the $^3S_1 \rightarrow {}^1S_0$ transition is forbidden (*f*), and those associated with the $^3P_{1,2} \rightarrow {}^1S_0$ transition are called intercombination lines (*i*); hence the name *fir* triplets. It is important to note that the metastable $^3S_1$ level can also be depleted by transitions to the ^3P level. Such transitions are either collisionally or radiatively excited (see Sects. 2.3.3, 3.6). The *f*/*i* ratio (often noted $\mathscr{R}$) therefore decreases when the density n_e is high or the photoionization rate ϕ is significant: as already mentioned in Sect. 3.6, a useful approximation is

$$\mathscr{R} = \frac{\mathscr{R}_0}{1 + \phi/\phi_c + n_e/N_c}, \tag{17}$$

where the critical values of the photoexcitation rate and the density, noted ϕ_c and N_c respectively, are entirely determined by atomic parameters (Blumenthal et al. 1972, see also Table 1). For hot stars, the density remains quite low, even close to the photosphere, and its impact is therefore often neglected;[4] however, the UV flux responsible for the $^3S_1 \rightarrow {}^3P_{1,2}$ transition is not negligible in these stars (see Fig. 23). The UV radiation is diluted, as the distance from the star increases, by a factor

$$w(r) = 0.5 \times \left(1 - \sqrt{1 - (R_*/r)^2}\right). \tag{18}$$

[4] Only the Si XIII triplet is marginally affected at very small radii ($<0.05\,R_*$) above the photosphere (see Fig. 2 in Waldron and Cassinelli 2001).

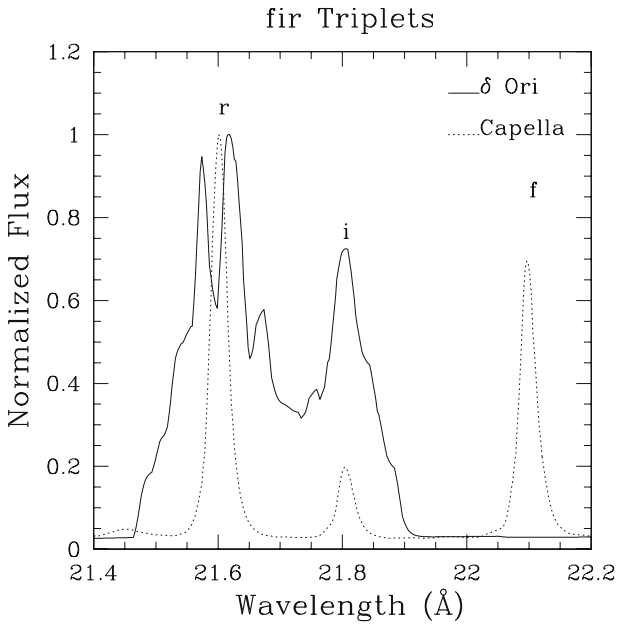

Fig. 23 Examples of observed He-like triplets (data taken from the Xatlas database and smoothed by a box of 4 pixels half width). Due to the presence of a strong UV flux, the forbidden line is nearly entirely suppressed for the hot star δ Ori while it appears with full strength in the spectrum of the late-type star Capella

Hence, its influence on the *f/i* ratio decreases with radius.[5] For hot stars, the observation of a given *f/i* ratio will thus yield an estimate of the dilution factor and thereby of the position in the wind of the X-ray emitting plasma. Leutenegger et al. (2006) have further shown that the *f/i* ratios could also be interpreted in the framework of a wind-shock model (i.e., with X-ray emission regions distributed throughout the wind). In this case, the integrated *f/i* ratio increases faster with radius than in the localized case. Furthermore, they predict slight differences in the profiles of the *fir* lines: the *i* line should be stronger where the UV flux is maximum, i.e., close to the star, and it should thus have weaker wings than the *f* line, which is produced further away and should appear more flat-topped. Those subtle differences might, however, not be easily detectable with current instrumentation. Finally, the $(f+i)/r$ ratio (often noted $\mathscr{G}$) can also pinpoint the nature of the X-ray plasma. For $\mathscr{G}$ values close to 4, the plasma is dominated by photoionization; if close to 1, the collisions are preponderant. In addition, the $(f+i)/r$ ratio is a sensitive indicator of the temperature, as is the ratio of H-like to He-like lines, although at very high densities the *r* line

[5] It should be noted that the reasoning above applies only to single objects. For some hot binaries, strong forbidden lines have been observed, while intercombination lines remain negligible (Pollock et al. 2005). This is sometimes taken as a typical signature of X-rays arising in wind–wind interactions (see also Sect. 4.5). The proposed explanation is twofold: first, the wind–wind interaction occurs far from the stellar surfaces, thereby decreasing the impact of the UV flux; second, the forbidden line could be boosted by inner-shell ionization of Li-like ions.

is affected by the collisional transition of $^1S_1 \rightarrow {}^1P_1$. To help in the interpretation of high-resolution spectra, Porquet et al. (2001) performed extensive calculations of $\mathscr{R}$ and $\mathscr{G}$ values for a large range of densities, plasma temperatures and stellar temperatures in the case of the most abundant He-like ions (C, N, O, Ne, Mg, Si). These results, available at CDS, do not rely on the approximate formula quoted above for the *f/i* ratio but take into account all atomic processes, notably the blending of *fir* lines with dielectronic satellite lines (whose exact contribution depends on the assumed temperature and spectral resolution). On the other hand, they were calculated assuming the stellar flux to be a blackbody, whereas most other authors rather use the approximate formula but rely on detailed atmosphere models (such as Kurucz or TLUSTY).

To go further in the interpretation of the new high-resolution data, Owocki and Cohen (2001) (see also the precursor works of Macfarlane et al. 1991) presented detailed calculations of the X-ray line profiles expected for hot stars, when assuming that the X-ray emitting material follows the bulk motion of the wind. Such so-called exospheric models depend on four parameters. First, the exponent β of the velocity law

$$v(r) = v_\infty \left[1 - \frac{R_*}{r}\right]^\beta . \tag{19}$$

Second, the exponent q involved in the radial dependence of the volume filling factor ($f[r] \propto r^{-q}$), which reflects variations with radius of the temperature or of the emission measure of the X-ray emitting plasma. Third, a typical optical depth τ_*, which depends on the wind properties:

$$\tau_* = \frac{\kappa \dot{M}}{4\pi v_\infty R_*}. \tag{20}$$

Finally, the onset radius R_0, below which there is no production of X-rays. The last two parameters were found to be the most critical ones: the blueshifts and line widths of the line profiles clearly increase with increasing τ_* and/or R_0, while the profiles are much less sensitive to changing values of q or β. In this framework, a coronal model can be reproduced by setting $R_0 = R_*$ and choosing high values of q, while a wind-shock model rather requires lower values of q and larger values of R_0. The former always produces narrow, symmetric profiles, with little or no blueshift; the latter generates broad lines (generally FWHM$\sim v_\infty$) whose exact shape depends on the opacity. In the optically thin case ($\tau_* \sim 0$), the line profile expected for a wind-shock model is flat-topped, unshifted and symmetric. For more absorbed winds, the redshifted part of the line, arising from the back side of the star's atmosphere, suffers more absorption and is therefore suppressed: the line profile appears blueshifted and skewed (see Fig. 24). In addition, there should be some wavelength dependence of the line profiles since the absorption is strongly wavelength-dependent: the high-energy lines should appear narrower (lower values of τ_* and R_0), although this effect is often mitigated by the larger instrumental broadening at these energies.

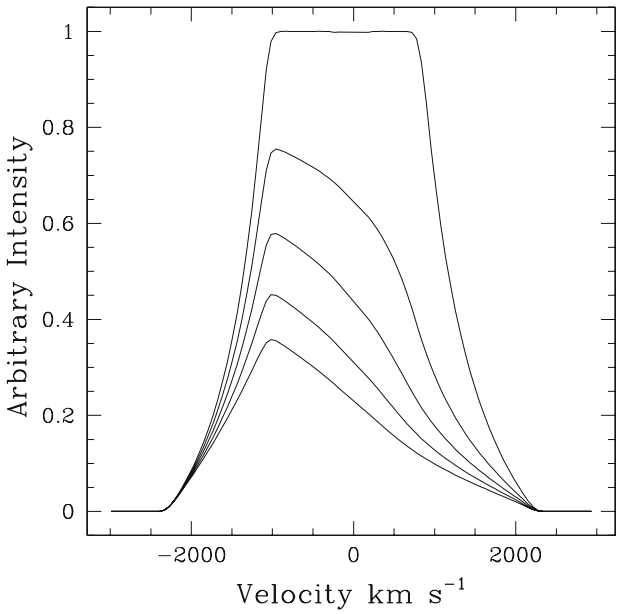

Fig. 24 Theoretical X-ray line profiles expected for an exospheric model with $v_\infty = 2{,}300\,\mathrm{km\,s^{-1}}$, $q = 0$, $\beta = 1$, $R_0 = 1.8\,R_*$ and increasing opacities τ_* (from 0 to 2 in steps of 0.5) (figure courtesy of G. Rauw)

4.2.2 Results from high-resolution spectra

Before the advent of XMM-*Newton* and CHANDRA, only low- or medium-resolution spectra were available to X-ray astronomers. These data led to the determination of four main observables: the temperature(s) of the plasma, the degree of absorption, the temporal variability, and the overall flux level. The current X-ray facilities have indeed given some better insights into these properties (see Sect. 4.1), but they have also provided high-resolution spectra which permit to study the line ratios and the detailed shape of the line profiles for the first time. Such observations (see example in Fig. 25) have resulted in new, strong constraints on the models.

One of the first hot stars observed at high-resolution was ζ Pup (O4Ief), an early supergiant which possesses a strong wind. Kahn et al. (2001) and Cassinelli et al. (2001) report on XMM-*Newton* and CHANDRA observations, respectively. They found that the line profiles are blueward skewed and broad (HWHM $\sim 1{,}000\,\mathrm{km\,s^{-1}}$), as expected for a wind-shock model. By estimating the emission measures (EMs) for each line ($\mathrm{EM} = 4\pi d^2 F_{\mathrm{line}}/\mathrm{Emissivity}(T_e)$, with d being the distance and F_{line} the line flux), Kahn et al. (2001) further showed that ζ Pup displays a large overabundance in nitrogen and that only a small fraction of the wind emits X-rays (since the measured EMs are much smaller than the EM available from the whole wind). The *fir* triplets indicate line formation regions at a few stellar radii, compatible with the radii of optical depth unity at the wavelengths considered. These radii appear smaller for high nuclear charge ions (such as Si and S) than for lighter elements (such as O, Ne, Mg, Cassinelli et al. 2001). Finally, the N VII Lyα 24.79 Å line seems broader and

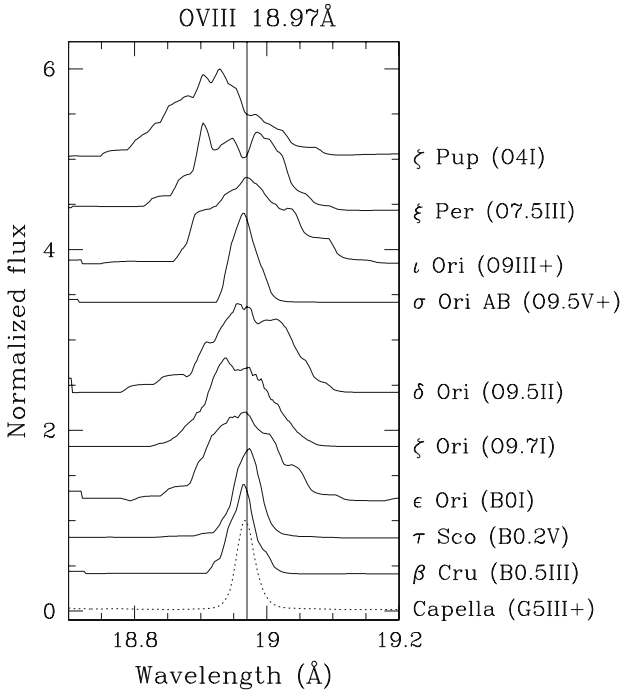

Fig. 25 Observed line profiles for O VIII λ18.97Å in a sample of bright OB objects and in the coronally active late-type star Capella (where the line width is mostly instrumental). The *vertical line* corresponds to the rest wavelength of the line; the normalized profiles have been shifted upward by an arbitrary amount for clarity (data taken from the Xatlas database and smoothed by a box of 4 pixels half width)

either flat-topped (Cassinelli et al. 2001) or structured (Kahn et al. 2001), suggesting a formation in more remote regions of the wind. However, this feature could rather be explained by a blend of this line with N VI Heβ 24.90 Å (Pollock 2007). Overall, although a qualitative agreement with the wind-shock model was readily found, a more detailed, quantitative comparison awaited the work of Kramer et al. (2003). These authors found that profiles of the kind derived by Owocki and Cohen (2001) yield rather good fits, but they discovered two intriguing problems. First, the good fits by a spherically symmetric wind model were found for a wind attenuation about five times smaller than the one expected from the known mass-loss rate ($\tau_*^{\rm exp} = 4$–30 vs. $\tau_*^{\rm obs} = 0$–5, see also Oskinova et al. 2006). Second, the derived τ_* appeared rather similar for all lines, i.e., it seemed independent of wavelength (Kramer et al. 2003), although the error bars were rather large. Cohen et al. (2009, submitted) recently re-investigated the CHANDRA spectrum of ζ Pup, by considering more lines and by using the HEG data in addition to the MEG data. They now found a significant variation of the optical depth with wavelength, compatible with the atomic opacity expected for a mass-loss rate of $\sim 3 \times 10^{-6}\, M_\odot\, {\rm year}^{-1}$ (about three times lower than in the literature).

The situation at first appeared quite different for the O9.7Ib star ζ Ori A. In Waldron and Cassinelli (2001), the line profiles were reported as broad (HWHM $= 850 \pm 40\ {\rm km\,s^{-1}}$) but symmetric, unshifted and Gaussian rather than flat-topped.

Again, as for ζ Pup, emission from high-energy ions seems to be produced closer to the stellar surface than for low-energy ions (at $1.2 \pm 0.5\ R_*$ for Si XIII, but at a few stellar radii for other elements). These results were confirmed by Raassen et al. (2008), but challenged by Leutenegger et al. (2006) and Cohen et al. (2006)—the latter two using the same CHANDRA data as Waldron and Cassinelli (2001)—as well as by Pollock (2007), who relies on the same XMM-*Newton* data as Raassen et al. (2008). Although they used different techniques, both Cohen et al. (2006) and Pollock (2007) detected slight asymmetries and blueshifts (up to $-300\,\mathrm{km\,s^{-1}}$) in the line profiles of ζ Ori A. Cohen et al. (2006) also showed that wind profiles with $\tau_* = 0.25$–0.5, $R_0 \sim 1.5\ R_*$ and $q \sim 0$ yield significantly better fits than simple Gaussians: some wind attenuation is thus needed. However, as first found for ζ Pup, the observed mean opacity is smaller than expected (Cohen et al. 2006) and no clear trend of the opacity with wavelength was detected. Cohen et al. (2006) argue that, taking into account a reduced mass-loss rate and the presence of numerous ionization edges, the opacity variations over the considered wavelength range might be smaller than first thought albeit compatible with the data, within uncertainties. As was done for ζ Pup, Wollman et al. (2009, in preparation) re-analyzed the CHANDRA data of ζ Ori: a significant, although small, trend in the optical depths is now detected, which is compatible with the wind opacity if the mass-loss rate from literature is decreased by a factor of 10.

The late-O stars δ Ori A (O9.5II + B0.5III) and ζ Oph (O9.5Ve) both display symmetric and broad X-ray lines although they are much narrower than those of ζ Pup and ζ Ori A (HWHM $= 430 \pm 60\,\mathrm{km\,s^{-1}}$, Miller et al. 2002, and HWHM $= 400 \pm 87\,\mathrm{km\,s^{-1}}$, Waldron 2005, respectively). On the basis of its mass-loss rate, δ Ori A should be an intermediate case between ζ Pup and ζ Ori A: narrower profiles are therefore quite surprising. In addition, the lines of δ Ori A are unshifted (centroid at $0 \pm 50\,\mathrm{km\,s^{-1}}$) and the *fir* ratios indicate a formation region one stellar radius above the photosphere (which is more in agreement with a wind-shock model than a coronal model), at a position similar to that of optical depth unity. However, δ Ori A is a binary and one may wonder whether peculiar effects such as interacting winds could have an impact on its X-ray emission. This does not seem to be the case since no phase-locked variations of the X-ray flux were ever reported for this object (Miller et al. 2002)—it must be noted, though, that the changes might be quite subtle for such late-type O + B systems, see, e.g., the case of CPD−41°7742 in Sect. 4.5. In contrast, the lines of ζ Oph appear slightly blueshifted; their width might decrease for low-energy lines, and the formation radii derived from the *fir* ratios differ from the radius of optical depth unity. This star is a known variable, in the optical as well as in X-rays (see, e.g., Oskinova et al. 2001), and Waldron (2005) reports a change in the formation radius derived from the Mg XI triplet between two CHANDRA observations separated by 2 days.

The narrowest profiles among O-type stars were found for σ Ori AB (O9.5V + B0.5V, Skinner et al. 2008a and Fig. 25): HWHM $= 264 \pm 80\,\mathrm{km\,s^{-1}}$, or 20% of the terminal velocity. For this star, the X-ray lines again show no significant shift and the most constraining *fir* ratios point to a formation region below $1.8\ R_*$.

Since more observations are now available, some authors have undertaken a consistent, homogeneous analysis of several objects. This indeed eases the comparison between different objects but, as already seen earlier, the results sometimes disagree between different teams. Using their "distributed" *fir* model, Leutenegger et al. (2006)

found onset radii of 1.25–1.67 R_* for ζ Pup, ζ Ori, ι Ori, and δ Ori A, without any large differences for high-mass species such as Si XIII. Such a radius rules out a coronal model but can still be reconciled with a wind-shock model. Leutenegger et al. (2006) further explain their differences with Waldron and Cassinelli (2001) by (1) calibration problems at the beginning of the CHANDRA mission, and (2) different atmosphere models (TLUSTY vs. Kurucz) which give fluxes different by a factor of 2–3 shortward of the Lyman edge, at wavelengths responsible for exciting the Si XIII transitions.

Waldron and Cassinelli (2007) (see errata in Waldron and Cassinelli 2008) examined the high-resolution spectra of 17 OB stars. The sample contains 2 known magnetic objects (see Sect. 4.6) and 15 stars considered as "normal" by the authors; however, we note that 3 of these, 9 Sgr and the stars in Cyg OB2, are well known binaries displaying wind–wind interactions detected at X-ray energies (Rauw et al. 2002a, 2005; De Becker et al. 2006); this likely explains the peculiar, deviant results sometimes found by the authors for these stars. Overall, when the lines are analyzed by simple Gaussian profiles, 80% of their peaks appear within $\pm 250\,\mathrm{km\,s^{-1}}$ of the rest wavelength. The distribution of the line positions peaks at $0\,\mathrm{km\,s^{-1}}$, but is heavily skewed (many more blueshifts than redshifts) and this asymmetry increases with the star's luminosity. The line HWHMs are distributed between 0 and $1{,}800\,\mathrm{km\,s^{-1}}$, i.e., they are always less than the terminal velocity and most of the time they are less than half that value; there is a slight trend toward narrower lines (expressed as a fraction of the terminal velocity) for main-sequence objects. These widths appear also larger than the velocity expected at the position derived from the *fir* triplets (using a localized approach and Kurucz atmosphere models). Both width and shift seem to be independent of wavelength (see however the results of new analyses mentioned above). Finally, the formation radii found from triplets of heavier ions are smaller than those of lighter ions and the lower temperatures, derived from the ratios of lines from H and He-like ions, are only found far from the photosphere.

Despite some discrepancies in the interpretations, as shown above, several conclusions are now emerging from the analysis of high-resolution spectra:

1. Only a small fraction of the wind emits, as expected.
2. The X-ray lines are broad, although not as broad as predicted (HWHM = 0.2–0.8 v_∞).
3. The profiles are more symmetric than expected, without evidence for flat-topped shapes.
4. Except for ζ Pup, the blueshifts are small or non-existent.
5. The opacities derived from fits to the profiles are lower than expected.
6. For a given star, the line profiles and fitted opacities are generally quite similar regardless of the wavelength, although error bars are large and shallow trends cannot be excluded (indeed, some were found in a few cases).
7. From the analysis of the *fir* ratios, the (minimum) radius of the X-ray emitting region appears rather close to the photosphere (often $<2\,R_*$ for the most stringent constraints), although there is disagreement about the possibility of a formation at or very close ($r < 1.1\,R_*$) to the photosphere. The formation radius is generally compatible with the radius of optical depth unity, which can be easily understood:

the emissivity scales with the square of the density; therefore, the flux will always be dominated by the densest regions that are observable. As the density decreases with radius, these regions are the closest to the star, i.e., they are just above the "X-ray photosphere" (radius of optical depth unity).

4.2.3 A new paradigm?

The characteristics of the X-ray lines enumerated above were not fully in agreement with the expectations of the wind-shock model. Therefore, some adjustments of the models have been proposed. They fall in five broad classes: resonance scattering, decrease of mass-loss rate, porosity, combination corona + wind, and a complete change of concept.

In most cases, X-ray plasmas associated with hot stars are considered to be optically thin, hence the use of optically-thin thermal plasma models. Ignace and Gayley (2002) rather suggested that resonant scattering could play a significant role, especially for the strongest lines. In fact, their detailed line profile modeling showed that an optically-thick line appears much more symmetric and less blueshifted than in the optically-thin case. This arises from the fact that the Sobolev line interaction region is radially elongated and that X-rays can thus escape more easily laterally than radially, reducing the strength of the blue/red wings. Their calculations of line shift and width agreed well with those of ζ Pup, but the line profiles of ζ Ori and θ^1 Ori C were more difficult to reproduce. An evaluation of the impact of resonance scattering for Fe XVII in δ Ori A showed that some weak opacity effect might affect the strongest X-ray lines, but the optically-thin case was still well within the error bars (Miller et al. 2002). Leutenegger et al. (2007) incorporated resonance scattering into the models of Owocki and Cohen (2001). They showed that for ζ Pup, including resonance scattering provides a better fit, but that some discrepancies remain. In addition, they showed that resonance scattering only has a significant effect for large filling factors ($\gg 10^{-3}$), which could be a problem for winds of massive stars (see below). Finally, it should be noted that in the above calculations including resonance scattering, Leutenegger et al. (2007) were able to fit the line profiles without any large reduction of the mass-loss rate.

Reducing the mass-loss rates can naturally solve many of the discrepancies mentioned earlier since it leads to more symmetric and less blueshifted line profiles (see Owocki and Cohen 2001) as well as reduced and less wavelength-dependent opacities. Cohen et al. (2006) strongly advocate in favor of that solution following their analysis of ζ Ori. The trends detected by Cohen et al. (2009, submitted) and Wollman et al. (2009, in preparation) again favor this scenario. Such a reduction of the mass-loss rate was also envisaged from results at other wavelengths (UV, optical), some authors even proposing a decrease by one or two orders of magnitude (e.g., Fullerton et al. 2006, see however remarks in Oskinova et al. 2007). However, such a drastic reduction of the mass-loss rates might be in conflict with the absorption values measured for high-mass X-ray binaries. Notably, to explain the X-ray observations, Watanabe et al. (2006) need a mass-loss rate of $1.5\text{–}2.0\times10^{-6} M_\odot$ year^{-1} for the B0.5Ib primary of Vela X-1. More reasonable decreases by a factor of a few (2–10) are now commonly envisaged, especially in the context of (micro)clumping (see below and the outcome

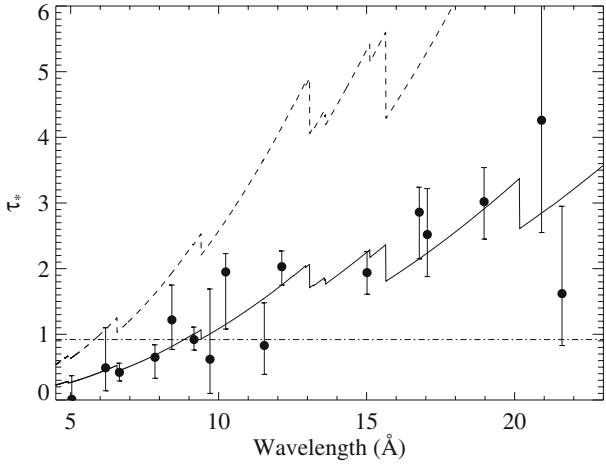

Fig. 26 Variation with wavelength of the opacity τ_* derived from line-profile models of Owocki and Cohen (2001) for the star ζ Pup. The observations correspond to the dots, the *dash-dot line* represents a constant opacity, the *dashed line* the opacity variation expected from the literature mass-loss rate and the *solid line* the opacity variation for a reduced mass-loss rate (figure courtesy of D. Cohen)

of the 2007 Potsdam meeting), and they are compatible with fits to the X-ray lines—at least for ζ Pup (Cohen et al. 2009, submitted; Fig. 26) and ζ Ori (Wollman et al. 2009, in preparation).

Because of the unstable line-driving mechanism propelling the wind, it is expected that the wind is not smooth. Indeed, evidence for clumping has been found observationally: stochastic variability of optical lines associated with the wind (e.g., Eversberg et al. 1998; Markova et al. 2005), model atmosphere fits of UV lines (Bouret et al. 2005), temporal and/or spectral properties of some high-mass X-ray binaries (Sako et al. 2003; van der Meer et al. 2005). A wind composed of dense clumps in a rarefied gas has two interesting consequences. First, a reduction of the mass-loss rate by a factor $\sqrt{f}$, where f is the volume filling factor of these clumps. This reduction amounts to less than 10 and is thus not as drastic as those mentioned above. Second, the possibility of leakage, resulting in reduced opacity and more symmetric profiles, in the case of optically-thick clumps (Fig. 27). In this case, X-rays can avoid absorption by the dense clumps if the radiation passes in the (nearly) empty space between them. The wind is then said to be porous and the opacity is no more atomic in nature, i.e., determined by the plasma physical properties, but is rather *geometric*, i.e., it depends only on the clump size and interclump distance. Feldmeier et al. (2003) and Oskinova et al. (2006) have envisaged the consequences of such a structured wind. Their model uses a wind composed of hot parcels emitting X-rays and cool dense fragments compressed radially and responsible for the absorption. The line profile is severely affected, being less broad and less blueshifted as well as more symmetric than in the homogeneous wind case of equivalent mass-loss rate (Fig. 27). For optically thick clumps, the resulting opacity is effectively gray, and the line profile should thus be independent of wavelength. As the clumps become more and more optically

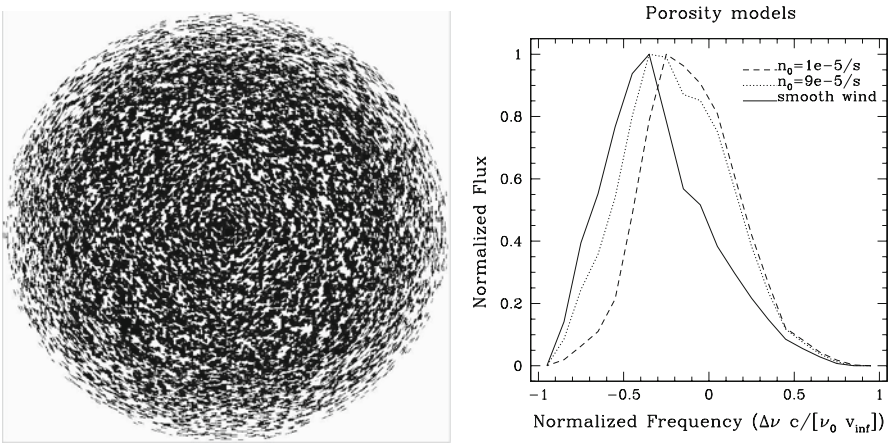

Fig. 27 *Left* Sketch of a porous wind (see Feldmeier et al. 2003). *Right* X-ray lines expected in a homogeneous wind and winds with optically thick clumps (the fragmentation frequency n_0 represents the number of clumps passing through some reference radius per unit time—data courtesy L. Oskinova)

thin, the differences with a homogeneous wind decrease and finally disappear. For ζ Pup, Oskinova et al. (2006) showed that using the strongly reduced mass-loss rate suggested by Fullerton et al. (2006) causes the blueshift to be too small compared to observations. However, a porous wind with only moderate reduction of the mass-loss provides good fits. Porosity can thus greatly help in reducing the opacity and getting wavelength-independent properties without a drastic reduction of the mass-loss rate which could potentially be problematic. However, the origin and consequence of porosity have been questioned by Owocki and Cohen (2006). These authors showed that, for a clumped wind, the opacity depends on the so-called porosity length l/f where l is the size of the clumps and f the volume filling factor. For optically-thick clumps, the most favorable case, getting symmetric lines requests $l/f \gtrsim r$: either the clumps have large scales, or the filling factor is small (hence the clump compression is high), or a combination of both is needed. However, hydrodynamic simulations show that the line-driven instability leads to small-scale (typically $l \sim 0.01\,R_*$) and moderately compressed ($f \sim 0.1$) clumps. A porosity in agreement with the observations would thus have another origin than the intrinsic instabilities of the wind. In addition, large clumps separated by large distances might lead to significant temporal variability in the X-ray light curve, which is not detected. Finally, the gray opacity contradicts the shallow but non-zero wavelength-dependence observed at least in ζ Pup and ζ Ori (Cohen et al. 2009, submitted and Wollman et al. 2009, in preparation). Therefore, the presence of large, optically thick clumps can most probably be discarded. However, we cannot rule out that smaller, less opaque clumps exist in the stellar winds.

Waldron and Cassinelli (2007, 2009) rather advocated for a partial return of the magnetic corona hypothesis. More precisely, they assumed a wind-shock model in the outer wind regions, where lines associated with low-mass ions arise, combined with a coronal model close to the star, which would produce the lines from the

highly-ionized high-mass species. As support for their combined idea, Waldron and Cassinelli (2007) emphasized three annoying facts. First, the formation radii derived from *fir* triplets agree quite well with radii of optical depth unity, as could have been expected. If a decrease of the mass-loss rate is considered, then one would have to explain why the formation region lies much above the X-ray photosphere. Second, the radii derived from *fir* triplets indicate, at least for Si XIII, formation regions very close to the photosphere. In some cases, the small estimated radii might even disagree with the typical onset radius, $0.5\,R_*$ above photosphere, of the wind-shock model. Third, the high-mass ions systematically display smaller formation radii than their lower-mass counterparts. At these small radii, the wind velocity is too low to get the observed broad lines and high post-shock temperatures. Waldron and Cassinelli (2009) proposed a theoretical model where plasmoids produced by magnetic reconnection events are rapidly accelerated; they emphasized that these plasmoids are not clumps but "isolated magnetic rarefactions". However, as mentioned above, Leutenegger et al. (2006), Cohen et al. (2006) and Oskinova et al. (2006) have challenged their radius calculations. Another caveat can be noted: Waldron and Cassinelli (2007) rely on the wind opacity calculated as in Waldron (1984); in that model, the wind is supposed to have a temperature of $0.8\times T_{\rm eff}$ at any position in the wind, which leads to a high ionization throughout the wind, thereby strongly reducing the opacity at low energies. However, such high temperatures at any radii might not be entirely physical (see, e.g., Macfarlane et al. 1993). In a different context, we will come back to the impact of magnetic fields on stellar winds in Sect. 4.6.

A more radical shift in thought was proposed by Pollock (2007). Up to now, it was considered that particle interactions in winds take place through long-range Coulomb interactions. This explained the redistribution of momentum from a minority of UV-driven ions to the rest of the flow. However, it seems that the mean free path for ion–ion Coulomb collisions is not small (Pollock 2007): for ζ Ori, it is $0.1\,R_*$ at $3\,R_*$ above the photosphere and $1\,R_*$ at $10\,R_*$. Therefore, Pollock (2007) proposes the shocks to be collisionless, like in SNRs. Any dissipation of energy would occur through other phenomena, probably linked to magnetic fields. In addition, the time scale for post-shock equilibrium appears very long (corresponding to a flow distance of a few stellar radii for electrons), thereby suggesting that no full equilibrium is ever established. In this model, the X-ray lines would arise far from the star, through ion–ion interactions such as ionization and charge exchange. Pollock (2007) claims that this would explain the faint continuum emission at X-ray wavelengths (the electrons being too cold for a significant bremsstrahlung in this domain) and the observed line profiles. As the author mentions in his paper, a more quantitative assessment of this idea must await a detailed modeling. It is, however, worth noting that collisionless shocks and non-equilibrium phenomena were also proposed, although in a different context, by Zhekov (2007, see below).

At present, it is still difficult to assert which solution applies best, or which combination of the above is closer to reality. Certainly, this will be a task for the next generation of X-ray facilities.

Table 5 Observed properties of the high-resolution X-ray spectra of early B-type stars

Name	Sp. type	HWHM ($km\,s^{-1}$)	kT (keV)	$\log(L_X/L_{bol})$	References
ϵ Ori	B0I	~1,000	0.2–0.3		Zhekov and Palla (2007)
τ Sco	B0.2V	200–450	1.7	−6.3	Mewe et al. (2003)
					Cohen et al. (2003)
θ Car	B0.2V + late	<400[c]	0.2	−7.0	Nazé and Rauw (2008)
β Cru A	B0.5III + B2V	140	0.2	−7.7	Cohen et al. (2008)
θ^1 Ori A	B0.5V + A0 + lateB	<160[c]	>1.3[a]	−6[b]	Schulz et al. (2003)
					Stelzer et al. (2005)
β Cep	B1V	<450[c]	0.2	−7.2	Favata et al. (2008)
β Cen	B1III	<440[c]	0.2	−7.2	Raassen et al. (2008)
Spica	B1III-IV		0.2–0.3		Zhekov and Palla (2007)

[a] 70% of the X-ray flux come from hot plasma (i.e., with $T > 1.5\times10^7$ K, Schulz et al. 2003)
[b] Note that the flux values of Stelzer et al. (2005) do not agree with those of Schulz et al. (2003)
[c] Unresolved lines

4.3 The case of early B-stars

The previous section focused on results derived from observations of O-type stars. However, a sample of early B-type stars was also observed at high resolution with the current facilities. In their case too, surprises are common and the overall picture appears quite contrasted.

While the X-ray lines of the O-type stars often appear broad, especially for luminous objects with strong winds, the X-ray lines of B-type stars were found to be particularly narrow, except for the B0I supergiant ϵ Ori (see Fig. 25; Table 5). These narrow lines were reported to be symmetric and unshifted, with the exception of a possible asymmetry in β Cen (Raassen et al. 2005). The *fir* triplets usually favored formation radii at distances of 1.5–5 R_* from the star.

The hardness of the spectrum and the overall emission level were found to vary from star to star (see Table 5). On the one hand, τ Sco emits hard X-rays and displays a clear overluminosity (Mewe et al. 2003; Cohen et al. 2003). This seems also to be the case of θ^1 Ori A and E (Schulz et al. 2003). Note, however, that the presence of a low-mass companion to θ^1 Ori E (Herbig and Griffin 2006) might lead to a revision of the above results for this star.

On the other hand, the X-ray emission from the B-type stars ϵ Ori, θ Car, β Cru A, Spica, β Cen, and β Cep appears much softer. For the first four stars, the distributions of the differential emission measure (DEM) as a function of temperature display peaks centered on 0.2–0.3 keV, with FWHMs of 0.1–0.3 keV, and without hard tails (Zhekov and Palla 2007; Nazé and Rauw 2008). Hottest thermal components (0.6 keV) were detected for β Cen, β Cep, and β Cru A, but they are clearly not dominant (the main component is at about 0.2 keV for these objects, Raassen et al. 2005; Favata et al. 2008; Cohen et al. 2008). The X-ray emission levels are also much more modest, with $L_X - L_{bol}$ ratios of about −7 dex (see Table 5).

Among the investigated B-stars were three known β Cephei pulsators: β Cru A, β Cen, and β Cep (Cohen et al. 2008; Raassen et al. 2005; Favata et al. 2008). While no significant variation of the flux was detected for the latter two objects, β Cru A displays some variability of its hard emission at the primary and tertiary pulsation periods. However, as the maxima of the optical and X-ray light curves appear phase-shifted by a quarter of a period and as the variability is of very modest amplitude, these changes need to be confirmed. The blue straggler θ Car, which is not a known pulsator, displays some variability but only on long-term ranges (between ROSAT, Einstein and XMM-*Newton* observations, Nazé and Rauw 2008).

While the soft character of the X-ray emission and the values of the formation radii are compatible with the wind-whock model described in Sect. 4.2, the narrow lines clearly constitute a challenge for this scenario. Hard X-ray emission is also a problem in such objects since they possess much weaker winds than O stars. The exact origin of the X-ray emission of these B-type stars therefore remains a mystery up to now (see, e.g., the extensive discussion in Cohen et al. 2008) but some proposed explanations rely on the possible impact of a magnetic field (see Sect. 4.6).

To conclude this section, a last comment on the peculiar case of Be stars should be made. One such star was studied in detail with CHANDRA: γ Cas (B0.5IV, Smith et al. 2004). γ Cas appears particularly bright in X-rays, although it is less luminous than X-ray binaries. Its X-ray emission consists of a strong continuum (a bremsstrahlung with $kT = 11$–$12\,\mathrm{keV}$), some broad (HWHM$\sim$600 km s^{-1}) and symmetric X-ray lines from ionized metals (an optically thin plasma with 4 components, with temperatures ranging from 0.15 to 12 keV), and fluorescence K features from iron and silicon. For the photoionized plasma, different iron abundances were found for the hot and the warm component, which might indicate the presence of the FIP effect and at least point toward different emission sites. In addition, while the warm and most of the hot components display similar absorption, part of the hot component appears more strongly absorbed. Smith et al. (2004) suggest that these hard X-rays are seen through the dense regions of the Be disk, while most of the X-ray emission (warm + most of the hot plasma) is only absorbed by the stellar wind or the outer, less dense regions of the disk. The presence of fluorescence features indeed suggests that some cold gas is present close to the X-ray emission regions. Li et al. (2008) further presented models for generating X-rays in Be stars. According to these authors, the collision of the magnetically channeled wind (see Sect. 4.6) with Be disks could explain the emission of B-stars down to types B8 without the need for a companion.

4.4 Do Wolf-Rayet stars emit X-rays?

Wolf-Rayet stars (WRs) are the evolved descendants of O-type stars. They come in three "flavors", WN, WC, and WO, which refer to spectra dominated by nitrogen, carbon, or oxygen lines, respectively. In the evolutionary sequence of hot stars, WC and WO objects are expected to correspond to later stages than WN stars, explaining their metal-rich composition. Both types display mass-loss rates on average ten times larger than for their O-type progenitors. These winds, denser and enriched in metals, are much more opaque to X-rays than those of O stars, especially in the WC case. One may thus naively expect WRs stars to be less X-ray bright than O stars.

The first X-ray observations of WRs indeed provided results quite in contrast with those of O-type stars. The detection fraction was much smaller for WRs and no $L_X - L_{bol}$ relation was found for the detected objects (Wessolowski 1996), although the latter fact could be explained theoretically by assuming a particular relation of the X-ray flux on the wind properties, and by taking into account the absorption by the dense, enriched winds (Ignace and Oskinova 1999). An overall view of the situation 10 years ago was presented by Pollock (1995) and Pollock et al. (1995): only 20 WRs were clearly detected by ROSAT (i.e., detection statistic $\lambda > 10$), which corresponds to about 10% of the WRs listed in the VIIth catalog of Galactic WRs (van der Hucht 2001). Using this catalog, it appears that 7 of these stars belonged to the WC category, 12 were WN and 1 WN/WC; 6 of these were supposedly single (4WN + 1WC[6] + 1WN/WC[7]), 4 were candidate binaries (3WN + 1WC), and 10 were known binaries (5WN + 5WC) at that time. As for O-type stars, WR binaries appear brighter than single objects, most probably because of wind–wind interactions (see Sect. 4.5). In addition, WN stars were found to be on average four times brighter than WC stars.

With so few WRs detected, small number statistics could bias the results; investigations with higher sensitivity were thus crucially needed in order to settle the question about the intrinsic strength of the WR X-ray emission. About 20% of the presumably single WCs were observed using ASCA, XMM-*Newton*, or CHANDRA: WR60, 111, 114, 118, 121, 144 (Oskinova et al. 2003) and WR5, 57, 90, 135 (Skinner et al. 2006a). These studies now place stringent constraints on the intrinsic emission of WC objects, with limits on $\log[L_X/L_{bol}]$ between -7.4 and -9.1 (Table 6). This suggests that either there is no intrinsic X-ray emission in WRs of WC type, which would be surprising because of the presence of radiatively driven winds similar to O-stars (see Sect. 4.2), or that the emission takes place deep in the wind and is then completely absorbed.

The case of single WN stars is less clear-cut (Table 6). On the one hand, a few putatively single WN-type objects were found to be clear X-ray emitters in recent observations. WR6 and WR110 are rather bright ($L_X^{unabs} \sim 5 \times 10^{32}$ erg s^{-1}) and display two main thermal components at 0.5 and >3 keV (Skinner et al. 2002b,a). For WR46, three temperatures provide the best fit: 0.15, 0.6, and 2–3 keV (Gosset et al. 2009, in preparation). The high temperature is quite unusual for single objects and is not predicted by shocked wind models—it is rather reminiscent of X-ray emission from interacting winds. The observed variations in the optical (WR6 and WR46) or in X-rays (WR46 and WR110) also suggest a possible binary nature for these stars. However, WR147 displays hints of a non-zero X-ray emission associated with the WR component (Pittard et al. 2002) and WR1 presents a soft spectrum, with little emission above 4 keV, in contrast to the three previous objects (Ignace et al. 2003). In the latter case, the possible presence of an absorption edge due to ionized sulfur further indicates absorption unrelated to the neutral ISM and rather linked to the hot wind: the X-ray emission would thus occur at some depth inside the wind. Ignace et al. (2003)

[6] This object is WR111, whose clear detection was subsequently challenged (Oskinova et al. 2003). It now appears that this old detection was a false alarm.

[7] This object is WR20a, subsequently found to be a very massive binary of type WN6ha + WN6ha (Rauw et al. 2004).

Table 6 X-ray properties of suspected single Wolf-Rayet stars in our Galaxy

Name	Sp. type	L_X (erg s^{-1})	$\log(L_X/L_{bol})$	Remarks	References
Detected Wolf-Rayet stars (XMM-Newton *and* CHANDRA)					
WR1	WN4	2.0×10^{32}	−6.6	P	Ignace et al. (2003)
WR3	WN3	2.5×10^{32}	−6.8		Oskinova (2005)
WR6	WN4	1.7×10^{32}	−6.6	HP	Skinner et al. (2002b)
WR20b	WN6	1.6×10^{33}	−6.2	H	Nazé et al. (2008a)
WR42d	WN5	4.0×10^{32}	−6.7		Oskinova (2005)
WR44a	WN5	1.6×10^{31}	−8.1		Oskinova (2005)
WR46	WN3	2.4×10^{32}	−7.0	P	Gosset et al. (in preparation)
WR110	WN5	7.2×10^{31}	−7.1	HP	Skinner et al. (2002a)
WR136	WN6	7.9×10^{30}	−8.8		Oskinova (2005)
WR152	WN3	3.2×10^{31}	−7.3		Oskinova (2005)
Other detected Wolf-Rayet stars (ROSAT)					
WR2[a]	WN2	7.9×10^{31}	−7.3		Oskinova (2005)
WR7	WN4	2.0×10^{32}	−6.6		Oskinova (2005)
WR18	WN5	2.5×10^{32}	−6.9		Oskinova (2005)
WR78	WN7	1.3×10^{31}	−8.7		Oskinova (2005)
WR79a	WN9	7.9×10^{31}	−7.7		Oskinova (2005)
Undetected Wolf-Rayet stars					
WR5	WC6	$<9.3\times10^{30}$	<−7.7		Skinner et al. (2006a)
WR16	WN8	$<1.0\times10^{30}$	<−8.9		Oskinova (2005)
WR40	WN8	$<4.0\times10^{31}$	<−7.6		Gosset et al. (2005)
WR57	WC8	$<8.9\times10^{30}$	<−8.1		Skinner et al. (2006a)
WR60	WC8		<−8.2		Oskinova et al. (2003)
WR61	WN5	$<5.0\times10^{30}$	<−8.1		Oskinova (2005)
WR90	WC7	$<1.9\times10^{30}$	<−8.7		Skinner et al. (2006a)
WR111	WC5		<−7.8		Oskinova et al. (2003)
WR114	WC5		<−9.2		Oskinova et al. (2003)
WR118	WC9		<−7.4		Oskinova et al. (2003)
WR121	WC9		<−7.4		Oskinova et al. (2003)
WR124	WN8	$<2.0\times10^{32}$	<−6.6	P	Oskinova (2005)
WR135	WC8	$<6.6\times10^{29}$	<−9.1		Skinner et al. (2006a)
WR144	WC4		<−7.4		Oskinova et al. (2003)
WR157	WN5	$<4.0\times10^{31}$	<−7.9		Oskinova (2005)

Quoted luminosities correspond to observed values, i.e., without dereddening, for detected objects and to upper limits for undetected stars. The letters H and P in the remarks column indicate the presence of a hard tail (or hot component) and of periodicities (either in optical, X-rays, or both), respectively. Note that the quoted limits correspond to different significance levels (e.g., conservative estimate from Gosset et al. 2005 vs. 1-σ in Oskinova et al. 2003)

[a] In a recent poster, Skinner et al. (2008b) presented the first results from CHANDRA observations of WR2 (L_X=1.3×10^{32} erg s^{-1}, $\log[L_X/L_{bol}] = -6.9$), but also of WR24 (WN6, L_X=9.5×10^{32} erg s^{-1}, $\log[L_X/L_{bol}] = -7.0$), and WR134 (WN6, L_X=2.7×10^{32} erg s^{-1}, $\log[L_X/L_{bol}] = -6.8$). As these authors consider their analysis preliminary, we prefer to include it only in a note

therefore proposed that the X-ray emission of WR1 would be typical of single WN objects and could explain the soft part of the spectra of WR6 and 110. On the other hand, WR40 remained undetected in a 20ks XMM-*Newton* observation (Gosset et al. 2005). This was quite surprising since this object is strongly variable in the optical domain and the changes are attributed to the unstable stellar wind: on the basis of the wind-shock model, WR40 was thus expected to be a moderate X-ray emitter. However, its non-detection yields a (very) conservative upper limit on its $\log[L_X/L_{bol}]$ of -7.6, about one order of magnitude below that of O-type stars and similar to the limits found for WCs. To reconcile the detection of WR1 and the invisibility of WR40, one might have to consider the structure of their winds in detail. The ratio $\dot{M}/v_\infty$, which intervenes in the estimation of the wind density, is 13 times larger for WR40; this difference is, however, slightly attenuated by the larger radius of WR40. In addition, WR1 presents an earlier spectral type, and its wind is consequently more ionized, i.e., less opaque. Indeed, WR1 and WR40 are not similar objects, as far as their wind and stellar properties are concerned, and their X-ray emission could thus well differ. Finally, differences in wind porosity/clumping might also impact the detection level of WRs. Contrary to WCs, whose winds invariably present large optical depths, the WN stars display a wider variety, in the visible as well as in X-rays: individual modeling is thus probably necessary for each case.

The first detection of a WO star, WR142, revealed a rather faint source with an inferred L_X/L_{bol} ratio of only 10^{-8} (e.g., similar to the upper limits on non-detections of other WRs, see above and Oskinova et al. 2009). The faintness of the source prevented any detailed spectral analysis but the hardness ratio clearly indicates a high temperature for the X-ray source which cannot be explained by the wind-shock model. This puzzling result might require to consider magnetic activity as a source of X-rays in WRs (Oskinova et al. 2009).

While most of the studies have been performed for galactic objects, Guerrero and Chu (2008a,b) as well as Guerrero et al. (2008) presented a first analysis of the X-ray emission of WRs belonging to the LMC. From the available ROSAT, CHANDRA, and XMM-*Newton* observations, which cover more than 90% of the known WRs in the LMC, only 32 objects (out of 125) were detected. They are mostly binaries: about half of the known WR binaries were observed as X-ray sources whereas the detection rate is only 10% for supposedly single objects. Many similarities with the Galactic case were found: non-detection of single WC stars, preferential detection of binaries. However, some clear differences were also discovered: larger values for the X-ray luminosities and L_X/L_{bol} ratios. While more sensitive data are certainly needed to confirm these trends, it remains to be seen whether these observations could be linked to the lower opacity of the winds in the low-metallicity environment of the LMC.

4.5 Interacting winds in hot binaries

It is well established that hot massive stars possess strong stellar winds. Therefore, if two such stars form a close pair, an interaction between the winds can be expected. The interaction region is likely to be planar if the winds are of equal strength or it will

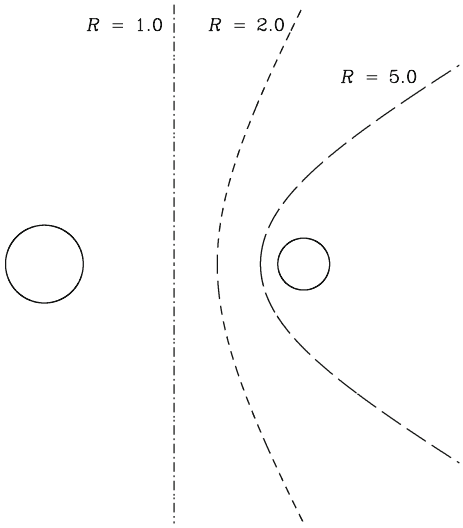

Fig. 28 Shape of the wind–wind interaction region derived from pressure equilibrium, for different wind momentum ratios R. For two winds of equal strengths ($R = 1$), the equilibrium occurs in a plane in-between the two stars; when the winds differ, the interaction region takes a more conical shape and begins to fold around the star with the weaker wind

rather appear cone-like if the winds are different (with the weaker wind inside the cone, Fig. 28). As the winds flow at tremendous speeds before colliding, the gas is heated to high temperatures: $kT = (3/16)mv^2$, which is about 4.7 keV assuming a wind of solar composition and a typical wind velocity of 2,000 km s^{-1} (Stevens et al. 1992). Plasma with such temperatures can only be observed in the high-energy domain, and X-rays thus constitute the best means to study this phenomenon. It must be noted that before the advent of sensitive X-ray facilities, only a handful of wind–wind interactions had been investigated in depth.

Theoretically, the wind–wind interactions introduced above can be separated in two classes, depending on the importance of cooling in the post-shock gas. To quantify this, one introduces the cooling parameter χ, defined as the ratio between the cooling time of the post-shock gas and the typical escape time from the shock region. It can be expressed as $\chi = v^4 D/\dot{M}$ where the wind velocity v is in units of 1,000 km s^{-1}, the distance D from the star to the shock[8] in 10^7 km, and the mass-loss rate $\dot{M}$ in $10^{-7}\ M_\odot$ year^{-1}. For $\chi \ll 1$, the gas cools rapidly and the collision is to be considered as radiative. This situation generally occurs in short-period binaries. In this case, hydrodynamic models predict that instabilities arise in the interaction region, making the collision quite turbulent, and the X-ray luminosity then follows a relation of the form $L_X \propto \dot{M} v^2$ (Stevens et al. 1992). For $\chi \geq 1$, the collision is adiabatic, the interaction thus appears smoother and the X-ray luminosity rather scales as $L_X \propto \dot{M}^2 v^{-3/2} D^{-1}$. This behavior is preferentially expected for long-period binaries.

[8] This distance can be found by considering the ram pressure equilibrium between the two flows. Considering the wind properties of the two stars (noted 1 and 2 in the following for the primary and secondary, respectively), the ratio of the separations between the shock and the star, measured along the binary axis, is $\frac{D_1}{D_2} = \sqrt{\frac{\dot{M}_1 v_1}{\dot{M}_2 v_2}} = R$ (the wind momentum ratio, see Fig. 28, Stevens et al. 1992).

According to the above considerations, several observational hints for the presence of a wind–wind interaction can be expected. First, this phenomenon provides an additional source of X-rays, on top of the intrinsic stellar contributions: such systems should thus appear overluminous. Indeed, the first X-ray observations showed that hot binaries are on average more luminous than single stars (e.g., Pollock 1987; Chlebowski and Garmany 1991). There are indications that this overluminosity might increase with the combined bolometric luminosity of the system (Linder et al. 2006). This could be readily explained if one considers that the winds are radiatively driven: larger luminosities mean stronger winds; hence stronger wind–wind interactions. Second, because of the high speeds of these winds which are colliding face-on, the X-ray emission should appear harder than the typical emission from O-type stars (kT of 1–10 vs. 0.3–0.7 keV). However, it should be noted that these first two criteria are not sufficient for ascertaining the presence of a wind–wind interaction in a given system, as other phenomena also produce additional hard X-ray emission (e.g., magnetically channeled winds, see Sect. 4.6). Finally, further evidence for the presence of a wind–wind interaction comes from the detection of modulations of the high-energy emission with orbital phase. These phase-locked variations are produced by changing absorption along the line-of-sight and/or changing separation in eccentric binaries.

Absorption changes occur as the interaction region is alternatively observed through the wind of one or the other star. These variations are, indeed, best seen in systems containing two very different winds, e.g., WR + O binaries. The most famous system in this category is definitely γ^2Vel (WC8 + O7.5III, $P = 78.5$ days). Willis et al. (1995) reported on multiple ROSAT observations of the system: they observed a recurrent strong increase of the observed X-ray emission when the O-type companion was in front of the WR star. This increase was detected in the "hard" ROSAT band, i.e., 0.5–2.5 keV,[9] and was interpreted as due to reduced absorption when the interaction region is seen through the less dense and less metal-rich (thus less opaque) O-star wind. The width of the light-curve peak was further related to an opening angle of about 50° for the shock cone. Short-term variations, detected by ASCA (Stevens et al. 1996), provide evidence for instabilities linked to the interaction region. Using high-resolution spectra, Schild et al. (2004) and Henley et al. (2005) showed that the X-ray emission was produced far from the UV sources (broad lines, large f/i ratio). The spectrum of the hot plasma was fitted with three temperatures, interpreted as coming from different regions (Schild et al. 2004): 0.25 keV (with constant absorption, this flux should be emitted far in the winds), 0.65 and 1.8 keV (both along the shock cone, the observed absorption decreasing when the line-of-sight lies inside the shock cone). For the latter components, reproducing exactly the change in the absorbing column proved rather difficult: either a decrease of a factor of four in the mass-loss rate is needed (microclumping, porosity?), or a change in the abundances (hints of a neon enrichment, suggesting a mix of O and WR material for the emitting plasma). Regarding the overall properties of the spectra, it must be noted that different metals sometimes

[9] Quite surprisingly, very soft (0.1–0.5 keV) emission was also detected in γ^2Vel but, as it seems stable with phase, it must be produced quite far in the winds, where the absorption is low. Since no single WC star was ever detected in X-rays (see Sect. 4.4), this soft flux can probably not be considered as intrinsic to the WR star.

yield different plasma temperatures, suggesting that non-equilibrium ionization could be present in γ^2Vel (Henley et al. 2005).

Similar effects are seen in a few other systems. In the eccentric system WR22 (WN+O7-9, $P = 80.3$ days), no emission is present at soft energies, but the flux at medium energies (0.7–2 keV) varies strongly due to changes in absorption (Gosset et al. 2009, submitted). The minimum absorption occurs when the O-type star is in front of the WR: as for γ^2Vel, the interaction region is then seen through the less opaque wind of the companion. The behavior of the absorption at other phases can be qualitatively understood if one considers the interaction region to dive deeper and deeper inside the WR wind, as seen from Earth. Outside our Galaxy, a similar phenomenon might occur in the peculiar system HD 5980 (WR+WR, Nazé et al. 2007a). Binaries composed of two O stars can also undergo similar absorption changes, although of smaller amplitude. The small decrease of the soft X-ray flux of Plaskett's star (O7.5I+O6I, $P = 14.4$ days) and HD 93403 (O5.5I+O7V, $P = 15.1$ days) can be explained by the optically thicker wind of the primary star obscuring our view to the interaction region (Linder et al. 2006; Rauw et al. 2002b, respectively). Absorption effects have also been proposed for HD 165052 (O6.5V+O6.5V, Corcoran 1996) and 29 CMa (O8.5I+O9.7V, Berghöfer and Schmitt 1995—although in this case it should concern the intrinsic emission of the stars, since there is apparently no overluminosity typical of an interacting region).

A changing separation in eccentric systems can also be responsible for a phase-locked modulation of the wind–wind X-ray emission. In adiabatic situations (where $L_X \propto \dot{M}^2 v^{-3/2} D^{-1}$), the stars are rather distant from one another and the stellar winds have plenty of time to reach their terminal velocity before interacting. Therefore, no variation in the wind speed is expected and changes in the X-ray luminosity can be attributed to the varying distance between the stars and the shock zone. As theory predicts a $1/D$ effect (see equation above), the intrinsic X-ray flux is expected to be maximum at periastron, where the plasma density is higher. Such a variation has now been observed in several systems: WR25 (WN+O4, $P = 208$ days, see Fig. 29, Gosset 2007), HD 93205 (O3.5V+O8V, $P = 6.1$ days, Antokhin et al. 2003), HD 93403 (O5.5I+O7V, $P = 15.1$ days, Rauw et al. 2002b). However, it must be noted that in other eccentric systems, like γ^2Vel and WR22, the hard X-ray flux is found to be constant, without evidence for a $1/D$ variation (Rauw et al. 2000, Gosset et al. 2009, submitted). The flux of the long-period binary WR140 (WC7+O4–5, $P = 7.94$ years, $e = 0.88$) rises toward periastron but then decreases suddenly as the WR star passes in front of the O-type star and its dense wind occults both the companion and the wind–wind interaction (Corcoran 2003). However, the flux does not follow perfectly the expected $1/D$ variation (Pollock et al. 2002), maybe because the collision becomes radiative near pariastron or because of the energy lost to accelerate non-thermal particles at that time (Pittard and Dougherty 2006). Interestingly, this system is one of the few where changes of the profiles of the X-ray lines have been detected. Pollock et al. (2005) report broad and blueshifted ($-600\,\mathrm{km\,s^{-1}}$) lines before periastron and even wider but slightly redshifted lines just after periastron. Such line profile changes clearly deserve an in-depth study: future X-ray facilities might help detect them for a wide range of interacting wind systems and the observations might then be compared to model predictions, see, e.g., those of Henley et al. (2003). It is worth noting that

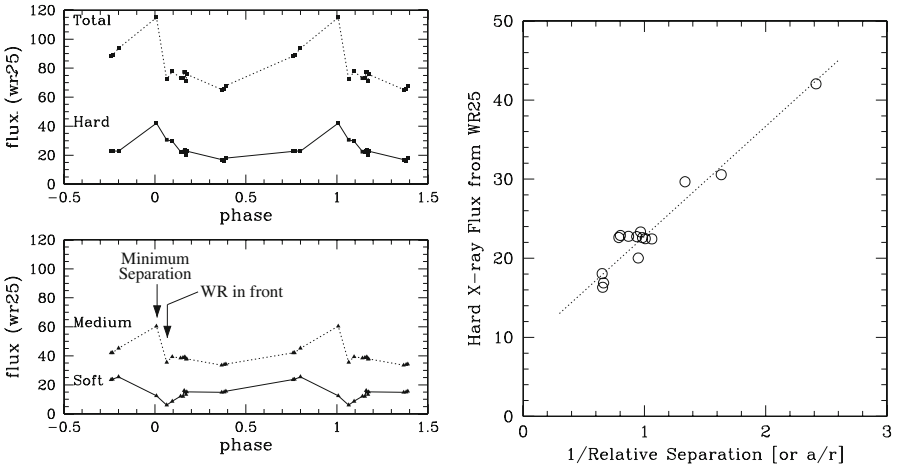

Fig. 29 *Left* X-ray light curves of WR 25 in different energy bands. At minimum separation ($\phi = 0$) the hard and medium fluxes are maximum, while the soft flux is minimum (or the absorption is maximum) when the Wolf-Rayet star is in front. *Right* The observed hard X-ray flux as a function of the inverse of the relative separation between the stars (r divided by the semi-major axis a). Figures adapted from Gosset (2007), which rely on XMM-*Newton* data

hints of a collisionless nature of the wind–wind shock as well as evidence for non-equilibrium ionization were reported for WR140 by Pollock et al. (2005) and Zhekov and Skinner (2000). Similar clues were also found for WR147 (Zhekov 2007).

In the case of a radiative interaction ($L_X \propto \dot{M} v^2$), the stars are closer to each other and the stellar winds are still in the acceleration zone when they interact. Therefore, the interaction occurs at lower speeds at periastron than at apastron: following the equation above, the X-ray flux should thus be minimum at periastron. A good example of this case is Cyg OB2 #8A (O6If+O5.5III(f), $P = 21.9$ days, De Becker et al. 2006) where the flux and plasma temperature present a minimum close to periastron. This is probably also the case of HD 152248 (O7.5III(f)+O7III(f), $P = 5.8$ days, Sana et al. 2004). Note that this idea can be applied on a more global scale, with longer-period systems permitting more acceleration for the wind thereby explaining their larger X-ray overluminosities (Linder et al. 2006)—of course, this is valid only in the radiative regime (i.e., up to $P \sim$ 10–20 days): for longer periods, the $1/D$ effect dominates.

A last case of wind interaction occurs when one of the star has little, if any, mass-loss rate. In this case, the wind of one star crashes onto the photosphere of its companion (or close to it): the X-ray emitting region thus roughly corresponds to the hemisphere facing the primary star. Such a possibility was envisaged to explain the peculiar shape of the light curve of CPD−41°7742 (O9V+B1-1.5V, $P = 2.4$ days, Sana et al. 2005). From a non-zero value, the count rate smoothly increases during a quarter of the orbit; this is followed by an equally smooth decrease during the next quarter of the orbit; when the maximum flux should be reached, a narrow dip makes the light curve come back to its original level. This level corresponds to the intrinsic emission of the two stars; the broad peak occurs when the X-ray emitting hemisphere comes slowly into

view as the system rotates (an effect analogous to the lunar phases); the narrow drop corresponds to an X-ray eclipse when the primary occults the secondary (with an inclination of 77°, the system is seen nearly edge-on). Such a phenomenon can be expected for other O+B systems, but has not yet been specifically searched for.

Further evidence for X-rays associated with a wind–wind interaction is the spatial extension of the high-energy source. Indeed, the X-ray emission is not point-like but occurs in an extended region close to the stagnation point (the intersection of the shock with the binary axis). Unfortunately, spatial resolution is still limited and one did not expect any direct evidence of this extension to be found with either XMM-*Newton* or CHANDRA. However, an indirect signature for the source extension was detected in a few systems. For example, in WR22, it is necessary to take extension into account to closely model the absorption at the most absorbed phase (Gosset et al. 2009, submitted). Such an effect could also help for a better modeling of absorption in γ^2Vel (Schild et al. 2004). In the very massive eclipsing binary WR20a (WN6ha+WN6ha, $P = 3.7$ days, Nazé et al. 2008a), the X-ray emission brightens during the optical eclipse: the lack of an X-ray eclipse is directly related to a non-zero extension of the X-ray emission; furthermore, the brightening requires the collision zone to be rather opaque when seen edge-on (which happens a quarter of phase after/before the eclipse). Finally, *direct* evidence for source extension was found in CHANDRA observations of WR147 (WN8+OB, see Pittard et al. 2002 and Fig. 30). This second closest WR system (the closest one being γ^2Vel) has been resolved at both radio and IR wavelengths: the non-thermal radio source corresponding to the wind–wind interaction lies 0.58″ north of the WR star and the OB companion is located 0.06" further away. The size of the observed X-ray emission is about 70% larger than the CHANDRA point spread function and its position does not correspond to that of the WR star. No other possibility than wind–wind collision can explain such observations and these data thus constitute important evidence showing the reality of the phenomenon. It should be noted that the best fit to the observations considers a main component associated with the extended interaction zone plus weaker contributions from the point-like stars: in this case, the WR star should thus have intrinsic, non-zero X-ray emission (see Sect. 4.4 for further discussion on this subject).

A strange feature discovered in two interacting systems of type WC+O (γ^2 Vel, Schild et al. 2004, and θ Mus, Sugawara et al. 2008) must also be mentioned: the presence of narrow radiative recombination continua (RRC) associated with highly ionized carbon. It indicates that cool gas ($kT =$ a few eV) is present not far from the X-ray sources. Its origin is not yet clear: because of the lack of phase-locked variations, Schild et al. (2004) favor recombination occurring far in the winds or far out in the post-collision flow while Sugawara et al. (2008) suggest that the RRC feature displays a similar shift as the X-ray lines arising from the hot plasma of the wind–wind interaction.

Once that clear evidence was found for wind–wind interactions, a better modeling was attempted. Indeed, when well understood, such interactions can help probe the stellar wind parameters, which are notoriously difficult to estimate (e.g., Antokhin et al. 2004; De Becker et al. 2006). However, one should not forget that there is more than just one interaction in the system: there are the stars. This has two consequences. First, for a meaningful comparison, the modeled wind–wind contribution should always be

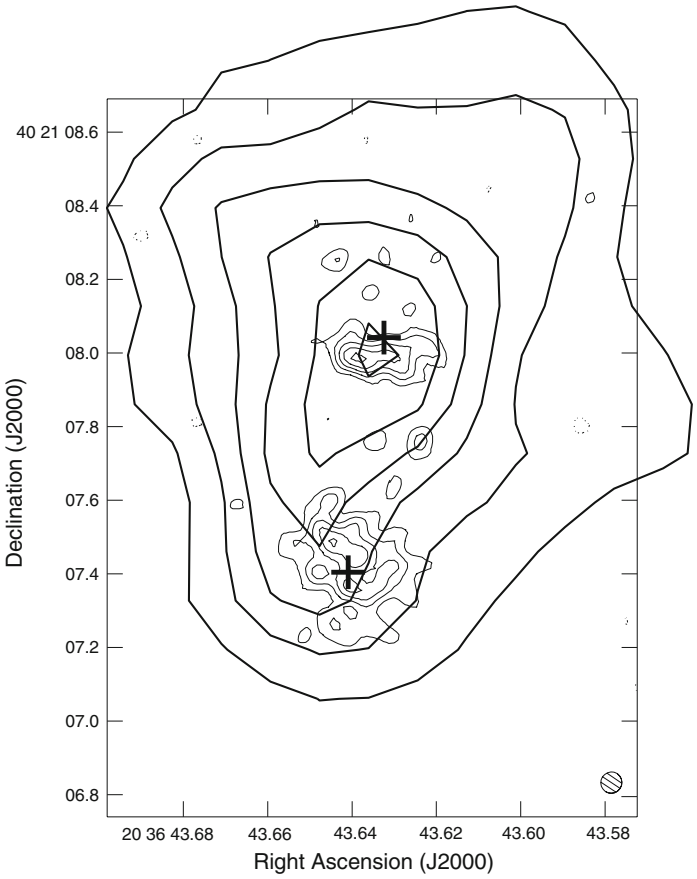

Fig. 30 The emission from WR147, with X-ray contours (*thick lines*) superimposed on radio contours (*thin lines*, figure reprinted from Pittard et al. 2002). The two *crosses* give the positions of the stars: the WR star is to the south, the O star to the north. The WR star is associated with the southern radio source, while the elongated radio source to the north is non-thermal radio emission from the wind–wind collision. The X-ray emission, which is extended, is not co-spatial with the WR star but is likely associated with the wind–wind interaction

added to the stars' intrinsic high-energy emissions. Indeed, the predicted changes are generally larger than the observed ones since the stellar X-rays dilute the variations of the interaction emission (e.g., HD 152248, Sana et al. 2004). Second, wind acceleration needs to be cautiously modeled. Indeed, in hot stars, the winds are accelerated by UV radiation; in hot binaries, there are two sources of UV photons: along the binary axis, the stellar winds might hence not be accelerated to their full strength (a process called radiative inhibition) and, in asymmetric systems (e.g., WR + O), the strongest wind might even suddenly decelerate as it approaches the companion (a process called sudden radiative braking). Such braking effects alter the wind velocity; hence the X-ray emission: the flux and plasma temperature will be lower than expected. Observational evidence for that process is still quite elusive in the X-ray domain. For γ^2Vel, Henley et al. (2005) used a geometrical model (with X-ray emission along a cone revolving

with the orbital period) to reproduce the observed unshifted line profiles: they found that the latter could only be fitted with a half-opening angle of 85°, i.e., much more than the 25° expected on the basis of the shape of the X-ray light curve. This result was interpreted as a possible consequence of sudden radiative braking close to the O star.

Finally, a last remark must be made: not all hot binaries display X-ray bright interactions and this is not solely due to the type of performed observations (a short snapshot prohibiting the production of light curves, contrary to a dedicated monitoring). In NGC 6231, only HD 152248 and CPD−41°7742 present a clear overluminosity in the $L_X - L_{bol}$ diagram, although several other binary systems exist in the cluster (Sana et al. 2006). In the case of ι Orionis (Pittard et al. 2000), no significant variation of the X-ray emission was detected between periastron and apastron observations, although they were eagerly expected. The reasons for these differences are unclear, and definitely require more investigation.

4.6 Hot magnetic objects

Up to recent years, magnetic fields were quite an elusive subject for hot stars. Indeed, hot stars lack outer convection zones, and there seemed to be no correlation between X-ray emission and rotation rate (as seen in cool stars). However, magnetism had been proposed to explain the variability of some peculiar objects, e.g., θ^1 Ori C, and it was also needed for producing the non-thermal radio emission observed in a few hot systems. Direct evidence for its presence is difficult to find as the broadening of the stellar lines in the spectra of hot stars prevents the direct observation of Zeeman splitting. However, the Zeeman effect also induces polarization of light and it was finally through spectropolarimetric studies that magnetic fields were first detected in 2002 (θ^1 Ori C, Donati et al. 2002). More efforts to search for magnetic fields are currently under way (Bouret et al. 2008; Hubrig et al. 2008; Petit et al. 2008; Schnerr et al. 2008). Table 7 summarizes the current status of magnetic field detections in hot stars.

To study the impact of a magnetic field on the stellar winds, hydrodynamical modeling was undertaken (ud-Doula and Owocki 2002). It revealed that the crucial factor is the importance of magnetic energy relative to the kinetic energy of the wind, better evaluated through the use of a wind confinement parameter

$$\eta = \frac{B_{eq}^2 R_*^2}{\dot{M} v_\infty}. \tag{21}$$

If $\eta \ll 1$, the field is weak and the outflowing wind remains rather unaltered; if $\eta > 1$, the field is strong enough to channel the wind toward the stellar equator. In the latter case, it must be noted that no stable disk forms. The head-on collision of the two channeled wind streams at the equator heats the gas to high temperatures: as for interacting wind binaries, hard X-ray emission should thus be produced. In addition, since the phenomenon occurs quite close to the photosphere, in shocked plasma with little radial velocity, the lines of the emitting hot plasma are expected to be

narrow ($\sigma < 250\,\mathrm{km\,s^{-1}}$) and only slightly blueshifted (-100 to $0\,\mathrm{km\,s^{-1}}$, Gagné et al. 2005b). Finally, if the magnetic and rotational axes differ, a periodic modulation of the X-ray emission should be observed, as the region of magnetically confined wind is alternatively observed edge-on/face-on (though this modulation can be of limited amplitude depending on the characteristics of the system, see e.g., Favata et al. 2008).

θ^1 Ori C was observed at four phases with CHANDRA gratings and also at medium resolution in the framework of the COUP campaign (Gagné et al. 2005a, see errata in Gagné et al. 2005b). The observed spectrum is indeed quite hard, with a dominant temperature at 2.5–3 keV, and a second, much weaker component at 0.7 keV. Flux variations of about 30% are detected, with a simultaneous maximum of X-ray and Hα emissions when the "disk" is seen face-on; a slightly larger absorption column is also observed when the "disk" is seen edge-on. Most X-ray lines are narrow ($350\,\mathrm{km\,s^{-1}}$, slightly larger than predicted) but the broader lines (e.g., O VIII) correspond to a cooler plasma and their formation could thus be explained by the "usual" wind-shock model. Moreover, the line centroids are on average close to $0\,\mathrm{km\,s^{-1}}$, though slightly variable (from a small blueshift of $-75\,\mathrm{km\,s^{-1}}$ when seen face-on to a redshift of $+125\,\mathrm{km\,s^{-1}}$ when edge-on). Finally, the comparison of the line triplets from He-like ions suggests a formation region very close to the stellar surface, at radial distances $r = 1.6 - 2.1\,R_*$. All in all, the case of θ^1 Ori C is well explained by the hydrodynamical models.

This is also the case for τ Sco, whose magnetic field was detected by Donati et al. (2006b) shortly after high-resolution X-ray spectroscopy had revealed its striking similarities to θ^1 Ori C: narrow (HWHM of 200–450 $\mathrm{km\,s^{-1}}$) and unshifted lines, hard emission (strong component at $kT = 1.7$ keV), clear overluminosity, X-ray formation region at r=1–3 R_* (Mewe et al. 2003; Cohen et al. 2003). The magnetic field geometry is however much more complex than a simple dipole, and MHD simulations still need to be performed to check if the agreement is also quantitative.

One can now easily imagine a whole continuum of magnetic effects in massive stars. On the one hand, strong magnetic confinement ($\eta \gg 1$) will produce hard X-rays, narrow lines, a large overluminosity, and a clear periodic modulation, as exemplified by θ^1 Ori C. On the other hand, small magnetic confinement will not affect the X-ray emission, which keeps its usual properties from the wind-shock model (soft X-rays, broader lines, constant emission, and $\log[L_X/L_{bol}] \sim -7$, see Sect. 4.2). This other extreme would be represented by ζ Ori A, whose magnetic field is very weak (Bouret et al. 2008) and which displays a "normal" X-ray emission (see Sect. 4.2.2). In between those two extreme cases, a whole range of possibilities opens up, which still needs to be tested.

In view of the surprising spectra of early B-type stars, which cannot be explained by the current wind-shock model (see Sect. 4.3), magnetic fields are often seen as a potential solution. Indeed, B-type stars possess weaker stellar winds than O-stars and even small magnetic fields can produce large magnetic confinements, as exemplified by β Cep (Table 7; Favata et al. 2008). Magnetically channeled winds naturally produce the observed narrow X-ray lines and the observed formation radii are compatible with this scenario. However, detailed MHD simulations are still missing, as well as sensitive polarimetric observations of problematic B-stars (θ Car, β Cru). It remains

Table 7 Properties of magnetic stars earlier than B1 (a '+' in the spectral type indicates the presence of companions)

Name	Sp. type	B_{obs} (G)	B_{dip} (G)	$v \sin i$	v_∞ (km s^{-1})	R_* ($R_\odot$)	$\dot{M}$ ($M_\odot$ year^{-1})	kT (keV)	HWHM (km s^{-1})	$\log(L_X/L_{bol})$	η	References
9 Sgr	O4V+	211 ± 57		128	2,950	16.0	2.4×10^{-6}	0.26	500–1,600	−6.4	0.3	Rauw et al. (2002a) and Hubrig et al. (2008)
HD 148937	O5.5f?p	-276 ± 88		45	2,600	15.0	$\lesssim 10^{-7}$	0.2	873	−6.0	13	Hubrig et al. (2008) and Nazé et al. (2008b,c)
θ^1 Ori C[b]	O5.5V+		$1,060 \pm 90$	24	2,980	8.3	1.4×10^{-6}	2.5–3	300	−6.0	3.6	Donati et al. (2002) and Gagné et al. (2005b)
	O7V+				2,760	9.1	5.5×10^{-7}				12	
HD 191612	O6.5f?p		1,500	45	2,700	14.5	1.6×10^{-6}	0.2–0.3	900	−6.1 . . . 2	21	Donati et al. (2006a), Nazé et al. (2007b, 2008b)
	–O8fp+											and Howarth et al. (2007)
HD 36879	O7V	180 ± 52		163	2,170–2,400	10	4×10^{-7}				0.6–0.7	Hubrig et al. (2008), Prinja et al. (1990) and Vilkoviskii and Tambovtseva (1992)
HD 155806	O7.5Ve	-115 ± 37		91	2,390	8.9	2×10^{-7}	soft		−6.7[a]	0.4	Hubrig et al. (2008), Prinja et al. (1990), Chlebowski and Garmany (1991), Berghöfer et al. (1996) and Martins et al. (2005)

Table 7 continued

Name	Sp. type	B_{obs} (G)	B_{dip} (G)	$v \sin i$	v_∞ (km s^{-1})	R_* ($R_\odot$)	$\dot{M}$ ($M_\odot$ year^{-1})	kT (keV)	HWHM (km s^{-1})	$\log(L_X/L_{bol})$	η	References
HD 152408	O8I	-89 ± 29		85	955–2,200	31	$5–12 \times 10^{-6}$			<−7.3[a]	0.05–0.3	Hubrig et al. (2008), Prinja et al. (1990), Vilkoviskii and Tambovtseva (1992), Chlebowski and Garmany (1991) and Berghöfer et al. (1996)
ζ Ori A	O9.7I		61 ± 10	110	2,100	25.0	$1.4–1.9 \times 10^{-6}$	0.2	850	−7.1	0.11–0.15	Raassen et al. (2008) and Bouret et al. (2008)
τ Sco	B0.2V	300 everywhere		5	2,000	5.2	2×10^{-8}	0.6	200–450	−6.5	12	Mewe et al. (2003), Cohen et al. (2003) and Donati et al. (2006b)
NU Ori	B0.5V+		650 ± 200	225				0.2		−6.7	55[c]	Stelzer et al. (2005) and Petit et al. (2008)
ξ^1 CMa	B0.5-1III	306		20	1,518	7.1	1.9×10^{-8}	0.3[a]		−6.6[a]	31	Cassinelli et al. (1994) and Hubrig et al. (2006)
β Cep	B1V+		360 ± 40	27	800–1,500	6.9	10^{-9}	0.2	<450	−7.2	790–1,481	Henrichs et al. (2000) and Favata et al. (2008)

The dipolar field strength is quoted when available; if absent, the values of η were calculated by assuming the observed field strength to be the dipolar one. Quoted X-ray temperatures correspond to the main component

[a] ROSAT observations (from Berghöfer et al. 1996)

[b] The two lines correspond respectively to the hot and cool models of Gagné et al. (2005b)

[c] Assuming the same values of radius, mass-loss rate and terminal velocity as for τ Sco

to be seen if the variety of temperatures and luminosities can also be reproduced by such models, e.g., hard and bright X-rays for τ Sco (with $\eta \sim 10$) versus soft emission without overluminosity for β Cep (which has a larger $\eta \sim 1{,}000$).

The magnetic models were, however, less successful in some cases. For example, the non-thermal radio emitter 9 Sgr, discussed above, displays a high-resolution X-ray spectrum quite typical of "normal" O-type stars (low kT, broad and slightly blueshifted lines, see Rauw et al. 2002a) although its magnetic field is significant (Hubrig et al. 2008). Indeed, wind–wind interactions most probably play a role in this system, and a full modeling taking into account both magnetic fields and colliding winds should help understand the high-energy characteristics of 9 Sgr. The problems are more critical for the Of?p stars. This category gathers at least three peculiar Galactic stars: HD 108, HD 191612, and HD 148937 (Walborn 1972, 1973). To explain their cyclic variability in the optical domain, a magnetic oblique rotator model was proposed. Indeed, a magnetic field has been detected for HD 191612 (Donati et al. 2006a) and HD 148937 (Hubrig et al. 2008), and the derived confinement parameters are large, with values similar to or larger than for θ^1 Ori C (Table 7). In the X-ray domain, all three stars present similar spectra but their properties do not fully agree with the predictions of the magnetic models (Nazé et al. 2004, 2007a, 2008b,c). On the positive side, two similarities with θ^1 Ori C can be underlined: a large overluminosity (an order of magnitude compared to the "canonical" relation) and the flux variations of HD 191612, in phase with those of the optical emissions. In addition, although the overall flux is soft, a second thermal component at 1–3 keV is present but it is of reduced intensity (it only accounts for 30% of the intrinsic flux) and it can certainly not explain the overluminosity. On the negative side, these stars display soft spectra with a dominant component at 0.2–0.3 keV, as expected for "typical" O-type stars (see Sect. 4.1.2), and broad X-ray lines (HWHM $\sim 900\,\mathrm{km\,s^{-1}}$). For these Of?p stars, it thus seems that an additional phenomenon must be at work to explain the characteristics observed at X-ray energies.

As spectropolarimetric analyses are still on-going, it is difficult to assess at the present time the overall validity of the magnetically-channeled wind model at high-energies. Sensitive magnetic detections and high-resolution X-ray spectroscopy of OB-stars need first to be accumulated. Once definitive values for the physical properties of the magnetic systems will become available, statistical analyses will be performed to test whether significant differences between magnetic and non-magnetic systems exist and detailed modeling will be able to check if their X-ray emission follows the expectations or not. Until then, hard X-ray emission with narrow unshifted lines might certainly be considered as a typical signature of strong magnetic fields. This result, at least valid for τ Sco and θ^1 Ori C, was also used to explain the observations of numerous X-ray bright O-type stars in very young clusters. Following some authors (e.g., Schulz et al. 2003), the number of bright, hard sources associated with O-type objects increases as the cluster age decreases. This result was linked to observational hints that magnetic field strength decreases with age (Donati et al. 2006a). However, the impact of binarity (and associated interacting wind emission) was not fully assessed. In this context, it should be remembered that young clusters still harbor the most massive stars: these objects, displaying the strongest winds, are the most susceptible to pro-

duce strong wind–wind interactions. Decreasing magnetic field might thus not be the only cause for the smaller number of X-ray bright sources observed in older clusters.

5 Conclusions

XMM-*Newton* and CHANDRA have provided entirely new views of stellar X-rays, in particular through high-resolution grating spectroscopy offering a resolving power of several hundred. Stellar X-ray sources are rich in emission lines from which information on physical conditions and processes can be extracted.

Coronae of cool stars reveal standard thermal spectra that have, nevertheless, offered a number of surprises, such as previously unknown systematics of element abundances. Subtle effects related to line broadening, optical depths, resonant scattering, and fluorescence have been crucial to develop models of the emitting sources or irradiated surfaces. Much attention has also been paid to the unique methodology of measuring average coronal densities that are pivotal for the construction of coronal models.

Density measurements were at the origin of new hypotheses related to pre-main sequence stars. Soft X-ray emission revealing very high densities has been interpreted as a signature of accretion shocks near the stellar surface. Outflows or jets are also X-ray sources, perhaps related to the same physical mechanisms also operating in winds of massive stars.

The current X-ray observatories have also clearly provided better insight into the properties of hot, massive stars. In particular, high-resolution spectra have proved a crucial tool to test the proposed models in detail: the new observations do not fully agree with expectations and require a change of paradigm.

Continuing investigations in the domain of high-resolution spectroscopy are clearly needed. The higher sensitivity facilities of the next generation should notably be able to resolve the profile variations of X-ray lines, which are expected in various contexts (wind–wind interaction in binaries, channeled wind in magnetic objects, and even in winds of single stars, rotating coronal plasma, plasma flows in magnetic fields, etc.). Studies of X-ray emission in different metallicity environments, e.g., the Magellanic Clouds, should also provide crucial information since the stellar wind strength and absorption depend on the metal content. In this context, it must be noted that high sensitivity and high spectral resolution must be complemented by a high spatial resolution—it is of little interest to get a well-exposed spectrum of a whole cluster!

Acknowledgments Both authors warmly thank the Editorial Board of *The Astronomy and Astrophysics Review* and in particular its Editor-in-Chief, Thierry Courvoisier, for the invitation to write this review article. They further thank Marc Audard for critically reviewing their paper. The authors are indebted to several colleagues who gave permission to use original figure material, namely Costanza Argiroffi, Markus Aschwanden, David Cohen, Stefan Czesla, Eric Gosset, Hans Moritz Günther, Mihalis Mathioudakis, Raanan Nordon, Lida Oskinova, Rachel Osten, Julian Pittard, Gregor Rauw, Luigi Scelsi, Stephen Skinner, and Masahiro Tsujimoto. YN acknowledges support from the Fonds National de la Recherche Scientifique (Belgium), the PRODEX XMM and Integral contracts, and the "Action de Recherche Concertée" (CFWB-Académie Wallonie Europe). YN also wishes to thank G. Rauw for his constant help and for providing useful suggestions on the manuscript; J.-P. Swings, J.-M. Vreux, and E. Gosset for a careful reading of the text; D. Cohen, E. Wollman, and L. Oskinova for interesting discussions. The X-Atlas, 2XMM, and ADS/CDS databases were used for preparing this document.

References

Albacete Colombo JF, Micela G (2005) X-ray analysis of the close binary system FO 15. In: Rauw G, Nazé Y, Blomme R, Gosset E (eds) Massive stars and high-energy emission in OB associations, pp 69–72

Albacete Colombo JF, Flaccomio E, Micela G, Sciortino S, Damiani F (2007) Unveiling the Cygnus OB2 stellar population with CHANDRA. A&A 464:211–227. doi:10.1051/0004-6361:20066101, arXiv:astro-ph/0610352

Antia HM, Basu S (2005) The discrepancy between solar abundances and helioseismology. ApJ 620:L129–L132. doi:10.1086/428652, arXiv:astro-ph/0501129

Antiochos SK (1980) Radiative-dominated cooling of the flare corona and transition region. ApJ 241:385–393. doi:10.1086/158351

Antiochos SK, Noci G (1986) The structure of the static corona and transition region. ApJ 301:440–447. doi:10.1086/163912

Antokhin II, Rauw G, Vreux JM, van der Hucht KA (2003) Search for X-ray variability in early-type stars in the Carina OB1 association with XMM-*Newton*. In: Balona LA, Henrichs HF, Medupe R (eds) Astronomical society of the Pacific conference series, astronomical society of the Pacific conference series, vol 305, pp 383–386

Antokhin II, Owocki SP, Brown JC (2004) A steady, radiative-shock method for computing X-ray emission from colliding stellar winds in close, massive-star binaries. ApJ 611:434–451. doi:10.1086/422093

Antokhin II, Rauw G, Vreux JM, van der Hucht KA, Brown JC (2008) XMM-*Newton* X-ray study of early type stars in the Carina OB1 association. A&A 477:593–609. doi:10.1051/0004-6361:20065711, 0711.3612

Antunes A, Nagase F, White NE (1994) ASCA observations of the coronal X-ray emission of Algol. ApJ 436:L83–L86. doi:10.1086/187638

Argiroffi C, Maggio A, Peres G (2003) On coronal structures and their variability in active stars: the case of Capella observed with CHANDRA/LETGS. A&A 404:1033–1049. doi:10.1051/0004-6361:20030497

Argiroffi C, Drake JJ, Maggio A, Peres G, Sciortino S, Harnden FR (2004) High-resolution X-ray spectroscopy of the post-T Tauri star PZ telescopii. ApJ 609:925–934. doi:10.1086/420692, arXiv:astro-ph/0403017

Argiroffi C, Maggio A, Peres G, Stelzer B, Neuhäuser R (2005) XMM-*Newton* spectroscopy of the metal depleted T Tauri star TWA 5. A&A 439:1149–1158. doi:10.1051/0004-6361:20052729, arXiv:astro-ph/0505075

Argiroffi C, Maggio A, Peres G (2007) X-ray emission from MP Muscae: an old classical T Tauri star. A&A 465:L5–L8. doi:10.1051/0004-6361:20067016, arXiv:astro-ph/0701765

Aschwanden MJ, Stern RA, Güdel M (2008) Scaling laws of solar and stellar flares. ApJ 672:659–673. doi:10.1086/523926, 0710.2563

Asplund M, Grevesse N, Güdel M, Sauval AJ (2005a) The solar model problem resurrected. ArXiv Astrophysics e-prints, arXiv:astro-ph/0510377

Asplund M, Grevesse N, Sauval AJ (2005b) The solar chemical composition. In: Barnes TG III, Bash FN (eds) Cosmic abundances as records of stellar evolution and nucleosynthesis, astronomical society of the Pacific conference series, vol 336, pp 25–38

Audard M, Güdel M, Drake JJ, Kashyap VL (2000) Extreme-ultraviolet flare activity in late-type stars. ApJ 541:396–409. doi:10.1086/309426

Audard M, Güdel M, Mewe R (2001) The XMM-*Newton* view of stellar coronae: flare heating in the coronae of HR 1099. A&A 365:L318–L323. doi:10.1051/0004-6361:20000085

Audard M, Güdel M, Sres A, Raassen AJJ, Mewe R (2003) A study of coronal abundances in RS CVn binaries. A&A 398:1137–1149. doi:10.1051/0004-6361:20021737, arXiv:astro-ph/0109268

Audard M, Telleschi A, Güdel M, Skinner SL, Pallavicini R, Mitra-Kraev U (2004) Some like it hot: the X-ray emission of the giant star YY Mensae. ApJ 617:531–550. doi:10.1086/424590, arXiv:astro-ph/0408345

Audard M, Güdel M, Skinner SL, Briggs KR, Walter FM, Stringfellow G, Hamilton RT, Guinan EF (2005) X-ray spectral variability during an outburst in V1118 Ori. ApJ 635:L81–L84. doi:10.1086/499237, arXiv:astro-ph/0510859

Audard M, Briggs KR, Grosso N, Güdel M, Scelsi L, Bouvier J, Telleschi A (2007) The XMM-*Newton* optical monitor survey of the Taurus molecular cloud. A&A 468:379–390. doi:10.1051/0004-6361:20066320, arXiv:astro-ph/0611367

Ayres TR, Brown A, Osten RA, Huenemoerder DP, Drake JJ, Brickhouse NS, Linsky JL (2001a) CHANDRA, EUVE, HST, and VLA multiwavelength campaign on HR 1099: instrumental capabilities, data reduction, and initial results. ApJ 549:554–577. doi:10.1086/319051

Ayres TR, Osten RA, Brown A (2001b) 3 Ms in the life of β Ceti: sustained flare activity on a clump giant detected by the extreme ultraviolet explorer. ApJ 562:L83–L86. doi:10.1086/337971

Baade D, Lucy LB (1987) A search for coronal line emission from early-type stars. I—Zeta Puppis. A&A 178:213–220

Bahcall JN, Basu S, Pinsonneault M, Serenelli AM (2005) Helioseismological implications of recent solar abundance determinations. ApJ 618:1049–1056. doi:10.1086/426070, arXiv:astro-ph/0407060

Bai T (1979) Iron K-alpha fluorescence in solar flares—A probe of the photospheric iron abundance. Solar Phys 62:113–121. doi:10.1007/BF00150138

Ball B, Drake JJ, Lin L, Kashyap V, Laming JM, García-Alvarez D (2005) Stellar coronal abundances at intermediate-activity levels: ξ UMa. ApJ 634:1336–1345. doi:10.1086/496909

Ballantyne DR, Fabian AC (2003) The contribution of particle impact to the production of Fe Kα emission from accreting black holes. ApJ 592:1089–1099. doi:10.1086/375798, arXiv:astro-ph/0304218

Bally J, Feigelson E, Reipurth B (2003) X-rays from the vicinity of the protostar L1551 IRS 5: reflection or fast shocks? ApJ 584:843–852. doi:10.1086/345850

Behar E, Cottam J, Kahn SM (2001) The CHANDRA Iron-L X-ray line spectrum of Capella. ApJ 548:966–975. doi:10.1086/318999, arXiv:astro-ph/0003099

Berghöfer TW, Schmitt JHMM (1995) The ROSAT view of the massive eclipsing 0-type binary system 29 UW Canis Majoris. In: van der Hucht KA, Williams PM (eds) Wolf-Rayet stars: binaries; colliding winds; evolution, IAU symposium, vol 163, pp 382–387

Berghöfer TW, Schmitt JHMM, Cassinelli JP (1996) The ROSAT all-sky survey catalogue of optically bright OB-type stars. A&A Suppl 118:481–494

Berghöfer TW, Schmitt JHMM, Danner R, Cassinelli JP (1997) X-ray properties of bright OB-type stars detected in the ROSAT all-sky survey. A&A 322:167–174

Blumenthal GR, Drake GWF, Tucker WH (1972) Ratio of line intensities in Helium-like ions as a density indicator. ApJ 172:205–212

Bopp BW, Stencel RE (1981) The FK Comae stars. ApJ 247:L131–L134. doi:10.1086/183606

Bouret JC, Lanz T, Hillier DJ (2005) Lower mass loss rates in O-type stars: spectral signatures of dense clumps in the wind of two Galactic O4 stars. A&A 438:301–316. doi:10.1051/0004-6361:20042531, arXiv:astro-ph/0412346

Bouret JC, Donati JF, Martins F, Escolano C, Marcolino W, Lanz T, Howarth ID (2008) The weak magnetic field of the O9.7 supergiant ζ Orionis A. MNRAS 389:75–85. doi:10.1111/j.1365-2966.2008.13575.x, 0806.2162

Bowyer S, Drake JJ, Vennes S (2000) Extreme ultraviolet astronomy. Ann Rev Astron Astrophys 38:231–288. doi:10.1146/annurev.astro.38.1.231

Bray RJ, Cram LE, Durrant C, Loughhead RE (1991) Plasma loops in the solar corona. In: Bray RJ, Cram LE, Durrant C, Loughhead RE (eds) Plasma loops in the solar corona. Cambridge University Press, Cambridge, p 522, ISBN 0521351073

Brickhouse NS, Dupree AK (1998) Extreme ultraviolet explorer observations of the W Ursa Majoris contact binary 44i Bootis: coronal structure and variability. ApJ 502:918–931. doi:10.1086/305916

Brickhouse NS, Raymond JC, Smith BW (1995) New model of iron spectra in the extreme ultraviolet and application to SERTS and EUV observations: a solar active region and Capella. ApJ Suppl 97:551–570. doi:10.1086/192150

Brickhouse NS, Dupree AK, Young PR (2001) X-ray doppler imaging of 44i Bootis with CHANDRA. ApJ 562:L75–L78. doi:10.1086/338121, arXiv:astro-ph/0110560

Brinkman AC, Behar E, Güdel M, Audard M, den Boggende AJF, Branduardi-Raymont G, Cottam J, Erd C, den Herder JW, Jansen F, Kaastra JS, Kahn SM, Mewe R, Paerels FBS, Peterson JR, Rasmussen AP, Sakelliou I, de Vries C (2001) First light measurements with the XMM-*Newton* reflection grating spectrometers: evidence for an inverse first ionisation potential effect and anomalous Ne abundance in the Coronae of HR 1099. A&A 365:L324–L328. doi:10.1051/0004-6361:20000047, arXiv:astro-ph/0011018

Brown JC (1971) The deduction of energy spectra of non-thermal electrons in flares from the observed dynamic spectra of hard X-ray bursts. Solar Phys 18:489–502. doi:10.1007/BF00149070

Calvet N, Gullbring E (1998) The structure and emission of the accretion shock in T Tauri stars. ApJ 509:802–818. doi:10.1086/306527

Canizares CR, Huenemoerder DP, Davis DS, Dewey D, Flanagan KA, Houck J, Markert TH, Marshall HL, Schattenburg ML, Schulz NS, Wise M, Drake JJ, Brickhouse NS (2000) High-resolution X-ray spectra of Capella: initial results from the CHANDRA high-energy transmission grating spectrometer. ApJ 539:L41–L44. doi:10.1086/312823, arXiv:astro-ph/0006457

Cargill PJ (1994) Some implications of the nanoflare concept. ApJ 422:381–393. doi:10.1086/173733

Cassinelli JP, Olson GL (1979) The effects of coronal regions on the X-ray flux and ionization conditions in the winds of OB supergiants and of stars. ApJ 229:304–317. doi:10.1086/156956

Cassinelli JP, Swank JH (1983) X-ray spectra of Orion OB supergiants. ApJ 271:681–690. doi:10.1086/161235

Cassinelli JP, Cohen DH, Macfarlane JJ, Sanders WT, Welsh BY (1994) X-ray emission from near-main-sequence B stars. ApJ 421:705–717. doi:10.1086/173683

Cassinelli JP, Miller NA, Waldron WL, MacFarlane JJ, Cohen DH (2001) CHANDRA detection of Doppler-shifted X-ray line profiles from the wind of ζ Puppis (O4 F). ApJ 554:L55–L58. doi:10.1086/320916, arXiv:astro-ph/0104107

Chen W, White RL (1991) Nonthermal X-ray emission from winds of OB supergiants. ApJ 366:512–528. doi:10.1086/169586

Chlebowski T, Garmany CD (1991) On winds and X-rays of O-type stars. ApJ 368:241–251. doi:10.1086/169687

Choi CS, Dotani T (1998) ASCA observation of a long-duration X-ray flare from the W UMa–type Binary VW Cephei. ApJ 492:761–766. doi:10.1086/305071

Chung SM, Drake JJ, Kashyap VL, Lin LW, Ratzlaff PW (2004) Doppler shifts and broadening and the structure of the X-ray emission from Algol. ApJ 606:1184–1195. doi:10.1086/383195, arXiv:astro-ph/0401583

Cohen DH, Cassinelli JP, Macfarlane JJ (1997) ROSAT PSPC observations of 27 near-main-sequence B stars. ApJ 487:867–884. doi:10.1086/304636

Cohen DH, de Messières GE, MacFarlane JJ, Miller NA, Cassinelli JP, Owocki SP, Liedahl DA (2003) High-resolution CHANDRA spectroscopy of τ Scorpii: a narrow-line X-ray spectrum from a hot star. ApJ 586:495–505. doi:10.1086/367553, arXiv:astro-ph/0211412

Cohen DH, Leutenegger MA, Grizzard KT, Reed CL, Kramer RH, Owocki SP (2006) Wind signatures in the X-ray emission-line profiles of the late-O supergiant ζ Orionis. MNRAS 368:1905–1916. doi:10.1111/j.1365-2966.2006.10259.x, arXiv:astro-ph/0602599

Cohen DH, Kuhn MA, Gagné M, Jensen ELN, Miller NA (2008) CHANDRA spectroscopy of the hot star β Crucis and the discovery of a pre-main-sequence companion. MNRAS 386:1855–1871. doi:10.1111/j.1365-2966.2008.13176.x, 0802.4084

Corcoran MF (1996) X-ray emission from colliding wind binaries. In: Niemela V, Morrell N, Pismis P, Torres-Peimbert S (eds) Revista Mexicana de astronomia y astrofisica conference series, vol 5, pp 54–60

Corcoran MF (2003) X-ray observations of massive colliding wind binaries. In: van der Hucht K, Herrero A, Esteban C (eds) A massive star odyssey: from main sequence to supernova, IAU Symposium, vol 212, pp 130–138

Craig IJD, Brown JC (1976) Fundamental limitations of X-ray spectra as diagnostics of plasma temperature structure. A&A 49:239–250

Crosby NB, Aschwanden MJ, Dennis BR (1993) Frequency distributions and correlations of solar X-ray flare parameters. Solar Phys 143:275–299. doi:10.1007/BF00646488

Czesla S, Schmitt JHHM (2007) The nature of the fluorescent iron line in V 1486 Orionis. A&A 470:L13–L16. doi:10.1051/0004-6361:20077741, 0706.3097

Damiani F, Micela G, Sciortino S, Harnden FR Jr (1994) Einstein X-ray observations of Herbig Ae/Be stars. ApJ 436:807–817. doi:10.1086/174957

De Becker M (2007) Non-thermal emission processes in massive binaries. A&A Rev 14:171–216. doi:10.1007/s00159-007-0005-2, 0709.4220

De Becker M, Rauw G, Pittard JM, Antokhin II, Stevens IR, Gosset E, Owocki SP (2004) An XMM-*Newton* observation of the massive binary HD 159176. A&A 416:221–233. doi:10.1051/0004-6361:20031710, arXiv:astro-ph/0402663

De Becker M, Rauw G, Sana H, Pollock AMT, Pittard JM, Blomme R, Stevens IR, van Loo S (2006) XMM-*Newton* observations of the massive colliding wind binary and non-thermal radio emitter CygOB2#8A [O6If + O5.5III(f)]. MNRAS 371:1280–1294. doi:10.1111/j.1365-2966.2006.10746.x

Dennis BR (1985) Solar hard X-ray bursts. Solar Phys 100:465–490. doi:10.1007/BF00158441

Donati JF, Semel M, Carter BD, Rees DE, Collier Cameron A (1997) Spectropolarimetric observations of active stars. MNRAS 291:658–682

Donati JF, Babel J, Harries TJ, Howarth ID, Petit P, Semel M (2002) The magnetic field and wind confinement of θ^1 Orionis C. MNRAS 333:55–70. doi:10.1046/j.1365-8711.2002.05379.x

Donati JF, Howarth ID, Bouret JC, Petit P, Catala C, Landstreet J (2006a) Discovery of a strong magnetic field on the O star HD 191612: new clues to the future of θ^1 Orionis C. MNRAS 365:L6–L10. doi:10.1111/j.1745-3933.2005.00115.x, arXiv:astro-ph/0510395

Donati JF, Howarth ID, Jardine MM, Petit P, Catala C, Landstreet JD, Bouret JC, Alecian E, Barnes JR, Forveille T, Paletou F, Manset N (2006b) The surprising magnetic topology of τ Sco: fossil remnant or dynamo output? MNRAS 370:629–644. doi:10.1111/j.1365-2966.2006.10558.x, arXiv:astro-ph/0606156

Doschek GA, Feldman U, Landecker PB, McKenzie DL (1981) High resolution solar flare X-ray spectra—the temporal behavior of electron density, temperature, and emission measure for two class M flares. ApJ 249:372–382. doi:10.1086/159294

Drake JJ (2003a) Chemical fractionation and abundances in coronal plasma. Adv Space Res 32:945–954. doi:10.1016/S0273-1177(03)00296-5, arXiv:astro-ph/0308231

Drake JJ (2003b) From the Heart of the Ghoul: C and N Abundances in the Corona of Algol B. ApJ 594:496–509. doi:10.1086/375837, arXiv:astro-ph/0308230

Drake JJ, Testa P (2005) The 'solar model problem' solved by the abundance of neon in nearby stars. Nature 436:525–528. doi:10.1038/nature03803, arXiv:astro-ph/0506182

Drake JJ, Laming JM, Widing KG (1995) Stellar coronal abundances. 2: the first ionization potential effect and its absence in the corona of Procyon. ApJ 443:393–415. doi:10.1086/175533

Drake JJ, Laming JM, Widing KG (1997) Stellar coronal abundances. V. Evidence for the first ionization potential effect in alpha Centauri. ApJ 478:403–416. doi:10.1086/303755

Drake JJ, Peres G, Orlando S, Laming JM, Maggio A (2000) On stellar coronae and solar active regions. ApJ 545:1074–1083. doi:10.1086/317820

Drake JJ, Brickhouse NS, Kashyap V, Laming JM, Huenemoerder DP, Smith R, Wargelin BJ (2001) Enhanced noble gases in the coronae of active stars. ApJ 548:L81–L85. doi:10.1086/318933

Drake JJ, Testa P, Hartmann L (2005) X-ray diagnostics of grain depletion in matter accreting onto T Tauri stars. ApJ 627:L149–L152. doi:10.1086/432468, arXiv:astro-ph/0506185

Drake JJ, Chung SM, Kashyap V, Korhonen H, Van Ballegooijen A, Elstner D (2008a) X-ray spectroscopic signatures of the extended corona of FK Comae. ApJ 679:1522–1530. doi:10.1086/587443

Drake JJ, Ercolano B, Swartz DA (2008b) X-ray-fluorescent Fe Kα lines from stellar photospheres. ApJ 678:385–393. doi:10.1086/524976, 0710.0621

Dupree AK, Brickhouse NS, Doschek GA, Green JC, Raymond JC (1993) The extreme ultraviolet spectrum of alpha Aurigae (Capella). ApJ 418:L41–L44. doi:10.1086/187111

Emslie AG, Phillips KJH, Dennis BR (1986) The excitation of the iron K-alpha feature in solar flares. Solar Phys 103:89–102

Ercolano B, Drake JJ, Reale F, Testa P, Miller JM (2008) Fe Kα and hydrodynamic loop model diagnostics for a large flare on II Pegasi. ApJ 688:1315–1319. doi:10.1086/591934, 0807.2093

Eversberg T, Lepine S, Moffat AFJ (1998) Outmoving clumps in the wind of the hot O supergiant zeta Puppis. ApJ 494:799–805. doi:10.1086/305218

Favata F, Micela G (2003) Stellar coronal astronomy. Space Sci Rev 108:577–708. doi:10.1023/B:SPAC.0000007491.80144.21, arXiv:astro-ph/0302565

Favata F, Schmitt JHMM (1999) Spectroscopic analysis of a super-hot giant flare observed on Algol by BeppoSAX on 30 August 1997. A&A 350:900–916, arXiv:astro-ph/9909041

Favata F, Fridlund CVM, Micela G, Sciortino S, Kaas AA (2002) Discovery of X-ray emission from the protostellar jet L1551 IRS5 (HH 154). A&A 386:204–210. doi:10.1051/0004-6361:20011387, arXiv:astro-ph/0110112

Favata F, Micela G, Silva B, Sciortino S, Tsujimoto M (2005) A survey for Fe 6.4 keV emission in young stellar objects in ρ Oph: the strong fluorescence from Elias 29. A&A 433:1047–1054. doi:10.1051/0004-6361:20042019, arXiv:astro-ph/0412510

Favata F, Neiner C, Testa P, Hussain G, Sanz-Forcada J (2008) Testing magnetically confined wind shock models for beta Cep using XMM-*Newton* and CHANDRA phase-resolved X-ray observations. ArXiv e-prints 0806.2275

Feldman U (1992) Elemental abundances in the upper solar atmosphere. Phys Scripta 46:202–220. doi:10.1088/0031-8949/46/3/002

Feldmeier A, Puls J, Pauldrach AWA (1997) A possible origin for X-rays from O stars. A&A 322:878–895
Feldmeier A, Oskinova L, Hamann WR (2003) X-ray line emission from a fragmented stellar wind. A&A 403:217–224. doi:10.1051/0004-6361:20030231, arXiv:astro-ph/0302516
Flaccomio E, Micela G, Sciortino S (2003) Time evolution of X-ray coronal activity in PMS stars; a possible relation with the evolution of accretion disks. A&A 402:277–292. doi:10.1051/0004-6361:20030203, arXiv:astro-ph/0302329
Franciosini E, Pallavicini R, Tagliaferri G (2001) BeppoSAX observation of a large long-duration X-ray flare from UX Arietis. A&A 375:196–204. doi:10.1051/0004-6361:20010830
Fuhrmeister B, Liefke C, Schmitt JHMM (2007) Simultaneous XMM-*Newton* and VLT/UVES observations of the flare star CN Leonis. A&A 468:221–231. doi:10.1051/0004-6361:20066229
Fullerton AW, Massa DL, Prinja RK (2006) The discordance of mass-loss estimates for galactic O-type stars. ApJ 637:1025–1039. doi:10.1086/498560, arXiv:astro-ph/0510252
Gabriel AH, Jordan C (1969) Interpretation of solar helium-like ion line intensities. MNRAS 145:241–248
Gagné M, Oksala ME, Cohen DH, Tonnesen SK, ud-Doula A, Owocki SP, Townsend RHD, MacFarlane JJ (2005a) CHANDRA HETGS multiphase spectroscopy of the young magnetic O star θ^1 Orionis C. ApJ 628:986–1005. doi:10.1086/430873, arXiv:astro-ph/0504296
Gagné M, Oksala ME, Cohen DH, Tonnesen SK, ud-Doula A, Owocki SP, Townsend RHD, MacFarlane JJ (2005b) Erratum: "CHANDRA HETGS multiphase spectroscopy of the young magnetic O star θ^1 Orionis C". ApJ 634:712–713. doi:10.1086/496876
García-Alvarez D, Drake JJ, Lin L, Kashyap VL, Ball B (2005) The coronae of AB Doradus and V471 Tauri: primordial angular momentum versus tidal spin-up. ApJ 621:1009–1022. doi:10.1086/427721, arXiv:astro-ph/0411614
García-Alvarez D, Drake JJ, Ball B, Lin L, Kashyap VL (2006) Evidence of the FIP effect in the coronae of late-type giants. ApJ 638:1028–1040. doi:10.1086/499030, arXiv:astro-ph/0512492
García-Alvarez D, Drake JJ, Kashyap VL, Lin L, Ball B (2008) Coronae of young fast rotators. ApJ 679:1509–1521. doi:10.1086/587611
Getman KV, Flaccomio E, Broos PS, Grosso N, Tsujimoto M, Townsley L, Garmire GP, Kastner J, Li J, Harnden FR Jr, Wolk S, Murray SS, Lada CJ, Muench AA, McCaughrean MJ, Meeus G, Damiani F, Micela G, Sciortino S, Bally J, Hillenbrand LA, Herbst W, Preibisch T, Feigelson ED (2005) CHANDRA Orion ultradeep project: observations and source lists. ApJ Suppl 160:319–352. doi:10.1086/432092, arXiv:astro-ph/0410136
Giampapa MS, Rosner R, Kashyap V, Fleming TA, Schmitt JHMM, Bookbinder JA (1996) The coronae of low-mass dwarf stars. ApJ 463:707–725. doi:10.1086/177284
Giardino G, Favata F, Micela G, Reale F (2004) A large X-ray flare from the Herbig Ae star V892 Tau. A&A 413:669–679. doi:10.1051/0004-6361:20034151, arXiv:astro-ph/0310355
Giardino G, Favata F, Micela G, Sciortino S, Winston E (2007a) The onset of X-ray emission in young stellar objects. A CHANDRA observation of the Serpens star-forming region. A&A 463:275–288. doi:10.1051/0004-6361:20066424, arXiv:astro-ph/0611520
Giardino G, Favata F, Pillitteri I, Flaccomio E, Micela G, Sciortino S (2007b) Results from Droxo. I. The variability of fluorescent Fe 6.4 keV emission in the young star Elias 29. High-energy electrons in the star's accretion tubes? A&A 475:891–900. doi:10.1051/0004-6361:20077899, 0710.1947
Glassgold AE, Najita J, Igea J (1997) X-ray ionization of protoplanetary disks. ApJ 480:344–350. doi:10.1086/303952
Gondoin P (2003) X-ray spectroscopy of UZ Librae. A&A 400:249–256. doi:10.1051/0004-6361:20021864
Gondoin P, Erd C, Lumb D (2002) Structure and evolution of FK Comae corona. A&A 383:919–932. doi:10.1051/0004-6361:20011810
Gosset E (2007) Études d'étoiles massives de types spectraux O, Wolf-Rayet et apparentés—Abilitation thesis. PhD thesis, AA(Institut d'Astrophysique et de Géophysique, Université de Liège)
Gosset E, Nazé Y, Claeskens JF, Rauw G, Vreux JM, Sana H (2005) An XMM-*Newton* look at the Wolf-Rayet star WR 40. The star itself, its nebula and its neighbours. A&A 429:685–704. doi:10.1051/0004-6361:20040286
Gotthelf EV, Jalota L, Mukai K, White NE (1994) An ASCA observation of the Castor system. ApJ 436:L91–L94. doi:10.1086/187640
Gregory SG, Jardine M, Cameron AC, Donati JF (2006) Rotationally modulated X-ray emission from T Tauri stars. MNRAS 373:827–835. doi:10.1111/j.1365-2966.2006.11086.x, arXiv:astro-ph/0609667
Grevesse N, Sauval AJ (1998) Standard solar composition. Space Sci Rev 85:161–174. doi:10.1023/A:1005161325181

Grosso N, Kastner JH, Ozawa H, Richmond M, Simon T, Weintraub DA, Hamaguchi K, Frank A (2005) Enhanced X-ray variability from V1647 Ori, the young star in outburst illuminating McNeil's Nebula. A&A 438:159–168. doi:10.1051/0004-6361:20042182, arXiv:astro-ph/0504111

Güdel M (2004) X-ray astronomy of stellar coronae. A&A Rev. 12:71–237. doi:10.1007/s00159-004-0023-2, arXiv:astro-ph/0406661

Güdel M (2006) X-ray spectroscopy of cool stars. In: High resolution X-ray spectroscopy: towards XEUS and Con-X

Güdel M, Telleschi A (2007) The X-ray soft excess in classical T Tauri stars. A&A 474:L25–L28. doi:10.1051/0004-6361:20078143, 0709.0881

Güdel M, Audard M, Magee H, Franciosini E, Grosso N, Cordova FA, Pallavicini R, Mewe R (2001) The XMM-*Newton* view of stellar coronae: coronal structure in the castor X-ray triplet. A&A 365: L344–L352. doi:10.1051/0004-6361:20000040

Güdel M, Audard M, Skinner SL, Horvath MI (2002) X-ray evidence for flare density variations and continual chromospheric evaporation in Proxima Centauri. ApJ 580:L73–L76. doi:10.1086/345404, arXiv:astro-ph/0210190

Güdel M, Audard M, Kashyap VL, Drake JJ, Guinan EF (2003) Are Coronae of magnetically active stars heated by flares? II. Extreme ultraviolet and X-ray flare statistics and the differential emission measure distribution. ApJ 582:423–442. doi:10.1086/344614, arXiv:astro-ph/0209075

Güdel M, Audard M, Reale F, Skinner SL, Linsky JL (2004) Flares from small to large: X-ray spectroscopy of Proxima Centauri with XMM-*Newton*. A&A 416:713–732. doi:10.1051/0004-6361:20031471, arXiv:astro-ph/0312297

Güdel M, Briggs KR, Arzner K, Audard M, Bouvier J, Feigelson ED, Franciosini E, Glauser A, Grosso N, Micela G, Monin JL, Montmerle T, Padgett DL, Palla F, Pillitteri I, Rebull L, Scelsi L, Silva B, Skinner SL, Stelzer B, Telleschi A (2007a) The XMM-*Newton* extended survey of the Taurus molecular cloud (XEST). A&A 468:353–377. doi:10.1051/0004-6361:20065724, arXiv:astro-ph/0609160

Güdel M, Skinner SL, Mel'Nikov SY, Audard M, Telleschi A, Briggs KR (2007b) X-rays from T Tauri: a test case for accreting T Tauri stars. A&A 468:529–540. doi:10.1051/0004-6361:20066318, arXiv:astro-ph/0612589

Güdel M, Telleschi A, Audard M, Skinner SL, Briggs KR, Palla F, Dougados C (2007c) X-rays from jet-driving protostars and T Tauri stars. A&A 468:515–528. doi:10.1051/0004-6361:20065736, arXiv:astro-ph/0609182

Güdel M, Skinner SL, Audard M, Briggs KR, Cabrit S (2008) Discovery of a bipolar X-ray jet from the T Tauri star DG Tauri. A&A 478:797–807. doi:10.1051/0004-6361:20078141, 0712.1330

Guerrero MA, Chu YH (2008a) An X-ray survey of Wolf-Rayet stars in the magellanic clouds. I. The CHANDRA ACIS data set. ApJ Suppl 177:216–237. doi:10.1086/587059, 0802.0503

Guerrero MA, Chu YH (2008b) An X-ray survey of Wolf-Rayet stars in the magellanic clouds. II. The ROSAT PSPC and HRI data sets. ApJ Suppl 177:238–254. doi:10.1086/587060, 0802.0493

Guerrero MA, Carter JA, Chu YH, Foellmi C, Moffat AFJ, Oskinova L, Schnurr O (2008) An X-ray survey of Wolf-Rayet stars in the magellanic clouds. In: Poster presented at the 'X-ray Universe 2008' meeting (Grenada, Spain). http://xmm.esac.esa.int/external/xmm_science/workshops/2008symposium/guerrero_martin.pdf

Günther HM, Schmitt JHMM (2008) Where are the hot ion lines in classical T Tauri stars formed? A&A 481:735–745. doi:10.1051/0004-6361:20078674, 0801.2273

Günther HM, Schmitt JHMM (2009) Jets, accretion, coronae and all that: the enigmatic X-rays from the Herbig star HD 163296. ArXiv e-prints 0812.0285

Günther HM, Liefke C, Schmitt JHMM, Robrade J, Ness JU (2006) X-ray accretion signatures in the close CTTS binary V4046 Sagittarii. A&A 459:L29–L32. doi:10.1051/0004-6361:20066306, arXiv:astro-ph/0610121

Günther HM, Schmitt JHMM, Robrade J, Liefke C (2007) X-ray emission from classical T Tauri stars: accretion shocks and coronae? A&A 466:1111–1121. doi:10.1051/0004-6361:20065669, arXiv:astro-ph/0702579

Hamaguchi K, Corcoran MF, Petre R, White NE, Stelzer B, Nedachi K, Kobayashi N, Tokunaga AT (2005) Discovery of extremely embedded X-ray sources in the R Coronae Australis star-forming core. ApJ 623:291–301. doi:10.1086/428434, arXiv:astro-ph/0503029

Harnden FR Jr, Branduardi G, Gorenstein P, Grindlay J, Rosner R, Topka K, Elvis M, Pye JP, Vaiana GS (1979) Discovery of an star association in VI Cygni /Cyg OB2/. ApJ 234:L51–L54. doi:10.1086/183107

Hartmann L, Kenyon SJ (1996) The FU Orionis phenomenon. Ann Rev Astron Astrophys 34:207–240. doi:10.1146/annurev.astro.34.1.207

Hawley SL, Fisher GH, Simon T, Cully SL, Deustua SE, Jablonski M, Johns-Krull CM, Pettersen BR, Smith V, Spiesman WJ, Valenti J (1995) Simultaneous extreme-ultraviolet explorer and optical observations of AD leonis: evidence for large coronal loops and the neupert effect in stellar flares. ApJ 453:464–479. doi:10.1086/176408

Henley DB, Stevens IR, Pittard JM (2003) Theoretical X-ray line profiles from colliding wind binaries. MNRAS 346:773–786. doi:10.1111/j.1365-2966.2003.07121.x, arXiv:astro-ph/0306451

Henley DB, Stevens IR, Pittard JM (2005) Probing the wind–wind collision in γ^2 Velorum with high-resolution CHANDRA X-ray spectroscopy: evidence for sudden radiative braking and non-equilibrium ionization. MNRAS 356:1308–1326. doi:10.1111/j.1365-2966.2004.08556.x, arXiv:astro-ph/0411012

Hénoux JC (1995) Models for explaining the observed spatial variation of element abundances—a review. Adv Space Res 15:23–32. doi:10.1016/0273-1177(94)00015-S

Henrichs HF, de Jong JA, Donati JF, Catala C, Wade GA, Shorlin SLS, Veen PM, Nichols JS, Kaper L (2000) The magnetic field of β Cep and the Be phenomenon. In: Smith MA, Henrichs HF, Fabregat J (eds) IAU Colloq. 175: the Be phenomenon in early-type stars, astronomical society of the pacific conference series, vol 214, pp 324–329

Herbig GH (1960) The spectra of Be- and Ae-type stars associated with nebulosity. ApJ Suppl 4:337–368. doi:10.1086/190050

Herbig GH (1977) Eruptive phenomena in early stellar evolution. ApJ 217:693–715. doi:10.1086/155615

Herbig GH, Griffin RF (2006) θ^1 Orionis E as a spectroscopic binary. Astron J 132:1763–1767. doi:10.1086/507769

Howarth ID, Walborn NR, Lennon DJ, Puls J, Nazé Y, Annuk K, Antokhin I, Bohlender D, Bond H, Donati JF, Georgiev L, Gies D, Harmer D, Herrero A, Kolka I, McDavid D, Morel T, Negueruela I, Rauw G, Reig P (2007) Towards an understanding of the Of?p star HD 191612: optical spectroscopy. MNRAS 381:433–446. doi:10.1111/j.1365-2966.2007.12178.x, 0707.0594

Hubrig S, Schöller M, Yudin RV (2004) Magnetic fields in Herbig Ae stars. A&A 428:L1–L4. doi:10.1051/0004-6361:200400091, arXiv:astro-ph/0410571

Hubrig S, Briquet M, Schöller M, De Cat P, Mathys G, Aerts C (2006) Discovery of magnetic fields in the β Cephei star ξ^1 CMa and in several slowly pulsating B stars. MNRAS 369:L61–L65. doi:10.1111/j.1745-3933.2006.00175.x, arXiv:astro-ph/0604283

Hubrig S, Schöller M, Schnerr RS, González JF, Ignace R, Henrichs HF (2008) Magnetic field measurements of O stars with FORS 1 at the VLT. A&A 490:793–800. doi:10.1051/0004-6361:200810171, 0808.2039

Huenemoerder DP, Canizares CR, Schulz NS (2001) X-ray spectroscopy of II Pegasi: coronal temperature structure, abundances, and variability. ApJ 559:1135–1146. doi:10.1086/322419, arXiv:astro-ph/0106007

Huenemoerder DP, Canizares CR, Drake JJ, Sanz-Forcada J (2003) The coronae of AR Lacertae. ApJ 595:1131–1147. doi:10.1086/377490, arXiv:astro-ph/0306380

Huenemoerder DP, Testa P, Buzasi DL (2006) X-ray spectroscopy of the contact binary VW Cephei. ApJ 650:1119–1132. doi:10.1086/507404, arXiv:astro-ph/0606690

Huenemoerder DP, Kastner JH, Testa P, Schulz NS, Weintraub DA (2007) Evidence for accretion in the high-resolution X-ray spectrum of the T Tauri star system Hen 3-600. ApJ 671:592–604. doi:10.1086/522921, 0708.4393

Hussain GAJ, van Ballegooijen AA, Jardine M, Collier Cameron A (2002) The coronal topology of the rapidly rotating K0 dwarf AB Doradus. I. Using surface magnetic field maps to model the structure of the stellar corona. ApJ 575:1078–1086. doi:10.1086/341429, arXiv:astro-ph/0207452

Hussain GAJ, Brickhouse NS, Dupree AK, Jardine MM, van Ballegooijen AA, Hoogerwerf R, Collier Cameron A, Donati JF, Favata F (2005) Inferring coronal structure from X-ray light curves and Doppler shifts: a CHANDRA study of AB Doradus. ApJ 621:999–1008. doi:10.1086/427647, arXiv:astro-ph/0411571

Hussain GAJ, Jardine M, Donati JF, Brickhouse NS, Dunstone NJ, Wood K, Dupree AK, Collier Cameron A, Favata F (2007) The coronal structure of AB Doradus determined from contemporaneous Doppler imaging and X-ray spectroscopy. MNRAS 377:1488–1502. doi:10.1111/j.1365-2966.2007.11692.x, arXiv:astro-ph/0703619

Ignace R, Gayley KG (2002) Profile shapes for optically thick X-ray emission lines from stellar winds. ApJ 568:954–964. doi:10.1086/339059

Ignace R, Oskinova LM (1999) An explanation of observed trends in the X-ray emission from single Wolf-Rayet stars. A&A 348:L45–L48
Ignace R, Oskinova LM, Brown JC (2003) XMM-*Newton* observations of the nitrogen-rich Wolf-Rayet star WR 1. A&A 408:353–361. doi:10.1051/0004-6361:20031024
Imanishi K, Koyama K, Tsuboi Y (2001) CHANDRA observation of the ρ Ophiuchi cloud. ApJ 557:747–760. doi:10.1086/321691
Jardine M, Collier Cameron A, Donati JF (2002a) The global magnetic topology of AB Doradus. MNRAS 333:339–346. doi:10.1046/j.1365-8711.2002.05394.x, arXiv:astro-ph/0205132
Jardine M, Wood K, Collier Cameron A, Donati JF, Mackay DH (2002b) Inferring X-ray coronal structures from Zeeman–Doppler images. MNRAS 336:1364–1370. doi:10.1046/j.1365-8711.2002.05877.x, arXiv:astro-ph/0207522
Kahn SM, Leutenegger MA, Cottam J, Rauw G, Vreux JM, den Boggende AJF, Mewe R, Güdel M (2001) High resolution X-ray spectroscopy of zeta Puppis with the XMM-*Newton* reflection grating spectrometer. A&A 365:L312–L317. doi:10.1051/0004-6361:20000093, arXiv:astro-ph/0011026
Kashyap VL, Drake JJ, Güdel M, Audard M (2002) Flare heating in stellar coronae. ApJ 580:1118–1132. doi:10.1086/343869, arXiv:astro-ph/0208546
Kastner JH, Huenemoerder DP, Schulz NS, Canizares CR, Weintraub DA (2002) Evidence for accretion: high-resolution X-ray spectroscopy of the classical T Tauri star TW hydrae. ApJ 567:434–440. doi:10.1086/338419, arXiv:astro-ph/0111049
Kastner JH, Huenemoerder DP, Schulz NS, Canizares CR, Li J, Weintraub DA (2004a) The coronal X-ray spectrum of the multiple weak-lined T Tauri star system HD 98800. ApJ 605:L49–L52. doi:10.1086/420769, arXiv:astro-ph/0403062
Kastner JH, Richmond M, Grosso N, Weintraub DA, Simon T, Frank A, Hamaguchi K, Ozawa H, Henden A (2004b) An X-ray outburst from the rapidly accreting young star that illuminates McNeil's nebula. Nature 430:429–431. doi:10.1038/nature02747, arXiv:astro-ph/0408332
Kastner JH, Franz G, Grosso N, Bally J, McCaughrean MJ, Getman K, Feigelson ED, Schulz NS (2005) X-ray emission from orion Nebula cluster stars with circumstellar disks and jets. ApJ Suppl 160:511–529. doi:10.1086/432096, arXiv:astro-ph/0506650
Kastner JH, Richmond M, Grosso N, Weintraub DA, Simon T, Henden A, Hamaguchi K, Frank A, Ozawa H (2006) V1647 Orionis: the X-ray evolution of a pre-main-sequence accretion burst. ApJ 648:L43–L46. doi:10.1086/507992, arXiv:astro-ph/0607653
Kramer RH, Cohen DH, Owocki SP (2003) X-ray emission-line profile modeling of O stars: fitting a spherically symmetric analytic wind-shock model to the CHANDRA spectrum of ζ Puppis. ApJ 592:532–538. doi:10.1086/375390, arXiv:astro-ph/0211550
Krucker S, Benz AO (1998) Energy distribution of heating processes in the quiet solar corona. ApJ 501:L213–L216. doi:10.1086/311474
Ku WHM, Chanan GA (1979) Einstein observations of the Orion Nebula. ApJ 234:L59–L63. doi:10.1086/183109
Laming JM (2004) A unified picture of the first ionization potential and inverse first ionization potential effects. ApJ 614:1063–1072. doi:10.1086/423780, arXiv:astro-ph/0405230
Laming JM, Drake JJ (1999) Stellar coronal abundances. VI. The first ionization potential effect and XI Bootis A: solar-like anomalies at intermediate-activity levels. ApJ 516:324–334. doi:10.1086/307112
Laming JM, Drake JJ, Widing KG (1996) Stellar coronal abundances. IV. Evidence of the FIP effect in the corona of ε Eridani? ApJ 462:948–959. doi:10.1086/177208
Landi E, Feldman U, Innes DE, Curdt W (2003) Mass motions and plasma properties in the 10^7 K flare solar corona. ApJ 582:506–519. doi:10.1086/344524
Leutenegger MA, Paerels FBS, Kahn SM, Cohen DH (2006) Measurements and analysis of helium-like triplet ratios in the X-ray spectra of O-type stars. ApJ 650:1096–1110. doi:10.1086/507147, arXiv:astro-ph/0606370
Leutenegger MA, Owocki SP, Kahn SM, Paerels FBS (2007) Evidence for the importance of resonance scattering in X-ray emission line profiles of the O star ζ Puppis. ApJ 659:642–649. doi:10.1086/512031, arXiv:astro-ph/0610181
Li Q, Cassinelli JP, Brown JC, Waldron WL, Miller NA (2008) X-ray emission from magnetically torqued disks of Oe/Be stars. ApJ 672:1174–1182. doi:10.1086/523879, 0710.2633
Liefke C, Schmitt JHMM (2006) The coronal Ne/O abundance of α Centauri. A&A 458:L1–L4. doi:10.1051/0004-6361:20066220, arXiv:astro-ph/0609015

Linder N, Rauw G, Pollock AMT, Stevens IR (2006) The XMM-*Newton* view of Plaskett's star and its surroundings. MNRAS 370:1623–1632. doi:10.1111/j.1365-2966.2006.10611.x

Lorenzetti D, Giannini T, Calzoletti L, Puccetti S, Antoniucci S, Arkharov AA, di Paola A, Larionov VM, Nisini B (2006) Evidence for T Tauri-like emission in the EXor V1118 Ori from near-IR and X-ray data. A&A 453:579–586. doi:10.1051/0004-6361:20054562, arXiv:astro-ph/0603388

Lucy LB, White RL (1980) X-ray emission from the winds of hot stars. ApJ 241:300–305. doi:10.1086/158342

Macfarlane JJ, Cassinelli JP, Welsh BY, Vedder PW, Vallerga JV, Waldron WL (1991) Predicted extreme-ultraviolet line emission for nearby main-sequence B stars. ApJ 380:564–574. doi:10.1086/170614

Macfarlane JJ, Waldron WL, Corcoran MF, Wolff MJ, Wang P, Cassinelli JP (1993) Effects of coronal and shock-produced X-rays on the ionization distribution in hot star winds. ApJ 419:813–823. doi:10.1086/173533

Magee HRM, Güdel M, Audard M, Mewe R (2003) An XMM-*Newton* observation of the flare star AU Mic. Adv Space Res 32:1149–1154. doi:10.1016/S0273-1177(03)00321-1

Maggio A, Ness JU (2005) Spectral indications of density variability in the corona of AD Leonis. ApJ 622:L57–L60. doi:10.1086/429487, arXiv:astro-ph/0502379

Maggio A, Drake JJ, Kashyap V, Harnden FR Jr, Micela G, Peres G, Sciortino S (2004) X-ray spectroscopy of the unsteady quiescent corona of AD Leonis with CHANDRA. ApJ 613:548–566. doi:10.1086/422904, arXiv:astro-ph/0405580

Maggio A, Flaccomio E, Favata F, Micela G, Sciortino S, Feigelson ED, Getman KV (2007) Coronal abundances in Orion Nebula cluster stars. ApJ 660:1462–1479. doi:10.1086/513088, arXiv:astro-ph/0703439

Markova N, Puls J, Scuderi S, Markov H (2005) Bright OB stars in the Galaxy. II. Wind variability in O supergiants as traced by Hα. A&A 440:1133–1151. doi:10.1051/0004-6361:20041774, arXiv:astro-ph/0505613

Martins F, Schaerer D, Hillier DJ (2005) A new calibration of stellar parameters of Galactic O stars. A&A 436:1049–1065. doi:10.1051/0004-6361:20042386, arXiv:astro-ph/0503346

Matranga M, Mathioudakis M, Kay HRM, Keenan FP (2005) Flare X-ray observations of AB Doradus: evidence of stellar coronal opacity. ApJ 621:L125–L128. doi:10.1086/429288, arXiv:astro-ph/0502063

McKenzie DL, Broussard RM, Landecker PB, Rugge HR, Young RM, Doschek GA, Feldman U (1980) Electron densities in a solar flare derived from X-ray spectra. ApJ 238:L43–L46. doi:10.1086/183254

Mewe R, Kaastra JS, Schrijver CJ, van den Oord GHJ, Alkemade FJM (1995) EUV spectroscopy of cool stars. I. The corona of α Centauri observed with EUVE. R. A&A 296:477–498

Mewe R, Kaastra JS, van den Oord GHJ, Vink J, Tawara Y (1997) ASCA and EUVE observations of II Pegasi: flaring and quiescent coronal emission. A&A 320:147–158

Mewe R, Raassen AJJ, Drake JJ, Kaastra JS, van der Meer RLJ, Porquet D (2001) CHANDRA-LETGS X-ray observations of Capella. Temperature, density and abundance diagnostics. A&A 368:888–900. doi:10.1051/0004-6361:20010026

Mewe R, Raassen AJJ, Cassinelli JP, van der Hucht KA, Miller NA, Güdel M (2003) High-resolution X-ray spectroscopy of tau Scorpii (B0.2V) with XMM-*Newton*. A&A 398:203–211. doi:10.1051/0004-6361:20021577

Miller NA, Cassinelli JP, Waldron WL, MacFarlane JJ, Cohen DH (2002) New challenges for wind shock models: the CHANDRA spectrum of the hot star δ Orionis. ApJ 577:951–960. doi:10.1086/342111

Mitra-Kraev U, Harra LK, Güdel M, Audard M, Branduardi-Raymont G, Kay HRM, Mewe R, Raassen AJJ, van Driel-Gesztelyi L (2005) Relationship between X-ray and ultraviolet emission of flares from dMe stars observed by XMM-Newton. A&A 431:679–686. doi:10.1051/0004-6361:20041201

Mutel RL, Lestrade JF, Preston RA, Phillips RB (1985) Dual polarization VLBI observations of stellar binary systems at 5 GHz. ApJ 289:262–268. doi:10.1086/162886

Nazé Y, Rauw G (2008) High-resolution X-ray spectroscopy of θ Carinae. A&A 490:801–806. doi:10.1051/0004-6361:200810364, 0808.3353

Nazé Y, Rauw G, Vreux JM, De Becker M (2004) HD 108: the mystery deepens with XMM-*Newton* observations. A&A 417:667–677. doi:10.1051/0004-6361:20034422, arXiv:astro-ph/0402480

Nazé Y, Corcoran MF, Koenigsberger G, Moffat AFJ (2007a) First detection of phase-dependent colliding wind X-ray emission outside the milky way. ApJ 658:L25–L28. doi:10.1086/513510, arXiv:astro-ph/0702403

Nazé Y, Rauw G, Pollock AMT, Walborn NR, Howarth ID (2007b) Towards an understanding of the Of?p star HD191612: phase-resolved multiwavelength observations. MNRAS 375:145–153. doi:10.1111/j.1365-2966.2006.11270.x, arXiv:astro-ph/0611230

Nazé Y, Rauw G, Manfroid J (2008a) CHANDRA monitoring of the very massive binary WR20a and the young massive cluster Westerlund 2. A&A 483:171–182. doi:10.1051/0004-6361:20078851, 0801.0647

Nazé Y, Walborn NR, Martins F (2008b) The mysterious Of?p class and the magnetic O-star θ^1 Ori C: confronting observations. Revista Mexicana de Astronomia y Astrofisica 44:331–340, 0807.3496

Nazé Y, Walborn NR, Rauw G, Martins F, Pollock AMT, Bond HE (2008c) Hd 148937: a multiwavelength study of the third galactic member of the Of?p class. Astron J 135:1946–1957. doi:10.1088/0004-6256/135/5/1946, 0803.0605

Ness JU, Schmitt JHMM (2005) Anomalous X-ray line ratios in the cTTS TW Hydrae. A&A 444:L41–L44. doi:10.1051/0004-6361:200500208, arXiv:astro-ph/0510749

Ness JU, Mewe R, Schmitt JHMM, Raassen AJJ, Porquet D, Kaastra JS, van der Meer RLJ, Burwitz V, Predehl P (2001) Helium-like triplet density diagnostics. Applications to CHANDRA-LETGS X-ray observations of Capella and Procyon. A&A 367:282–296. doi:10.1051/0004-6361:20000419, arXiv:astro-ph/0012223

Ness JU, Schmitt JHMM, Burwitz V, Mewe R, Predehl P (2002) CHANDRA LETGS observation of the active binary Algol. A&A 387:1032–1046. doi:10.1051/0004-6361:20020445, arXiv:astro-ph/0203431

Ness JU, Brickhouse NS, Drake JJ, Huenemoerder DP (2003a) Modeling the Ne IX triplet spectral region of capella with the CHANDRA and XMM-*Newton* gratings. ApJ 598:1277–1289. doi:10.1086/379059, arXiv:astro-ph/0308317

Ness JU, Schmitt JHMM, Audard M, Güdel M, Mewe R (2003b) Are stellar coronae optically thin in X-rays? A systematic investigation of opacity effects. A&A 407:347–358. doi:10.1051/0004-6361:20030880, arXiv:astro-ph/0306308

Ness JU, Güdel M, Schmitt JHMM, Audard M, Telleschi A (2004) On the sizes of stellar X-ray coronae. A&A 427:667–683. doi:10.1051/0004-6361:20040504, arXiv:astro-ph/0407231

Neupert WM (1968) Comparison of solar X-ray line emission with microwave emission during flares. ApJ 153:L59–L64. doi:10.1086/180220

Nordon R, Behar E (2007) Six large coronal X-ray flares observed with CHANDRA. A&A 464:309–321. doi:10.1051/0004-6361:20066449, arXiv:astro-ph/0611386

Nordon R, Behar E (2008) Abundance variations and first ionization potential trends during large stellar flares. A&A 482:639–651. doi:10.1051/0004-6361:20078848, 0712.0482

Nordon R, Behar E, Güdel M (2006) On temperature and abundance effects during an X-ray flare on σ Geminorum. A&A 446:621–626. doi:10.1051/0004-6361:20054018, arXiv:astro-ph/0510023

Nordsieck KH, Cassinelli JP, Anderson CM (1981) Search for optical coronal line emission from the X-ray sources Epsilon Orionis /B0 Ia/ and Kappa Orionis /B0.5 Ia/. ApJ 248:678–683. doi:10.1086/159192

Oskinova LM (2005) Evolution of X-ray emission from young massive star clusters. MNRAS 361:679–694. doi:10.1111/j.1365-2966.2005.09229.x, arXiv:astro-ph/0505512

Oskinova LM, Clarke D, Pollock AMT (2001) Rotationally modulated X-ray emission from the single O star ζ Ophiuchi. A&A 378:L21–L24. doi:10.1051/0004-6361:20011222

Oskinova LM, Ignace R, Hamann WR, Pollock AMT, Brown JC (2003) The conspicuous absence of X-ray emission from carbon-enriched Wolf-Rayet stars. A&A 402:755–765. doi:10.1051/0004-6361:20030300, arXiv:astro-ph/0303025

Oskinova LM, Feldmeier A, Hamann WR (2006) High-resolution X-ray spectroscopy of bright O-type stars. MNRAS 372:313–326. doi:10.1111/j.1365-2966.2006.10858.x, arXiv:astro-ph/0603286

Oskinova LM, Hamann WR, Feldmeier A (2007) Neglecting the porosity of hot-star winds can lead to underestimating mass-loss rates. A&A 476:1331–1340. doi:10.1051/0004-6361:20066377, 0704.2390

Oskinova LM, Hamann W, Feldmeier A, Ignace R, Chu Y (2009) Discovery of X-ray emission from the Wolf-Rayet star WR142 of oxygen subtype. ArXiv e-prints 0901.4553

Osten RA, Brown A, Ayres TR, Linsky JL, Drake SA, Gagné M, Stern RA (2000) Radio, X-ray, and extreme-ultraviolet coronal variability of the short-period RS canum venaticorum binary σ^2 Coronae Borealis. ApJ 544:953–976. doi:10.1086/317249

Osten RA, Ayres TR, Brown A, Linsky JL, Krishnamurthi A (2003) CHANDRA, extreme ultraviolet explorer, and very large array observations of the active binary system σ^2 Coronae Borealis. ApJ 582:1073–1101. doi:10.1086/344797

Osten RA, Brown A, Ayres TR, Drake SA, Franciosini E, Pallavicini R, Tagliaferri G, Stewart RT, Skinner SL, Linsky JL (2004) A multiwavelength perspective of flares on HR 1099: 4 years of coordinated campaigns. ApJ Suppl 153:317–362. doi:10.1086/420770, arXiv:astro-ph/0402613

Osten RA, Hawley SL, Allred JC, Johns-Krull CM, Roark C (2005) From radio to X-ray: flares on the dMe flare star EV Lacertae. ApJ 621:398–416. doi:10.1086/427275, arXiv:astro-ph/0411236

Osten RA, Drake S, Tueller J, Cummings J, Perri M, Moretti A, Covino S (2007) Nonthermal hard X-ray emission and iron Kα emission from a superflare on II Pegasi. ApJ 654:1052–1067. doi:10.1086/509252, arXiv:astro-ph/0609205

Ottmann R, Schmitt JHMM, Kuerster M (1993) A study of the spatial and spectral characteristics of the corona of AR Lacertae. ApJ 413:710–723. doi:10.1086/173039

Owocki SP, Cohen DH (1999) A simple scaling analysis of X-ray emission and absorption in hot-star winds. ApJ 520:833–840. doi:10.1086/307500, arXiv:astro-ph/9901250

Owocki SP, Cohen DH (2001) X-ray line profiles from parameterized emission within an accelerating stellar wind. ApJ 559:1108–1116. doi:10.1086/322413, arXiv:astro-ph/0101294

Owocki SP, Cohen DH (2006) The effect of porosity on X-ray emission-line profiles from hot-star winds. ApJ 648:565–571. doi:10.1086/505698, arXiv:astro-ph/0602054

Owocki SP, Castor JI, Rybicki GB (1988) Time-dependent models of radiatively driven stellar winds. I—Nonlinear evolution of instabilities for a pure absorption model. ApJ 335:914–930. doi:10.1086/166977

Palla F, Stahler SW (1993) The pre-main-sequence evolution of intermediate-mass stars. ApJ 418:414–425. doi:10.1086/173402

Pallavicini R, Serio S, Vaiana GS (1977) A survey of soft X-ray limb flare images—the relation between their structure in the corona and other physical parameters. ApJ 216:108–122. doi:10.1086/155452

Pallavicini R, Golub L, Rosner R, Vaiana GS, Ayres T, Linsky JL (1981) Relations among stellar X-ray emission observed from Einstein, stellar rotation and bolometric luminosity. ApJ 248:279–290. doi:10.1086/159152

Parker EN (1988) Nanoflares and the solar X-ray corona. ApJ 330:474–479. doi:10.1086/166485

Parnell CE, Jupp PE (2000) Statistical analysis of the energy distribution of nanoflares in the quiet Sun. ApJ 529:554–569. doi:10.1086/308271

Peres G, Orlando S, Reale F, Rosner R (2001) The distribution of the emission measure, and of the heating budget, among the loops in the corona. ApJ 563:1045–1054. doi:10.1086/323769, arXiv:astro-ph/0111192

Petit V, Wade GA, Drissen L, Montmerle T, Alecian E (2008) Discovery of two magnetic massive stars in the Orion Nebula Cluster: a clue to the origin of neutron star magnetic fields? MNRAS 387:L23–L27. doi:10.1111/j.1745-3933.2008.00474.x, 0803.2691

Phillips KJH, Bhatia AK, Mason HE, Zarro DM (1996) High coronal electron densities in a solar flare from Fe XXI and Fe XXII X-ray line measurements. ApJ 466:549–560. doi:10.1086/177531

Phillips KJH, Mathioudakis M, Huenemoerder DP, Williams DR, Phillips ME, Keenan FP (2001) X-ray and extreme-ultraviolet emission from the coronae of Capella. MNRAS 325:1500–1510. doi:10.1046/j.1365-8711.2001.04555.x

Pittard JM, Dougherty SM (2006) Radio, X-ray, and γ-ray emission models of the colliding-wind binary WR140. MNRAS 372:801–826. doi:10.1111/j.1365-2966.2006.10888.x, arXiv:astro-ph/0603787

Pittard JM, Stevens IR, Corcoran MF, Gayley KG, Marchenko SV, Rauw G (2000) Coordinated monitoring of the eccentric O-star binary Iota Orionis: the X-ray analysis. MNRAS 319:137–153, arXiv:astro-ph/0007036

Pittard JM, Stevens IR, Williams PM, Pollock AMT, Skinner SL, Corcoran MF, Moffat AFJ (2002) High-resolution X-ray imaging of the colliding wind shock in WR 147. A&A 388:335–345. doi:10.1051/0004-6361:20020465, arXiv:astro-ph/0204212

Pizzolato N, Maggio A, Micela G, Sciortino S, Ventura P (2003) The stellar activity-rotation relationship revisited: Dependence of saturated and non-saturated X-ray emission regimes on stellar mass for late-type dwarfs. A&A 397:147–157. doi:10.1051/0004-6361:20021560

Pollock AMT (1987) The Einstein view of the Wolf-Rayet stars. ApJ 320:283–295. doi:10.1086/165539

Pollock AMT (1995) The X-ray view of the Wolf-Rayet stars (Invited). In: van der Hucht KA, Williams PM (eds) Wolf-Rayet stars: binaries; colliding winds; evolution, IAU symposium, vol 163, pp 429–437

Pollock AMT (2007) A new paradigm for the X-ray emission of O stars from XMM-*Newton* observations of the O9.7 supergiant ζ Orionis. A&A 463:1111–1123. doi:10.1051/0004-6361:20053838, arXiv:astro-ph/0612500

Pollock AMT, Haberl F, Corcoran MF (1995) The ROSAT PSPC survey of the Wolf-Rayet stars. In: van der Hucht KA, Williams PM (eds) Wolf-Rayet stars: binaries; colliding winds; evolution, IAU symposium, vol 163, pp 512–517

Pollock AMT, Corcoran MF, Stevens IR (2002) Testing colliding-wind X-ray theories with WR140. In: Moffat AFJ, St-Louis N (eds) Interacting winds from massive stars, astronomical society of the Pacific conference series, vol 260, pp 537–546

Pollock AMT, Corcoran MF, Stevens IR, Williams PM (2005) Bulk velocities, chemical composition, and ionization structure of the X-ray shocks in WR 140 near Periastron as revealed by the CHANDRA gratings. ApJ 629:482–498. doi:10.1086/431193

Porquet D, Mewe R, Dubau J, Raassen AJJ, Kaastra JS (2001) Line ratios for helium-like ions: applications to collision-dominated plasmas. A&A 376:1113–1122. doi:10.1051/0004-6361:20010959, arXiv:astro-ph/0107329

Pravdo SH, Feigelson ED, Garmire G, Maeda Y, Tsuboi Y, Bally J (2001) Discovery of X-rays from the protostellar outflow object HH2. Nature 413:708–711

Preibisch T, Kim YC, Favata F, Feigelson ED, Flaccomio E, Getman K, Micela G, Sciortino S, Stassun K, Stelzer B, Zinnecker H (2005) The origin of T Tauri X-ray emission: new insights from the CHANDRA orion ultradeep project. ApJ Suppl 160:401–422. doi:10.1086/432891, arXiv:astro-ph/0506526

Prinja RK, Barlow MJ, Howarth ID (1990) Terminal velocities for a large sample of O stars, B supergiants, and Wolf-Rayet stars. ApJ 361:607–620. doi:10.1086/169224

Prisinzano L, Micela G, Flaccomio E, Stauffer JR, Megeath T, Rebull L, Robberto M, Smith K, Feigelson ED, Grosso N, Wolk S (2008) X-ray properties of protostars in the Orion Nebula. ApJ 677:401–424. doi:10.1086/528842, 0712.2975

Raassen AJJ, Mewe R, Audard M, Güdel M, Behar E, Kaastra JS, van der Meer RLJ, Foley CR, Ness JU (2002) High-resolution X-ray spectroscopy of Procyon by CHANDRA and XMM-*Newton*. A&A 389:228–238. doi:10.1051/0004-6361:20020529, arXiv:astro-ph/0204385

Raassen AJJ, Mewe R, Audard M, Güdel M (2003a) The X-ray spectra of the flaring and quiescent states of AT Microscopii observed by XMM-*Newton*. A&A 411:509–515. doi:10.1051/0004-6361:20031389, arXiv:astro-ph/0309383

Raassen AJJ, Ness JU, Mewe R, van der Meer RLJ, Burwitz V, Kaastra JS (2003b) CHANDRA-LETGS X-ray observation of alpha Centauri: a nearby (G2V + K1V) binary system. A&A 400:671–678. doi:10.1051/0004-6361:20021899

Raassen AJJ, Cassinelli JP, Miller NA, Mewe R, Tepedelenlioğlu E (2005) XMM-*Newton* observations of β Centauri (B1 III): the temperature structure in the hot plasma and the photosphere-wind connection. A&A 437:599–609. doi:10.1051/0004-6361:20052650

Raassen AJJ, van der Hucht KA, Miller NA, Cassinelli JP (2008) XMM-*Newton* observations of ζ Orionis (O9.7 Ib): a collisional ionization equilibrium model. A&A 478:513–520. doi:10.1051/0004-6361:20077891, 0803.0873

Randich S, Schmitt JHMM, Prosser CF, Stauffer JR (1996) The X-ray properties of the young open cluster around α Persei. A&A 305:785–805

Rauw G (2008) Colliding wind signatures in early-type binaries. In: Revista Mexicana de astronomia y astrofisica conference series, vol 33, pp 59–64

Rauw G, Stevens IR, Pittard JM, Corcoran MF (2000) ASCA spectroscopy of the hard X-ray emission from the colliding wind interaction in γ^2 Velorum. MNRAS 316:129–136

Rauw G, Blomme R, Waldron WL, Corcoran MF, Pittard JM, Pollock AMT, Runacres MC, Sana H, Stevens IR, Van Loo S (2002a) A multi-wavelength investigation of the non-thermal radio emitting O-star 9 Sgr. A&A 394:993–1008. doi:10.1051/0004-6361:20020926

Rauw G, Vreux JM, Stevens IR, Gosset E, Sana H, Jamar C, Mason KO (2002b) Phase-resolved X-ray and optical spectroscopy of the massive binary HD 93403. A&A 388:552–562. doi:10.1051/0004-6361:20020523

Rauw G, De Becker M, Nazé Y, Crowther PA, Gosset E, Sana H, van der Hucht KA, Vreux JM, Williams PM (2004) WR 20a: a massive cornerstone binary system comprising two extreme early-type stars. A&A 420:L9–L13. doi:10.1051/0004-6361:20040150, arXiv:astro-ph/0404551

Rauw G, De Becker M, Linder N (2005) XMM-*Newton* observations of the Cyg OB2 association. In: Rauw G, Nazé Y, Blomme R, Gosset E (eds) Massive stars and high-energy emission in OB associations, pp 103–106

Reale F, Güdel M, Peres G, Audard M (2004) Modeling an X-ray flare on Proxima Centauri: evidence of two flaring loop components and of two heating mechanisms at work. A&A 416:733–747. doi:10.1051/0004-6361:20034027, arXiv:astro-ph/0312267

Robrade J, Schmitt JHMM (2005) X-ray properties of active M dwarfs as observed by XMM-*Newton*. A&A 435:1073–1085. doi:10.1051/0004-6361:20041941, arXiv:astro-ph/0504145

Robrade J, Schmitt JHMM (2006) XMM-*Newton* X-ray spectroscopy of classical T Tauri stars. A&A 449:737–747. doi:10.1051/0004-6361:20054247, arXiv:astro-ph/0601234

Robrade J, Schmitt JHMM (2007) X-rays from RU Lupi: accretion and winds in classical T Tauri stars. A&A 473:229–238. doi:10.1051/0004-6361:20077644, 0706.2879

Robrade J, Schmitt JHMM, Favata F (2008) Neon and oxygen in low activity stars: towards a coronal unification with the Sun. A&A 486:995–1002. doi:10.1051/0004-6361:200809690, 0806.0775

Rodonò M, Pagano I, Leto G, Walter F, Catalano S, Cutispoto G, Umana G (1999) Beppo-SAX observations of AR Lacertae. A&A 346:811–818

Rosner R, Tucker WH, Vaiana GS (1978) Dynamics of the quiescent solar corona. ApJ 220:643–645. doi:10.1086/155949

Sako M, Kahn SM, Paerels F, Liedahl DA, Watanabe S, Nagase F, Takahashi T (2003) Structure and dynamics of stellar winds in high-mass X-ray binaries. ArXiv Astrophysics e-prints arXiv:astro-ph/0309503

Sana H, Stevens IR, Gosset E, Rauw G, Vreux JM (2004) A phase-resolved XMM-*Newton* campaign on the colliding-wind binary HD 152248. MNRAS 350:809–828. doi:10.1111/j.1365-2966.2004.07719.x, arXiv:astro-ph/0402412

Sana H, Antokhina E, Royer P, Manfroid J, Gosset E, Rauw G, Vreux JM (2005) The massive binary CPD−41°7742. II. Optical light curve and X-ray observations. A&A 441:213–229. doi:10.1051/0004-6361:20052746, arXiv:astro-ph/0509542

Sana H, Rauw G, Nazé Y, Gosset E, Vreux JM (2006) An XMM-*Newton* view of the young open cluster NGC 6231—II. The OB star population. MNRAS 372:661–678. doi:10.1111/j.1365-2966.2006.10847.x, arXiv:astro-ph/0607486

Sanz-Forcada J, Brickhouse NS, Dupree AK (2002) Quiescent and flaring structure in RS Canum Venaticorum stars. ApJ 570:799–819. doi:10.1086/339730

Sanz-Forcada J, Maggio A, Micela G (2003) Three years in the coronal life of AB Dor. I. Plasma emission measure distributions and abundances at different activity levels. A&A 408:1087–1102. doi:10.1051/0004-6361:20031025, arXiv:astro-ph/0307088

Sanz-Forcada J, Favata F, Micela G (2004) Coronal versus photospheric abundances of stars with different activity levels. A&A 416:281–290. doi:10.1051/0004-6361:20034466, arXiv:astro-ph/0311367

Sanz-Forcada J, Favata F, Micela G (2007) Eclipsed X-ray flares in binary stars: geometrical constraints on the flare's location and size. A&A 466:309–316. doi:10.1051/0004-6361:20065743, arXiv:astro-ph/0701814

Scelsi L, Maggio A, Peres G, Pallavicini R (2005) Coronal properties of G-type stars in different evolutionary phases. A&A 432:671–685. doi:10.1051/0004-6361:20041739, arXiv:astro-ph/0501631

Scelsi L, Maggio A, Micela G, Briggs K, Güdel M (2007) Coronal abundances of X-ray bright pre-main sequence stars in the Taurus molecular cloud. A&A 473:589–601. doi:10.1051/0004-6361:20077792, 0707.2857

Schild H, Güdel M, Mewe R, Schmutz W, Raassen AJJ, Audard M, Dumm T, van der Hucht KA, Leutenegger MA, Skinner SL (2004) Wind clumping and the wind–wind collision zone in the Wolf-Rayet binary γ^2 Velorum observations at high and low state. XMM-*Newton* observations at high and low state. A&A 422:177–191. doi:10.1051/0004-6361:20047035, arXiv:astro-ph/0404610

Schmelz JT, Nasraoui K, Roames JK, Lippner LA, Garst JW (2005) Neon lights up a controversy: the Solar Ne/O abundance. ApJ 634:L197–L200. doi:10.1086/499051, arXiv:astro-ph/0510230

Schmitt JHMM, Favata F (1999) Continuous heating of a giant X-ray flare on Algol. Nature 401:44–46. doi:10.1038/43389, arXiv:astro-ph/9909040

Schmitt JHMM, Collura A, Sciortino S, Vaiana GS, Harnden FR Jr, Rosner R (1990) Einstein observatory coronal temperatures of late-type stars. ApJ 365:704–728. doi:10.1086/169525

Schmitt JHMM, Haisch BM, Drake JJ (1994) A spectroscopic measurement of the Coronal density of Procyon. Science 265:1420–1422. doi:10.1126/science.265.5177.1420

Schmitt JHMM, Drake JJ, Haisch BM, Stern RA (1996) A close look at the Coronal density of Procyon. ApJ 467:841–850. doi:10.1086/177657

Schmitt JHMM, Ness JU, Franco G (2003) A spatially resolved limb flare on Algol B observed with XMM-*Newton*. A&A 412:849–855. doi:10.1051/0004-6361:20034057, arXiv:astro-ph/0308394

Schmitt JHMM, Robrade J, Ness JU, Favata F, Stelzer B (2005) X-rays from accretion shocks in T Tauri stars: The case of BP Tau. A&A 432:L35–L38. doi:10.1051/0004-6361:200500014, arXiv:astro-ph/0503144
Schmitt JHMM, Reale F, Liefke C, Wolter U, Fuhrmeister B, Reiners A, Peres G (2008) A coronal explosion on the flare star CN Leonis. A&A 481:799–805. doi:10.1051/0004-6361:20079017, 0801.3752
Schneider PC, Schmitt JHMM (2008) The nature of the soft X-ray source in DG Tauri. A&A 488:L13–L16. doi:10.1051/0004-6361:200810261, 0807.2156
Schnerr RS, Henrichs HF, Neiner C, Verdugo E, de Jong J, Geers VC, Wiersema K, van Dalen B, Tijani A, Plaggenborg B, Rygl KLJ (2008) Magnetic field measurements and wind-line variability of OB-type stars. A&A 483:857–867. doi:10.1051/0004-6361:20077740
Schrijver CJ, Haisch B (1996) On the Coronal field topology in warm stars: is Procyon a warm hybrid. ApJ 456:L55–L58. doi:10.1086/309849
Schrijver CJ, Mewe R, Walter FM (1984) Coronal activity in F-, G-, and K-type stars. II—Coronal structure and rotation. A&A 138:258–266
Schrijver CJ, Lemen JR, Mewe R (1989) Coronal activity in F-, G-, and K-type stars. IV—Evidence for expanding loop geometries in stellar coronae. ApJ 341:484–492. doi:10.1086/167509
Schrijver CJ, van den Oord GHJ, Mewe R (1994) The optical thickness of stellar coronae in EUV lines. A&A 289:L23–L26
Schrijver CJ, Mewe R, van den Oord GHJ, Kaastra JS (1995) EUV spectroscopy of cool stars. II. Coronal structure of selected cool stars observed with the EUVE. A&A 302:438–456
Schulz NS, Canizares C, Huenemoerder D, Tibbets K (2003) X-ray modeling of very young early-type stars in the Orion Trapezium: signatures of magnetically confined plasmas and evolutionary implications. ApJ 595:365–383. doi:10.1086/377214, arXiv:astro-ph/0306008
Sciortino S (2008) Results and perspectives of young stellar object long look programs. Astronomische Nachrichten 329:214–217. doi:10.1002/asna.200710916, 0712.0281
Sciortino S, Vaiana GS, Harnden FR Jr, Ramella M, Morossi C, Rosner R, Schmitt JHMM (1990) Relationship between optical and X-ray properties of O-type stars surveyed with the Einstein observatory. ApJ 361:621–643. doi:10.1086/169225
Serio S, Peres G, Vaiana GS, Golub L, Rosner R (1981) Closed coronal structures. II—Generalized hydrostatic model. ApJ 243:288–300. doi:10.1086/158597
Seward FD, Forman WR, Giacconi R, Griffiths RE, Harnden FR Jr, Jones C, Pye JP (1979) X-rays from Eta Carinae and the surrounding nebula. ApJ 234:L55–L58. doi:10.1086/183108
Shibata K, Yokoyama T (1999) Origin of the Universal correlation between the flare temperature and the emission measure for solar and stellar flares. ApJ 526:L49–L52. doi:10.1086/312354
Shibata K, Yokoyama T (2002) A Hertzsprung–Russell-like diagram for solar/stellar flares and corona: emission measure versus temperature diagram. ApJ 577:422–432. doi:10.1086/342141, arXiv:astro-ph/0206016
Siarkowski M, Pres P, Drake SA, White NE, Singh KP (1996) Corona(e) of AR Lacertae. II. The spatial structure. ApJ 473:470–482. doi:10.1086/178159
Skinner SL, Zhekov SA, Güdel M, Schmutz W (2002a) XMM-*Newton* and very large array observations of the variable Wolf-Rayet star EZ Canis Majoris: evidence for a close companion? ApJ 579:764–773. doi:10.1086/342841, arXiv:astro-ph/0207171
Skinner SL, Zhekov SA, Güdel M, Schmutz W (2002b) XMM-*Newton* detection of hard X-ray emission in the nitrogen-type Wolf-Rayet star WR 110. ApJ 572:477–486. doi:10.1086/340307, arXiv:astro-ph/0203270
Skinner SL, Güdel M, Audard M, Smith K (2004) New perspectives on the X-ray emission of HD 104237 and other nearby herbig Ae/Be stars from XMM-*Newton* and CHANDRA. ApJ 614:221–234. doi:10.1086/422708, arXiv:astro-ph/0405450
Skinner S, Güdel M, Schmutz W, Zhekov S (2006a) X-ray observations of binary and single Wolf-Rayet stars with XMM-*Newton* and CHANDRA. Astrophys Space Sci 304:97–99. doi:10.1007/s10509-006-9082-3, arXiv:astro-ph/0511137
Skinner SL, Briggs KR, Güdel M (2006b) The unusual X-ray spectrum of FU Orionis. ApJ 643:995–1002. doi:10.1086/502967, arXiv:astro-ph/0603378
Skinner SL, Simmons AE, Audard M, Güdel M (2007) Hard X-rays and fluorescent iron emission from the embedded infrared cluster in NGC 2071. ApJ 658:1144–1151. doi:10.1086/511815, arXiv:astro-ph/0612563

Skinner SL, Sokal KR, Cohen DH, Gagné M, Owocki SP, Townsend RD (2008a) High-resolution CHANDRA X-ray imaging and spectroscopy of the σ Orionis cluster. ApJ 683:796–812. doi:10.1086/589917, 0805.0714

Skinner SL, Zhekov S, Güdel M, Schmutz W, Sokal K (2008b) X-ray emission from Wolf-Rayet stars. In: Poster presented at the "Lifetime of influence" meeting (Flagstaff, Lowell Observatory)

Skinner SL, Sokal KR, Güdel M, Briggs KR (2009) X-ray emission from the FU Orionis Star V1735 Cygni. ArXiv e-prints 0901.3514

Smith K, Pestalozzi M, Güdel M, Conway J, Benz AO (2003) VLBI observations of T Tauri South. A&A 406:957–967. doi:10.1051/0004-6361:20030764, arXiv:astro-ph/0305543

Smith MA, Cohen DH, Gu MF, Robinson RD, Evans NR, Schran PG (2004) High-resolution CHANDRA spectroscopy of γ Cassiopeiae (B0.5e). ApJ 600:972–985. doi:10.1086/379873, arXiv:astro-ph/0309293

Smith K, Güdel M, Audard M (2005) Flares observed with XMM-*Newton* and the VLA. A&A 436:241–251. doi:10.1051/0004-6361:20042054, arXiv:astro-ph/0503022

Stassun KG, van den Berg M, Feigelson E, Flaccomio E (2006) A simultaneous optical and X-ray variability study of the Orion Nebula cluster. I. Incidence of time-correlated X-ray/optical variations. ApJ 649:914–926. doi:10.1086/506422, arXiv:astro-ph/0606079

Stelzer B, Schmitt JHMM (2004) X-ray emission from a metal depleted accretion shock onto the classical T Tauri star TW Hya. A&A 418:687–697. doi:10.1051/0004-6361:20040041, arXiv:astro-ph/0402108

Stelzer B, Burwitz V, Audard M, Güdel M, Ness JU, Grosso N, Neuhäuser R, Schmitt JHMM, Predehl P, Aschenbach B (2002) Simultaneous X-ray spectroscopy of YY Gem with CHANDRA and XMM-*Newton*. A&A 392:585–598. doi:10.1051/0004-6361:20021188, arXiv:astro-ph/0206429

Stelzer B, Flaccomio E, Montmerle T, Micela G, Sciortino S, Favata F, Preibisch T, Feigelson ED (2005) X-ray emission from early-type stars in the Orion Nebula cluster. ApJ Suppl 160:557–581. doi:10.1086/432375, arXiv:astro-ph/0505503

Stelzer B, Micela G, Hamaguchi K, Schmitt JHMM (2006) On the origin of the X-ray emission from Herbig Ae/Be stars. A&A 457:223–235. doi:10.1051/0004-6361:20065006, arXiv:astro-ph/0605590

Stelzer B, Flaccomio E, Briggs K, Micela G, Scelsi L, Audard M, Pillitteri I, Güdel M (2007) A statistical analysis of X-ray variability in pre-main sequence objects of the Taurus molecular cloud. A&A 468:463–475. doi:10.1051/0004-6361:20066043, arXiv:astro-ph/0608651

Stelzer B, Robrade J, Schmitt JHMM, Bouvier J (2009) New X-ray detections of Herbig stars. A&A 493:1109–1119. doi:10.1051/0004-6361:200810540, 0810.1836

Stern RA, Lemen JR, Schmitt JHMM, Pye JP (1995) EUVE observations of Algol: detection of a continuum and implications for the coronal (Fe/H) abundance. ApJ 444:L45–L48. doi:10.1086/187856

Stevens IR, Blondin JM, Pollock AMT (1992) Colliding winds from early-type stars in binary systems. ApJ 386:265–287. doi:10.1086/171013

Stevens IR, Corcoran MF, Willis AJ, Skinner SL, Pollock AMT, Nagase F, Koyama K (1996) ASCA observations of γ^2 Velorum (WC8+O9I): the variable X-ray spectrum of colliding winds. MNRAS 283:589–605

Sugawara Y, Tsuboi Y, Maeda Y (2008) Redshifted emission lines and radiative recombination continuum from the Wolf-Rayet binary θ Muscae: evidence for a triplet system? A&A 490:259–264. doi:10.1051/0004-6361:20079302, 0810.1208

Swartz DA, Drake JJ, Elsner RF, Ghosh KK, Grady CA, Wassell E, Woodgate BE, Kimble RA (2005) The Herbig Ae star HD 163296 in X-rays. ApJ 628:811–816. doi:10.1086/429984, arXiv:astro-ph/0503076

Telleschi A, Güdel M, Briggs K, Audard M, Ness JU, Skinner SL (2005) Coronal evolution of the Sun in time: high-resolution X-ray spectroscopy of solar analogs with different ages. ApJ 622:653–679. doi:10.1086/428109, arXiv:astro-ph/0503546

Telleschi A, Güdel M, Briggs KR, Audard M, Palla F (2007a) X-ray emission from T Tauri stars and the role of accretion: inferences from the XMM-*Newton* extended survey of the Taurus molecular cloud. A&A 468:425–442. doi:10.1051/0004-6361:20066565, arXiv:astro-ph/0612338

Telleschi A, Güdel M, Briggs KR, Audard M, Scelsi L (2007b) High-resolution X-ray spectroscopy of T Tauri stars in the Taurus-Auriga complex. A&A 468:443–462. doi:10.1051/0004-6361:20066193, arXiv:astro-ph/0611024

Telleschi A, Güdel M, Briggs KR, Skinner SL, Audard M, Franciosini E (2007c) The first high-resolution X-ray spectrum of a Herbig star: AB Aurigae. A&A 468:541–556. doi:10.1051/0004-6361:20065422, arXiv:astro-ph/0610456

Testa P, Drake JJ, Peres G (2004a) The density of coronal plasma in active stellar coronae. ApJ 617:508–530. doi:10.1086/422355, arXiv:astro-ph/0405019

Testa P, Drake JJ, Peres G, DeLuca EE (2004b) Detection of X-ray resonance scattering in active stellar coronae. ApJ 609:L79–L82. doi:10.1086/422747, arXiv:astro-ph/0405520
Testa P, Peres G, Reale F (2005) Emission measure distribution in loops impulsively heated at the footpoints. ApJ 622:695–703. doi:10.1086/427900, arXiv:astro-ph/0412482
Testa P, Drake JJ, Peres G, Huenemoerder DP (2007) On X-ray optical depth in the coronae of active stars. ApJ 665:1349–1360. doi:10.1086/519920, 0706.4080
Testa P, Drake JJ, Ercolano B, Reale F, Huenemoerder DP, Affer L, Micela G, Garcia-Alvarez D (2008a) Geometry diagnostics of a stellar flare from fluorescent X-rays. ApJ 675:L97–L100. doi:10.1086/533461, 0801.3857
Testa P, Huenemoerder DP, Schulz NS, Ishibashi K (2008b) X-ray emission from young stellar objects in the ϵ Chamaeleontis group: the Herbig Ae star HD 104237 and associated low-mass stars. ApJ 687:579–597. doi:10.1086/591485, 0807.0059
Tout CA, Pringle JE (1995) X-ray coronae from dynamos in young Ae/Be stars. MNRAS 272:528–530
Tsuboi Y, Koyama K, Murakami H, Hayashi M, Skinner S, Ueno S (1998) ASCA detection of a super-hot 100 million K X-ray flare on the weak-lined T Tauri star V773 Tauri. ApJ 503:894–901. doi:10.1086/306024
Tsujimoto M, Feigelson ED, Grosso N, Micela G, Tsuboi Y, Favata F, Shang H, Kastner JH (2005) Iron fluorescent line emission from young stellar objects in the Orion Nebula. ApJ Suppl 160:503–510. doi:10.1086/432093, arXiv:astro-ph/0412608
ud-Doula A, Owocki SP (2002) Dynamical simulations of magnetically channeled line-driven stellar winds. I. Isothermal, nonrotating, radially driven flow. ApJ 576:413–428. doi:10.1086/341543, arXiv:astro-ph/0201195
Ulrich RK (1976) An infall model for the T Tauri phenomenon. ApJ 210:377–391. doi:10.1086/154840
van den Besselaar EJM, Raassen AJJ, Mewe R, van der Meer RLJ, Güdel M, Audard M (2003) AD Leonis: flares observed by XMM-*Newton* and CHANDRA. A&A 411:587–593. doi:10.1051/0004-6361:20031398, arXiv:astro-ph/0309315
van den Oord GHJ, Schrijver CJ, Camphens M, Mewe R, Kaastra JS (1997) EUV spectroscopy of cool stars. III. Interpretation of EUVE spectra in terms of quasi-static loops. A&A 326:1090–1102
van der Hucht KA (2001) The VIIth catalogue of galactic Wolf-Rayet stars. New Astron Rev 45:135–232. doi:10.1016/S1387-6473(00)00112-3
van der Meer A, Kaper L, di Salvo T, Méndez M, van der Klis M, Barr P, Trams NR (2005) XMM-*Newton* X-ray spectroscopy of the high-mass X-ray binary 4U 1700-37 at low flux. A&A 432:999–1012. doi:10.1051/0004-6361:20041288, arXiv:astro-ph/0412021
Ventura R, Maggio A, Peres G (1998) Loop modeling of coronal X-ray spectra. V. One- and two-loop model fitting of G-type star ROSAT/PSPC spectra. A&A 334:188–200
Vesecky JF, Antiochos SK, Underwood JH (1979) Numerical modeling of quasi-static coronal loops. I—Uniform energy input. ApJ 233:987–997. doi:10.1086/157462
Vilkoviskii EI, Tambovtseva LV (1992) Variability and theoretical upper limit of the mass loss rate in OB-stars. A&A Suppl 94:109–120
Wade GA, Drouin D, Bagnulo S, Landstreet JD, Mason E, Silvester J, Alecian E, Böhm T, Bouret JC, Catala C, Donati JF (2005) Discovery of the pre-main sequence progenitors of the magnetic Ap/Bp stars? A&A 442:L31–L34. doi:10.1051/0004-6361:200500184, arXiv:astro-ph/0509295
Walborn NR (1972) Spectral classification of OB stars in both hemispheres and the absolute-magnitude calibration. Astron J 77:312–318
Walborn NR (1973) The space distribution of the O stars in the solar neighborhood. Astron J 78:1067–1073
Walborn NR (2008) Multiwavelength systematics of OB spectra. In: Revista Mexicana de astronomia y astrofisica conference series vol 33, pp 5–14
Waldron WL (1984) Recombination stellar wind model for the coronae of early-type stars. ApJ 282:256–266. doi:10.1086/162198
Waldron WL (2005) Multiple X-ray periodicity in the rapidly rotating O-star, ζ Ophiuchi. In: Ignace R, Gayley KG (eds) The nature and evolution of disks around hot stars, Astronomical society of the Pacific conference series, vol 337, pp 329–332
Waldron WL, Cassinelli JP (2001) CHANDRA Discovers a very high density X-ray Plasma on the O star ζ Orionis. ApJ 548:L45–L48. doi:10.1086/318926, arXiv:astro-ph/0012190
Waldron WL, Cassinelli JP (2007) An extensive collection of stellar wind X-ray source region emission line parameters, temperatures, velocities, and their radial distributions as obtained from CHANDRA observations of 17 OB stars. ApJ 668:456–480. doi:10.1086/520919, 0707.0024

Waldron WL, Cassinelli JP (2008) Erratum: An extensive collection of stellar wind X-ray source region emission line parameters, temperatures, velocities, and their radial distributions as obtained from CHANDRA observations of 17 OB stars. ApJ 680:1595–1602. doi:10.1086/588041
Waldron WL, Cassinelli JP (2009) Highly accelerated diamagnetic plasmoids: a new X-ray production mechanism for OB stellar winds. ApJ 692:L76–L79. doi:10.1088/0004-637X/692/2/L76, 0901.1405
Walter FM (1981) On the coronae of rapidly rotating stars. II—A period-activity relation in G stars. ApJ 245:677–681. doi:10.1086/158843
Walter FM, Gibson DM, Basri GS (1983) First observations of stellar coronal structure—the coronae of AR Lacertae. ApJ 267:665–681. doi:10.1086/160904
Wargelin BJ, Kashyap VL, Drake JJ, García-Alvarez D, Ratzlaff PW (2008) X-ray flaring on the dMe star, Ross 154. ApJ 676:610–627. doi:10.1086/528702, 0712.2791
Watanabe S, Sako M, Ishida M, Ishisaki Y, Kahn SM, Kohmura T, Nagase F, Paerels F, Takahashi T (2006) X-ray spectral study of the photoionized stellar wind in Vela X-1. ApJ 651:421–437. doi:10.1086/507458, arXiv:astro-ph/0607025
Wessolowski U (1996) X-ray emission from (apparently) single galactic Wolf-Rayet stars. In: Vreux JM, Detal A, Fraipont-Caro D, Gosset E, Rauw G (eds) Liege international astrophysical colloquia, Liege international astrophysical colloquia, vol 33, pp 345–651
White NE, Shafer RA, Parmar AN, Horne K, Culhane JL (1990) X-ray eclipse mapping of AR Lacertae. ApJ 350:776–795. doi:10.1086/168430
White NE, Arnaud K, Day CSR, Ebisawa K, Gotthelf EV, Mukai K, Soong Y, Yaqoob T, Antunes A (1994) An ASCA observation of one orbital cycle of AR Lacertae. Publ Astron Soc Jpn 46:L97–L100
Willis AJ, Schild H, Stevens IR (1995) ROSAT observations of γ Velorum (WC8+O9I). I. The discovery of colliding-wind X-ray emission. A&A 298:549–566
Wojdowski PS, Schulz NS (2005) Ion-by-ion differential emission measure determination of collisionally ionized plasma. II. Application to Hot stars. ApJ 627:953–959. doi:10.1086/430586, arXiv:astro-ph/0503430
Wood BE, Linsky JL (2006) Coronal emission measures and abundances for moderately active K Dwarfs observed by CHANDRA. ApJ 643:444–459. doi:10.1086/501521, arXiv:astro-ph/0601551
Young PR (2005) The Ne/O abundance ratio in the quiet Sun. A&A 444:L45–L48. doi:10.1051/0004-6361:200500206, arXiv:astro-ph/0510264
Zhekov SA (2007) Colliding stellar wind models with non-equilibrium ionization: X-rays from WR 147. MNRAS 382:886–894. doi:10.1111/j.1365-2966.2007.12450.x, 0709.1686
Zhekov SA, Palla F (2007) X-rays from massive OB stars: thermal emission from radiative shocks. MNRAS 382:1124–1132. doi:10.1111/j.1365-2966.2007.12286.x, 0708.0085
Zhekov SA, Skinner SL (2000) X-ray emission from colliding wind shocks in the Wolf-Rayet binary WR 140. ApJ 538:808–817. doi:10.1086/309176
Zinnecker H, Preibisch T (1994) X-ray emission from Herbig Ae/Be stars: a ROSAT survey. A&A 292:152–164